SYNTHESIS AND STEREOSELECTIVE REDUCTION OF α-FLUORO-β-KETOESTERS BY KETOREDUCTASES

By

Matthew G. Vanagel, B.S.

A Thesis submitted in partial fulfillment of the requirements

for the degree of

Master of Science

in

Chemistry

University of Alaska Fairbanks

May 2024

APPROVED:

Dr. Tom Green, Committee Chair

Dr. Brian Rasley, Committee Co-Chair

Dr. Thomas Kuhn, Committee Member

Dr. Brian Rasley, Chair

Department of Chemistry and Biochemistry

Dr. Karsten Heuffer, Dean

College of Natural Science and Mathematics

Dr. Richard Collins, Director

The Graduate School

Abstract

Using commercially available ketoreductase (KRED) enzymes, α-fluoro-β-hydroxy esters were stereoselectively synthesized from racemic α-fluoro-β-keto esters through dynamic reductive kinetic resolution (DYRKR). The α-fluoro-β-keto esters were synthesized via Reformatsky reactions between an aromatic aldehyde and ethyl bromofluoroacetate and subsequent oxidation with Dess Martin Periodinane (DMP). Two enzymes were selected for their ability to yield either *syn* or *anti* diastereomers. Three aromatic substrates were reduced in high diastereomeric and enantiomeric excess and good yields. The KRED products were derivatized with (*R*)- and (*S*)-α-methoxy-α-trifluoromethylphenylacetic acid (MTPA) and analyzed via ^{19}F NMR spectroscopy to determine their absolute stereochemistry via Mosher ester analysis. For the three substrates, KRED 110 yielded the *anti* 2*S*,3*S* isomer. KRED 130 predominantly yielded the *syn* 2*S*,3*R* isomer but with less specificity. The use of these commercially available KRED enzymes provides access to enantio- and diastereomerically pure α-fluoro-β-hydroxy esters from readily accessible racemic substrates. Optically pure α-fluoro-β-hydroxy esters may serve as useful intermediates in the synthesis of medicinally relevant compounds such as fluorinated amino acids or fluorinated sphingolipid derivatives.

Acknowledgments

I would like to acknowledge and thank the various professors and mentors I have had throughout my many years at UAF. First and foremost I'd like to thank my advisor, Dr. Thomas Green, for guiding me throughout the course of my M.S. degree. I'd also like to thank Dr. Fenton Heirtzler who allowed me to do research in his lab when I was an undergrad student. That experience inspired my love for organic synthesis and set me on my current path. I'd also like to thank Dr. Brain Rasley and Dr. Kelly Drew for all their support and assistance. Additionally, I'd like to thank my friend and fellow graduate student Anil Kumar Damarancha for his assistance throughout the course of this project. Finally, I'd like to thank Dr. Carl Murphy for all his assistance in the NMR lab.

Table of Contents

List of Figures

Chapter 1. Introduction

1.1. The Relevance of Fluorine in Medicinal Chemistry

Fluorine is the 13th most abundant of all the elements, and the most abundant halogen in the earth's crust, but it exists in an insoluble form making it largely biologically unavailable [1]. As a result of this, organically bound fluorine is rare in nature. As of 2011, only twelve naturally formed organic compounds containing fluorine have been identified, all of which possess only a single fluorine atom, and only two of them (nucleocidin and fluorocitric acid) contain a fluorine atom bonded directly to a chiral center [2]. Most of the natural products containing fluorine are found in a small number of tropical and subtropical plants. The only ones found in bacteria have been found in two species of actinomycetes. No organofluoro compounds have been isolated from any organism in the animal kingdom or marine environments, despite the relative abundance of other halogenated natural products and metabolites [2].

Because there is a low natural abundance of compounds containing fluorine, fluorinated compounds were rare in medicine up until the 1970s since traditional medicinal chemistry was based and relied on natural compounds. However, today, there are more than 1.8 million fluorine containing organic chemicals listed by Chemical Abstract Services (CAS) and fluorinated compounds are almost ubiquitous in medicine and used to treat a wide variety of diseases. Examples include anti-cancer agents, anti-inflammatory agents, antidepressants, anesthetics, etc. As of 2011, 20% of all pharmaceutical drugs contain at least one fluorine atom. And as of 2007, 9 of the top 20 best-selling drugs worldwide contained fluorine [3].

The first fluorinated drug brought to market was fludrocortisone, which was first prescribed in 1954. Fludrocortisone is a corticosteroid which contains a fluorine atom at the 9a stereocenter in place of hydrogen (Figure 1.1). Fludrocortisone exhibits strong mineralocorticoid and glucocorticoid activities relative to cortisol and is used to treat cerebral salt-wasting

syndrome (CSWS) - a rare condition of the endocrine system characterized by low blood sodium concentration [4].

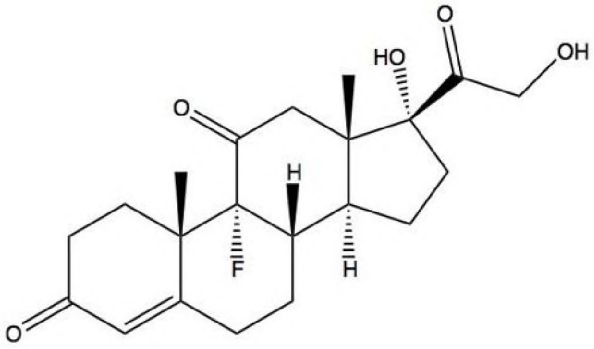

Figure 1.1. Fludrocortisone structure.

Shortly after, other fluorinated drugs were synthesized. 5-fluorouracil (Figure 1.2), now sold under the brand name Adrucil, was first synthesized in 1957 [5].

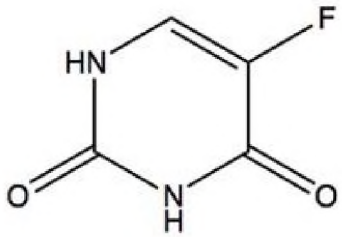

Figure 1.2. 5-fluorouracil structure.

5-fluorouracil is used to treat a variety of different cancers. 5-fluorouracil works by inhibiting thymidylate synthase. Inhibition of thymidylate synthase inhibits the synthesis of deoxythymidine monophosphate (dTMP) by preventing the methylation of deoxyuridine monophosphate (dUMP). Since dTMP is a required precursor for deoxythymidine triphosphate (dTTP), which is required for DNA synthesis, 5-flurouracil ultimately has the effect of promoting cell death as the cell can no longer synthesize DNA, a process known as thymineless death [6].

The synthesis and development of fluoroquinolones in the 1980s marked another historically significant advancement for fluorine use in pharmaceuticals. Quinolone antibiotics belong to a large group of broad-spectrum bactericides that share a bicyclic core structure related to that of 4-quinolone. Quinolones are commonly prescribed to treat bacterial infections in humans and other animals as they display broad spectrum oral activity and are typically accompanied by mild side effects that dissipate upon discontinued use. They are effective against both Gram-negative and Gram-positive bacteria. Their bactericidal properties result from their ability to inhibit the ligase activity of topoisomerases II and IV which results in a bacterial cell with both single and double strand breaks in their DNA which results in cell death [7].

The first in this class of antimicrobials was nalidixic acid, first reported in 1962 [8]. It showed moderate antimicrobial activity towards Gram negative organisms and its use was limited, restricted largely to urinary tract infections. In subsequent decades many other compounds in this class were synthesized and investigated. Flumequine was one of the earliest examples that contained a fluorine atom at the 6 position (Figure 1.3) [9].

The widespread use of these early compounds was restricted due to their lack of potency against a wider range of bacteria. Eventually in 1980, a systematic study by Koga et al. resulted in the synthesis and development of much more potent and broad-spectrum agents, norfloxacin and later pefloxacin (Figure 1.4) [10]. Almost all quinolones currently in use as antibiotics are fluoroquinolones which contain at least one fluorine atom attached to the central ring, commonly at the C-6 or C-7 position. The addition of fluorine to the quinolone structure resulted in drugs with enhanced tissue penetration allowing them to achieve therapeutically relevant concentrations in target organs such as lungs, kidneys, and intestines.

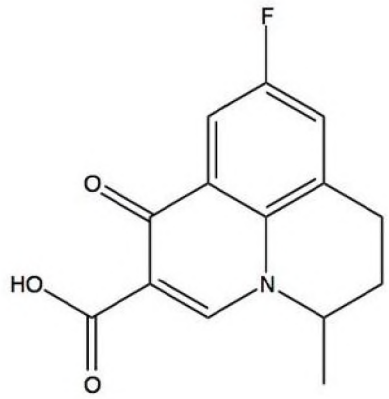

Figure 1.3. Flumequine structure

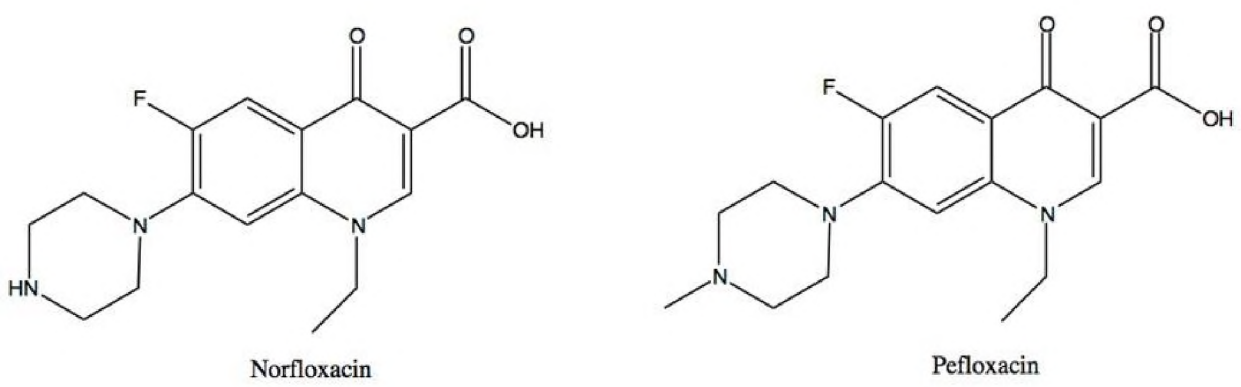

Figure 1.4. Structures of Norfloxacin and Pefloxacin

The addition of fluorine also broadened the spectrum of antibacterial activity such that fluoroquinolones are active against many Gram-positive and Gram-negative bacteria [11].

Fluorine substitution has become a common strategy in medicinal chemistry to improve a drug's properties. The addition of fluorine at key positions in a molecule can have profound effects on the bioactivity of the molecule and dramatically alter its pharmacological properties via its ability to influence the pK_a, metabolism, conformation, lipophilicity/membrane permeability, binding affinity, potency, and pharmacokinetics of the molecule.

1.1.1 The Effect of Fluorine on pK_a

Changes to the pK_a of a drug can strongly affect the drugs affinity for its receptors and alter its pharmacokinetic properties. Because of its high electronegativity, the inclusion of fluorine can affect the pK_a of a drug via its ability to affect the acidity or basicity of neighboring functional groups [12, 13].

In aliphatic systems successive fluorination has an additive effect regarding its modulation of pK_a. For example, each fluorine substitution at the β-position in ethylamine lowers the pK_a of the conjugate acid by about 1.6 units, which translates to a weaker base. (Figure 1.5) [14].

Amine	pKa
$CH_3CH_2NH_2$	10.7
$CH_2FCH_2NH_2$	9.0
$CHF_2CH_2NH_2$	7.3
$CF_3CH_2NH_2$	5.7

Figure 1.5. The effect of fluorine substitution on the pK_a of ethylamine. Successive fluorination results in a reduction of pK_a [14].

The effect of fluorination on amine basicity decreases the further fluorine is from the amine. Introduction of fluorine at the β carbon of dimethylalkyl amines lowers the pK_a by about 1.7 units while fluorine introduction at a gamma carbon lowers pK_a by only 0.3 units (Figure 1.6). This affect can be used to precisely modulate the basicity of an alkylamine [14].

An example of the utilization of this effect in drug development can be found in the development of a series of kinesin spindle protein (KSP) inhibitors (Figure 1.7) [15]. Compound 1 was tested as a treatment for taxane-refractory tumors but had limited efficacy due to its P-glycoprotein (P-gp) efflux [16]. Through structure activity studies it was revealed that the

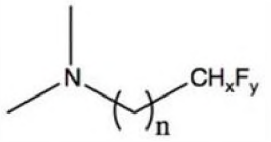

n	position	ΔpK_a
1	β-F	-1.7
2	γ-F	-0.7
3	δ-F	-0.3
4	ε-F	-0.1

Figure 1.6. Effect of distance of the fluorine from the amino group on the basicity of fluorinated amines [14].

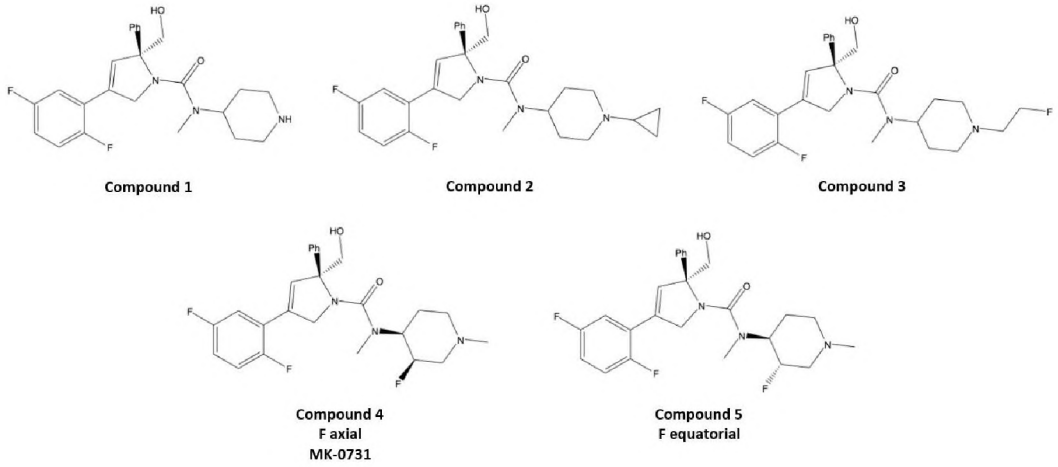

Figure 1.7. Structures in a series of KSP inhibitors that were developed for the treatment of taxane refractory solid tumors. The first in the series (compound 1) had limited efficacy due to P-gp efflux resulting from too great a basicity. Derivatives with reduced basicity were synthesized by introducing electron withdrawing substituents. Ultimately compound 4 (MK-0731) was selected for clinical trials [14, 16, 17].

recognition of this compound by the P-gp transporter was minimized if the pK_a of the piperidine moiety was lowered to between 6.5 and 8. Analogs of compound 1 were synthesized with various electron withdrawing substituents to reduce the basicity to the target range. One of the fluorinated derivatives was the N-β-fluoroethyl substituted derivative (compound 3) which had the required basicity, but metabolic N-dealkylation produced toxic fluoroacetic acid [17]. Installation of fluorine within the piperidine ring alleviated this problem resulting in compound 4

with fluorine in an axial position and compound 5 with fluorine in an equatorial position. Ultimately the axial isomer named MK-0731 (compound 4) was selected for clinical trials [14, 16].

In another study on a series of 3-piperidinylindole antipsychotic drugs (Figure 1.8), fluorination was found to decrease the basicity of the amine resulting in improved bioavailability of the drug. The study found that gamma-fluorination of the amine reduced the pK_a from 10.4 in the non-fluorinated compound to 8.5 and showed moderate bioavailability in rats. The compound was found to be metabolized at the 6 position of the indole ring and blocking this site of hydroxylation with another fluorine atom further improved bioavailability [18]. This effect is shown in another study on a series of piperidinyl and piperazinyl indoles which were synthesized for possible new and improved migraine treatments. Again, bioavailability was dramatically improved via fluorination of the compounds due to the reduction in the basicity of the amine (Figure 1.9) [15, 19].

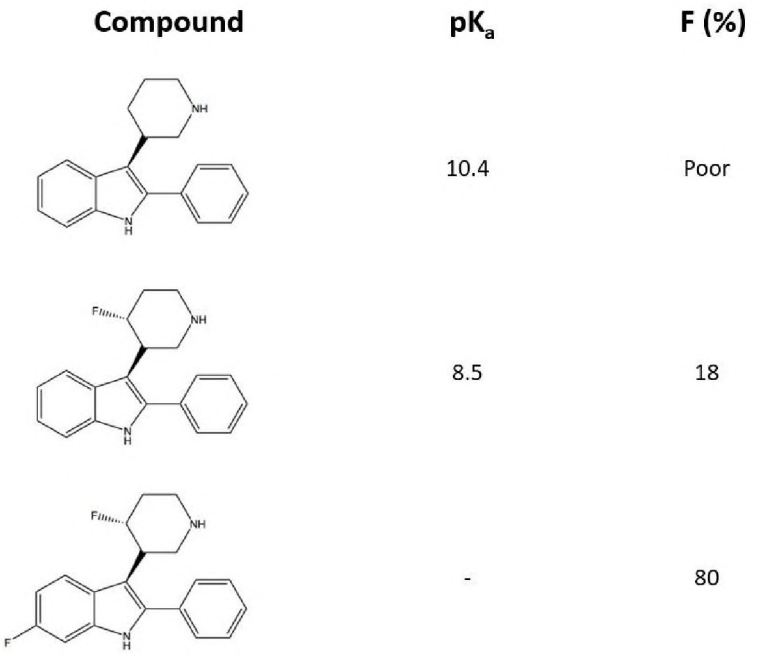

Figure 1.8. Basicity and bioavailability of a series of 3-piperdinylindoles developed as antipsychotics. Fluorination of the parent compound lowered pK_a and increased bioavailability (F%) [18, 19].

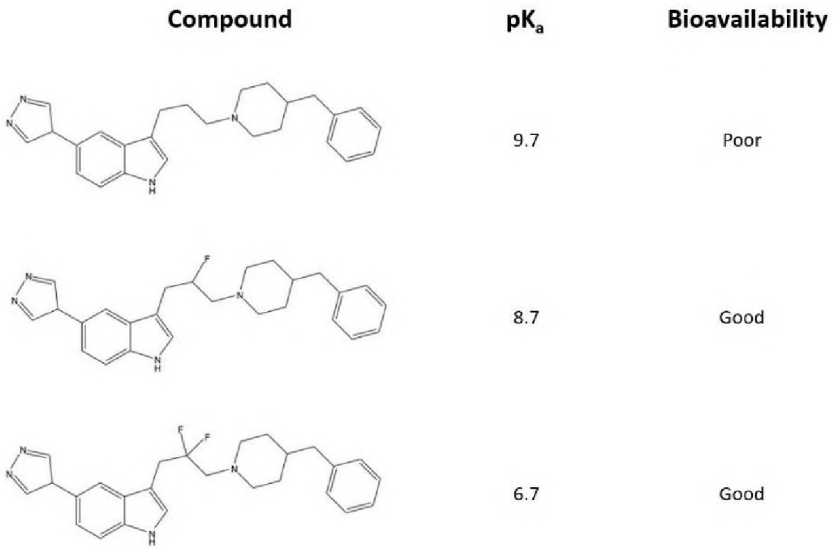

Figure 1.9. Basicity and bioavailability in a series of piperidinyl and piperazinyl indoles. By reducing the basicity of the amine through fluorination, bioavailability was improved [15, 19].

1.1.2. The Effect of Fluorine on Metabolism

Often, medicinal chemists aim to increase the metabolic stability of a given drug. A drug's metabolic stability can have a large effect on its bioavailability. Metabolic stability can be a major challenge in drug discovery and design as a drug can have a pharmacologically favorable interaction with a target receptor or protein, but if it is not sufficiently metabolically stable it may not be able to reach its target. Lipophilic compounds are especially susceptible to oxidative metabolism by cytochrome P450 and other liver enzymes [20].

Fluorine substitution is often employed to overcome issues arising from poor metabolic stability and to make drugs more resistant to certain types of metabolism. This effect is partially due to the strength of the C-F bond relative to the C-H bond (116 kcal/mol vs 99 kcal/mol) and the size of fluorine which can replace metabolically labile hydrogen atoms in aliphatic and aromatic compounds with minimal steric consequences [21, 22]. Even substitution of hydrogen with fluorine adjacent or distal to sites of attack can have a similar metabolic effect due to

inductive and resonance effects [21]. Fluorine can also be incorporated into electron-rich phenyl and heterocyclic rings as well as olefins and other compounds prone to oxidation to enhance their metabolic stability. The inductive effect of fluorine in saturated systems should result in decreased susceptibility of adjacent groups to metabolic attack by cytochrome P450. On the other hand, fluorine, if inserted ortho to a phenolic group can increase its reactivity as a nucleophile in methylation and glucuronidation reactions [21].

The development of the drug ezetimibe provides a good example of how the metabolic stability of a drug can be improved through selective fluorination. Ezetimibe was approved by the FDA in 2002 to reduce cholesterol levels in people with hypercholesterolemia. The precursor to ezetimibe was SCH 48461, a potent cholesterol absorption inhibitor that was particularly liable to metabolic attack at 4 different sites. (Figure 1.10a) The incorporation of two fluorine atoms blocked two of the metabolically labile sites and showed a 50x increase in activity compared to the lead compound SCH 48461 (Figure 1.10b) [23-25].

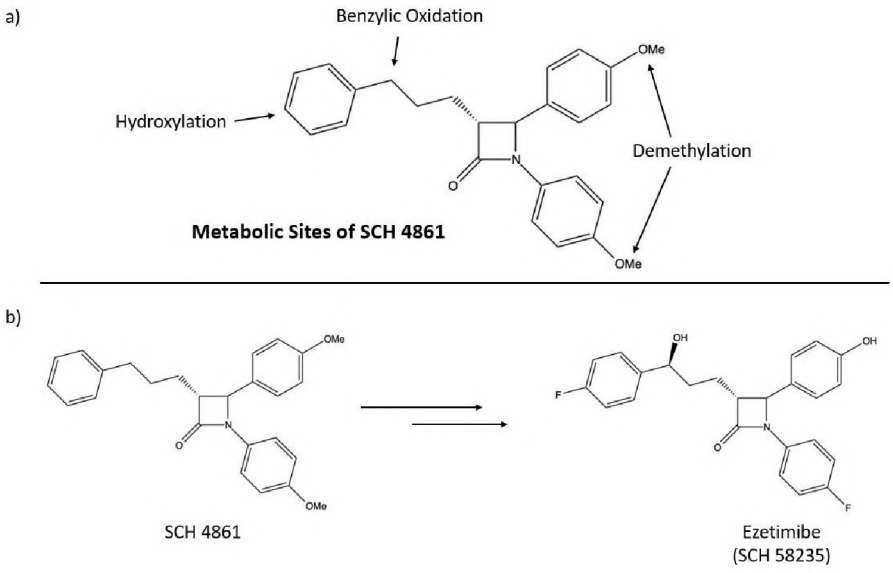

Figure 1.10. The development of Ezetimibe **a)** Sites of metabolism of parent compound SCH 4861 **b)** Fluorine incorporation at metabolically labile sites resulted in a significant increase in activity resulting in the drug Ezetimibe [19, 25].

While drug metabolism generally has a detoxifying role, occasionally metabolism of a particular drug results in the formation of toxic metabolites which may be carcinogenic or cause apoptosis or necrosis [26]. Fluorine can be incorporated into a drug to prevent the formation of toxic metabolites and this strategy has been used to develop safer drugs. Idiosyncratic drug reactions are rare, adverse reactions to a drug that can occur unpredictably in a population [27]. The causes of such reactions are varied and largely unknown, but covalent modifications to proteins by the drug and/or its metabolites and the immune responses they can cause have been implicated in some adverse reactions. Some strategies to lower the potential for such reactions have been to minimize the formation of reactive compounds that result from oxidative metabolism [28, 29].

In a study on a series of cannabinoid-1 receptor (CB1R) inverse agonists for the treatment of obesity, researchers used selective fluorination to reduce the potential for idiosyncratic allergic reactions resulting from covalent drug - protein binding (Figure 1.11) [30].

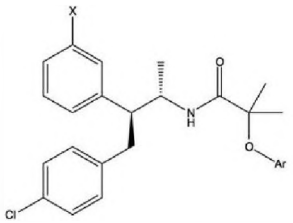

					Pharmacokinetics in rats			
Compound	Ar	X	CB1 IC_{50} (nM)	Covalent binding	Cl_p ((mL/min)/kg)	$T_{1/2}$ (h)	C_{max} (μM)	F (%)
6	Ph	H	2.03	3900	33	2.8	0.18	9
7	3,5-F_2-Ph	H	1.47	1700	35	2.4	0.30	19
8	2-pyr	H	1.80	910	25	2.2	0.44	29
9	5-CF_3-pyr	H	0.54	88	35	2.2	1.2	100
10	5-CF_3-pyr	CN	0.29	27	33	2.7	0.49	74

Figure 1.11. Fluorine incorporation in CB1R inverse agonists to reduce idiosyncratic drug reactions. Compound 10 (taranabant) had the lowest degree of adverse covalent protein binding and went under clinical trials for obesity. Cl_p = rate of clearance from plasma. $T_{1/2}$ = compound half life in circulating plasma. C_{max} = maximum concentration of compound achieved after an oral dose of 2 mg/kg. F = oral bioavailability [31].

One of the early leads in the study, the triphenylamide (compound 6) displayed a high degree of covalent protein binding as determined by incubating the tritiated compounds with human and rat liver microsomes and measuring radioactivity. It was determined that the electron rich phenoxy ring (Ar) was a major target for oxidative metabolism resulting in the formation of intermediates that could form adducts with proteins. The addition of two fluorine atoms to the phenoxy ring (compound 7) resulted in a 2-fold attenuation of covalent protein binding. Replacement of the phenoxy ring altogether with a 2-pyridyloxy group (compound 8) reduced covalent protein binding even further, and the addition of a trifluoromethyl group at the 5 position of the pyridyloxy group (compound 9) reduced covalent binding even more while also improving binding to CB1R [32]. The addition of a cyano group to the 3 position of the distal phenyl ring (compound 10) gave the lowest amount of covalent protein binding and made it into phase 3 clinical trials for the treatment of obesity under the name taranabant [33]. It never completed phase 3 trials due to the high level of depression and anxiety experienced by some participants [31, 34].

The prolonged treatment of experimental animals with exogenous estrogens is accompanied by the development of various tumors [35]. The formation of metabolites (primarily 2- and 4-hydroxyestradiol as well as 2- and 4- hydroxyestrone) that can covalently bind to proteins and DNA has been proposed as a mechanism for this phenomenon. This carcinogenesis could be inhibited by using fluorine as a metabolism inhibiting substituent. 2-fluoroestradiol was found to be highly estrogenic but non carcinogenic in animals, possibly due to the inability of oxidative enzymes to cleave the C-F bond [25, 36].

Selective fluorine incorporation is routinely used to extend the biological half-life of drugs. Prostanoids are a class of eicosanoid signaling molecules that are involved in

inflammation response and consist of the prostaglandins, thromboxanes, and prostacyclins. Prostanoids have relatively short in vivo half-lives of 5 minutes or less. For example, thromboxane A_2 (TxA_2) (Figure 1.12) which stimulates activation of platelets and increases platelet aggregation has an in vivo half-life of just 30 seconds due to the oxetane acetal moiety which is highly susceptible to hydrolytic cleavage at neutral pH. Through fluorination of the oxetane ring, the half-life of 7,7-difluoro-TxA2 is extended due to its rate of hydrolysis being 10^8 times slower than that of the non-fluorinated TxA2 [25, 37].

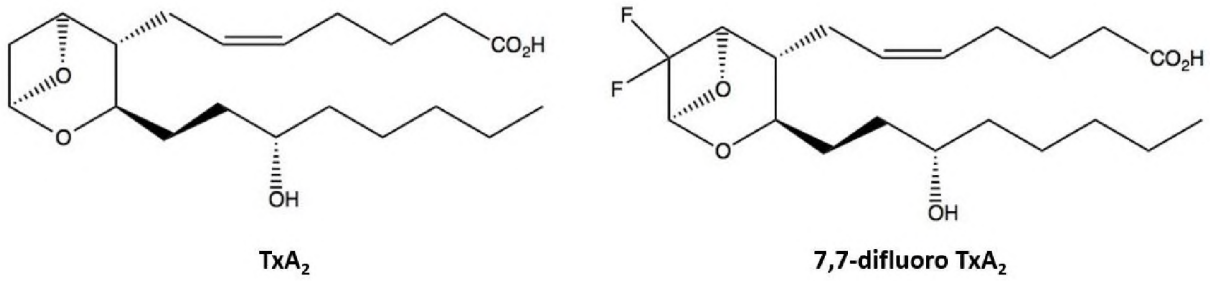

Figure 1.12. Use of fluorination to extend biological half-life by blocking site of hydrolytic cleavage [25].

Prostacyclin, also known as prostaglandin I2, (PGI_2) is another prostanoid. It is a vasodilator and inhibits platelet aggregation. As such, it's been considered as a drug candidate for the treatment of thrombosis and other vascular diseases. However, its acid labile enol ether moiety severely limits its clinical potential since it is easily hydrolyzed in vivo producing the inactive 6-keto-$PGF_{1\alpha}$ derivative (Figure 1.13) [19, 38].

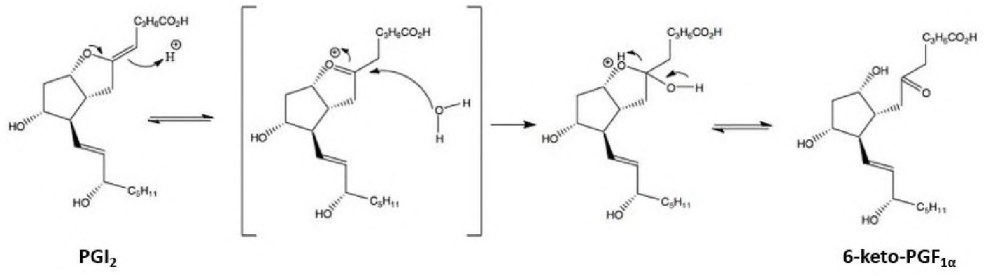

Figure 1.13. Production of 6-keto-$PGF_{1\alpha}$ via hydrolysis of PGI_2 [19].

Fluorination of PGI_2 has been shown to significantly enhance its hydrolytic stability. The highly electronegative fluorine withdraws electrons from the enol ether reducing the electron density of the enol and decreasing the rate of hydrolysis. For the monofluorinated analog, 7-F-PGI_2, its half-life was determined to be 1 month relative to the 10-minute half-life of PGI_2, and for the difluorinated derivative AFP-07, it has been found to have an even longer half-life of 90 days (Figure 1.14) [19, 39, 40].

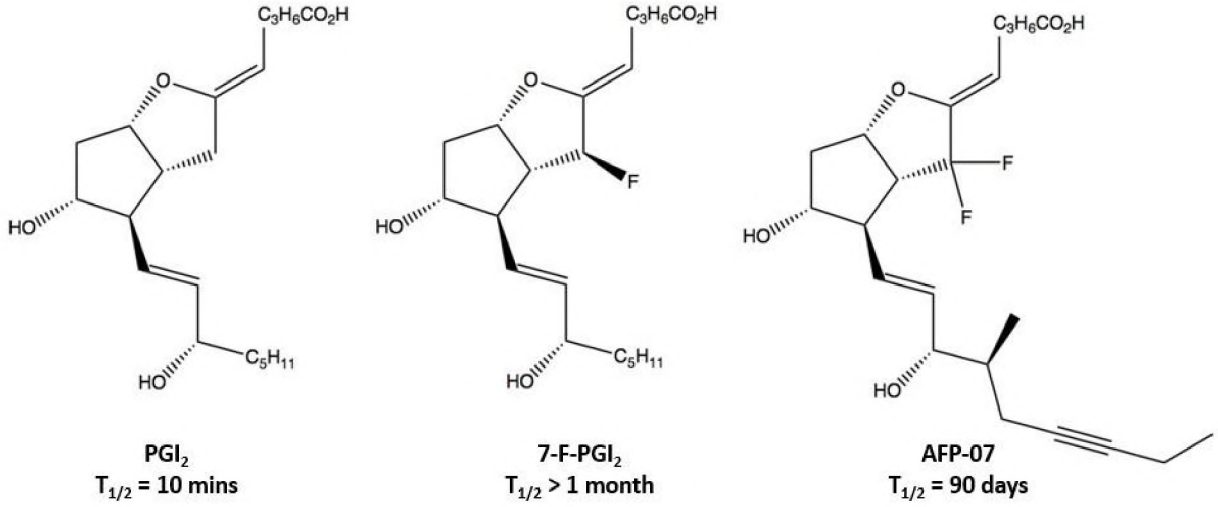

Figure 1.14. Fluorination to increase the half-life of PGI_2 [19]

While increased metabolic stability is often beneficial in drug development, it's also possible for a drug to be too stable resulting in unacceptably long half-lives. The role of fluorine in improving metabolic stability is further highlighted by its need to be removed in the development of the drug celecoxib. A series of 1,5-diarlypyrazole derivatives were synthesized to evaluate their ability to inhibit the cyclooxygenase (COX-2) enzyme which is involved in the conversion of arachidonic acid to prostaglandin H_2, a precursor to prostacyclin which is involved in inflammation. One of the lead compounds in the development of celecoxib had a fluorinated phenyl group and was found to have a half-life of 220 hours in rats. Replacement of the fluorine

atom with the metabolically labile methyl group reduced the half-life to a more reasonable 3.5 hours (Figure 1.15) [25, 41].

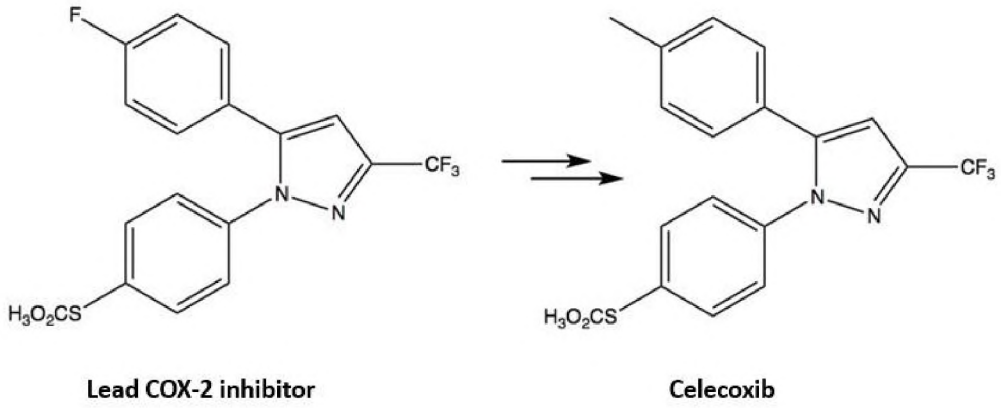

Figure 1.15. Removal of fluorine to reduce half-life in Celecoxib [25, 41].

The metabolic stability of alkyl groups is routinely improved via substitution for a trifluoromethyl group. For example, the substitution of one of the methyl groups in a *tert*-butyl substituent of the neurokinin 1 (NK1) receptor antagonist in Figure 1.16 for a trifluoromethyl group increased metabolic stability as evidenced by the decrease in clearance [14, 42].

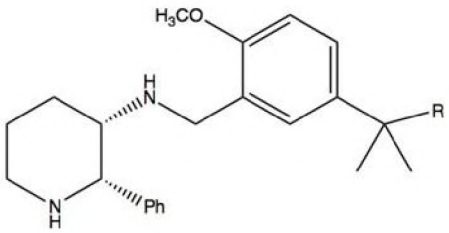

	R = CH_3	R = CF_3
NK1 binding IC_{50} (nM)	0.6	0.3
HLM Cl_{int} (µL/min/mg)	87.9	44.7

Figure 1.16. Replacement of a methyl group with a trifluoromethyl group in NK1 receptor antagonist resulted in an increase in metabolic stability as evidenced by a decrease in clearance. HLM = human liver microsome. Cl_{int} = intrinsic clearance [14, 42].

An example of fluorine being used to block multiple metabolic sites can be found in the cathepsin K inhibitor odanacatib (Figure 1.17) which was in late-stage clinical trials for the treatment of osteoporosis before being discontinued after it was found to increase the risk of stroke [43, 44]. Hydroxylative metabolism at the leucine moiety was blocked via the introduction of a fluorine atom. Additionally, the introduction of a trifluoroethylamine moiety blocked proteolysis [45]. The difluoroethylamine moiety in compound 11 (Figure 1.17) served a similar function but had the effect of increasing the basicity enough to form stable salts with strong acids which allowed for a more orally available formulation [14, 46].

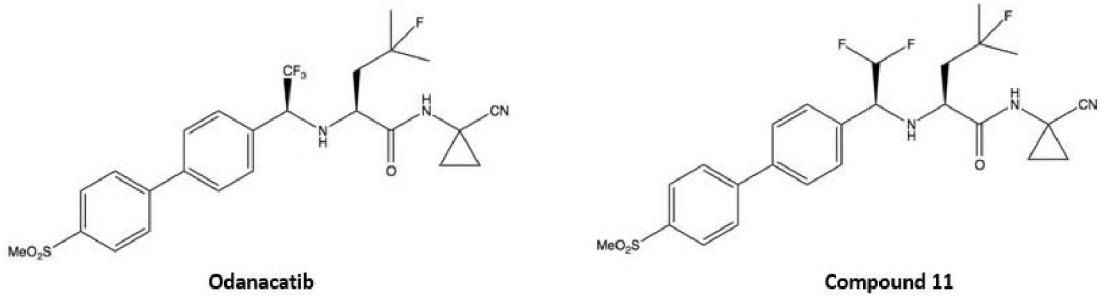

Figure 1.17. Fluorine incorporation to block multiple sites of metabolism in cathepsin K inhibitor. Introduction of a fluorine atom within the leucine moiety blocked one site of hydroxylative metabolism. The introduction of a trifluoroethylamine moiety blocked a site of proteolysis. The difluoroethylamine moiety in Compound 11 served a similar function but resulted in a more orally bioavailable formulation via the formation of stable salts through an increase in basicity [14, 45, 46].

1.1.3. The Effect of Fluorine on Lipophilicity

Lipophilicity is an important parameter in drug discovery and medicinal chemistry because it, in part, controls a drugs absorption and distribution. Orally administered drugs can be absorbed and distributed via two main pathways - active and passive transport. The distinction between the two methods is whether energy (ATP) is consumed in the process. The more common route is via passive transport which requires no ATP but is highly dependent on membrane permeability. Whether or not a drug can be distributed across cellular membranes

depends on the drugs lipophilicity. The drug must be lipophilic enough to pass into the membrane's lipid core, but not so lipophilic that it becomes trapped there and is unable to pass through. Lipophilicity is expressed as a partition coefficient (log P) between octanol and water. The more lipophilic the compound, the greater its partitioning in octanol.

While a drug needs to be lipophilic enough to pass through membranes, too high of a lipophilicity typically results in reduced solubility, and erratic absorption, among other things, so a balance must be met. Generally, the introduction of fluorine into a compound increases the lipophilicity of that compound. This is especially the case in aromatic compounds, per/polyfluorinated compounds, and fluorination adjacent to atoms with pi-bonds (with the exception of some α-fluorinated carbonyl compounds) [47]. Trifluoromethyl benzene for example is 57% more lipophilic than toluene. The reason for this effect on lipophilicity relates to the highly electronegative nature of the fluorine atom and its ability to withdraw electrons from neighboring polar functional groups, reducing their electron densities and thus their abilities to form hydrogen bonds with water. However, it is not *always* true that fluorine introduction increases lipophilicity. Fluorination of saturated alkyl groups typically results in decreased lipophilicity due to the large dipole in the carbon-fluorine bonds of fluoroalkanes [47, 48].

Fluorine substitution effects on lipophilicity were explored in a study on the development of a series of fluorinated 3-benzyl-5-indolecarboxamides as leukotriene receptor inhibitors (antagonists) to reduce bronchoconstriction in asthma patients. The study found that increasingly lipophilic amide substituents afforded more potent orally administered drug candidates. This strategy was limited however because amide substituents containing more than 6 carbon atoms resulted in a reduction of affinity for the leukotriene receptor. This effect was overcome by the introduction of fluorinated amide substituents, specifically a trifluoromethyl group, which

resulted in an average of 10x increase in *in vivo* potency relative to the non-fluorinated counterparts. Measurements of Log P values showed that each of the fluorinated compounds were more lipophilic than their non-fluorinated analogues (Figure 1.18) [19, 49].

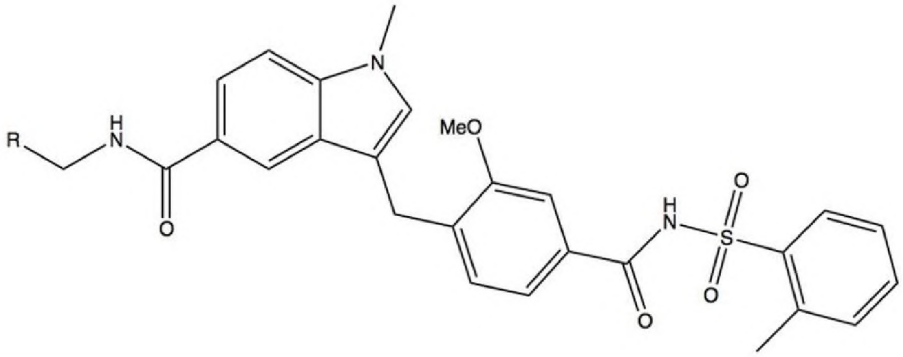

R	Log P
$CH_3CH_2CH(CH_3)$	5.85
$CF_3CH_2CH(CH_3)$	6.18
$(CH_3CH_2)_2CHCH_2$	6.29
$CF_3CH_2CH(CH_3CH_2)CH_2$	6.45
$CF_3CH(CH_3)CH2CH_2$	6.30
$CF_3CH(CH_3)CH_2$	5.89

Figure 1.18. Effect of fluorine substitution on lipophilicity in a series of fluorinated 3-benzyl-5-indolecarboxamides. The fluorinated compounds were all found to be more lipophilic than their non fluorinated counterparts [19, 49].

Interactions between fluorine and hydrogen bond donors also appears to play a role in lipophilicity. In the case of the tachykinin hNK2 receptor antagonist, compound 12, the N-H of the N-terminal amide was found to be crucial for potency but contributed to the poor membrane permeability of the compound. Introduction of a chlorine atom at the ortho position of the aromatic ring (compound 13) improved permeability, but it was found that the introduction of fluorine at the ortho position of the aromatic ring (compound 14) resulted in even more substantially improved permeability compared to its non-fluorinated parent compound (Figure1.19) [50].

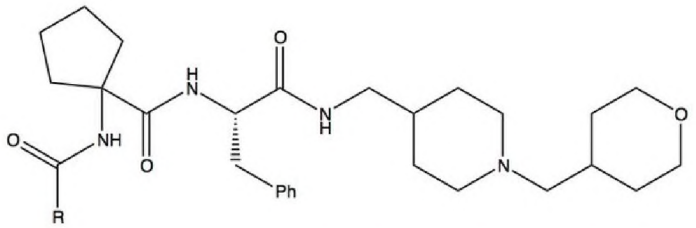

Compound	R	hNK_2 (pK_i)	Caco-2 P_{app} ($x10^{-6}$ cm/s)	PAMPA P_{app} ($x10^{-6}$ cm/s)
12	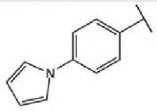	9.63	<1	ND
13	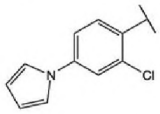	8.40	4.21	0.16
14	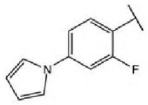	8.49	13.80	0.66

Figure 1.19. Effect of fluorine incorporation on lipophilicity and membrane permeability in a series of tachykinin hNK2 receptor antagonists. Incorporation of a fluorine atom at the ortho position of the aromatic ring resulted in a compound with the greatest permeability. Parallel artificial membrane permeability assay (PAMPA), and Caco-2 are methods for modeling *in vitro* passive transcellular permeation. [14, 50].

1.1.4. The Effect of Fluorine on Conformation

Because of their similarity in size (van der Waals radius 1.47Å for fluorine vs 1.2 Å for hydrogen), fluorine for hydrogen substitution often exerts little to no steric strain at receptors. However, the introduction of a trifluoromethyl group within a molecule can impose significant steric demands and can alter the preferred conformational state of a molecule. For example, while methoxy benzene adopts a planar conformation, trifluoromethoxybenzene does not, with its $-OCF_3$ group out of plane. Such conformational changes resulting from the incorporation of trifluoromethyl, or other larger fluorinated groups can be used to modify the binding affinity of a drug, as in the case of inhibitors of cholesteryl ester transfer protein. The cholesteryl ester transfer protein (CETP), also known as the plasma lipid transfer protein, is a plasma protein that facilitates the transport of cholesterol esters and triglycerides between lipoproteins. CETP is

implicated in coronary heart disease and its inhibition has been explored as a possible treatment. In the case of one class of inhibitors it was found that replacing the ethoxy group in compound 15 with a tetrafluoroethoxy group (compound 16) resulted in an 8-fold increase in potency (Figure 1.20). Molecular modelling showed that, in contrast to the ethoxy group, the tetrafluoroethoxy group prefers an out of plane conformation with respect to the phenyl ring which resulted in an increased binding affinity to the target CETP protein [19, 51].

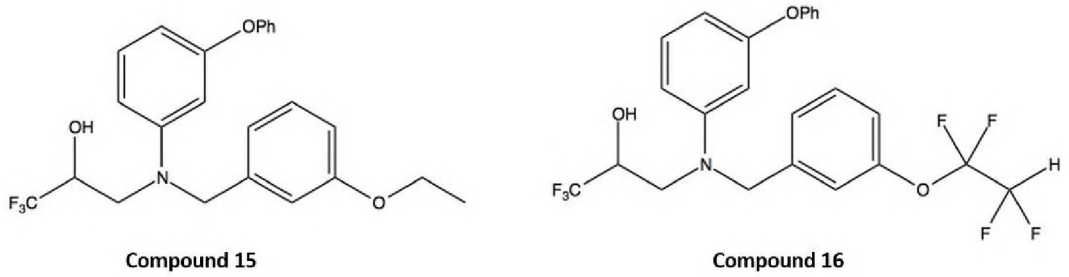

Figure 1.20. Fluorine incorporation resulting in increased binding affinity of the compound to the target CETP protein due to conformational effects of the tetrafluoroethoxy group and its preferred out of plane conformation [19, 51].

The highly polarized nature of the C-F bond can impact how a fluorine containing drug interacts with its environment. For example, the partial negative charge on the fluorine atom often results in the drug binding to its receptor in such a way that the fluorine atom is oriented towards a partial positive charged moiety of the receptor such as an amide carbon atom or acidic hydrogen atom [19, 51].

In the case of 1,3-difluoroalkanes the conformation in which the two C-F bonds are aligned in a parallel configuration is energetically disfavored. Because of the small size of the fluorine atom, it is unlikely that this effect is explained by steric constraint and is more likely explained by electrostatic dipole repulsion of the two partial negatively charged fluorine atoms. Such compounds prefer to adopt a twisted conformation as in Figure 1.21.

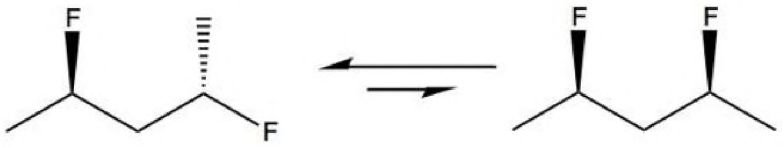

Figure 1.21. Conformational effects of 1,3-difluoroalkanes. Repulsion of the two partial negatively charged fluorine atoms results in a more energetically disfavor able conformation when the two C-F bonds are aligned parallel to one another [52].

When a neighboring group contains a formal rather than a partial charge, the electrostatic interactions of the C-F bond are even more extreme. In the case of the 2-fluoroethylammonium ion the gauche conformation in which the fluorine atom is nearer the positively charged nitrogen atom is strongly preferred (Figure 1.22) [52].

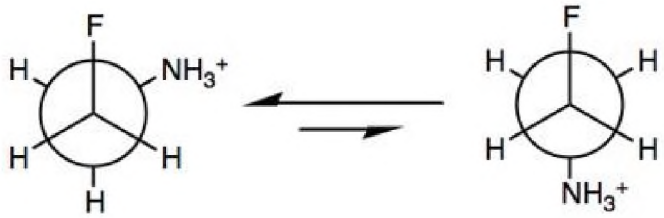

Figure 1.22. The 2-fluoroethylammonium ion will adopt the gauche conformation such that the partial negatively charged fluorine is nearer the positively charged nitrogen atom [52].

1.1.5. The Effect of Fluorine on Binding Affinity

Previous examples showed that by influencing the conformation of a molecule, fluorine substitution can affect that molecule's affinity for its receptor. Fluorine for hydrogen substitution is routinely used in medicinal chemistry to improve ligand binding to proteins. This is possible since fluorine and hydrogen are similar in size, so the overall size of the molecule is not significantly affected [53]. In some cases, fluorine, due to its ability to act as a hydrogen bond acceptor, can also be substituted for a hydroxyl group and interact with enzymes which would normally act on the corresponding hydroxyl groups [54].

Carbonic anhydrase II (CAII), a zinc metalloenzyme, catalyzes the hydration of CO_2 to give bicarbonate and a proton. Inhibition of CAII is used in the treatment of a variety of diseases

such as in glaucoma where CAII inhibition reduces intraocular pressure. CAII inhibitors are also used to treat altitude sickness where lack of oxygen causes a decrease in the partial pressure of CO_2 in the lungs resulting in respiratory alkalosis. By preventing bicarbonate uptake in the kidney, CAII inhibitors can correct the alkalosis. Fluorine can interact with CAII and strategically substituting fluorine for hydrogen in the CAII inhibitor N-(4-sulfamylbenzoyl) benzylamine (SBB), resulting in increased binding affinity via enhanced polar interactions with parts of the enzyme. Specifically, the residues within the CAII active site are Pro202 and Phe131, which engage in dipole-dipole interactions with the fluorinated inhibitors [53]. Substitution of hydrogen atoms with fluorine in the benzoyl group of SBB further enhanced the binding affinity of the inhibitor [55]. Methazolamide is a CAII inhibitor used to treat glaucoma. It was found that fluorinated analogues bind nearly 10 times more strongly to CAII than methazolamide itself due to stacking interactions between the fluorinated aromatic ring of the drug and the aromatic ring in residue Phe131 of the enzyme [25, 56, 57].

1.1.6. The Use of Fluorine in Positron Emission Tomography (PET) Imaging

Positron Emission Tomography (PET) is a nuclear imaging technique that uses radiotracers to visualize and measure changes in a variety of physiological processes and activities including metabolism, blood flow, regional chemical composition, etc. During PET, positrons are emitted as the radioisotope undergoes positron emission decay (β decay), the positron eventually interacts with an electron at which point both particles are annihilated resulting in the production of a pair of gamma rays which are ultimately detected. The result is a three-dimensional image of various functional processes taking place in the body. ^{18}F has become one of the most important radioisotopes used in PET. The properties of ^{18}F lends itself very well to PET imaging. Compared to other radionuclides, ^{18}F has a relatively long half-life of

110 minutes allowing ^{18}F labeled drugs to be produced off site of hospitals. ^{18}F also has a high percentage of β+ emission and a relatively low positron energy of 635 keV which allows for imaging at high resolution [25].

[^{18}F]-fluorodeoxyglucose (FDG), an analogue of glucose where an ^{18}F atom replaces the hydroxyl group at the C-2 position (structure shown in Figure 1.23), is one of the most commonly used radiopharmaceuticals.

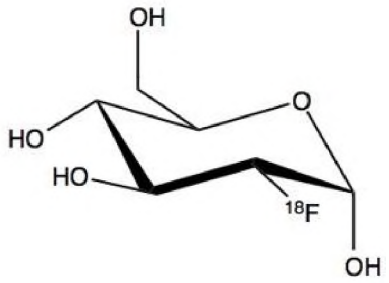

Figure 1.23. Structure of [^{18}F]-fluorodeoxyglucose (FDG)

FDG is used to show glucose uptake and energy consumption in cells. Like glucose, FDG is taken into cells via glucose transporters where it is phosphorylated by hexokinase at the C-1 position. Due to the fluorine atom at the C-2 position, the resulting FDG-6-phosphate cannot be further metabolized since the next step in glucose's metabolism involves glycolysis and requires the hydroxyl group that is replaced by ^{18}F in FDG. Thus, the FDG-6-phosphate becomes trapped in the cell and undergoes radio decay providing a good reflection of the distribution and uptake of glucose by cells. After its decay the 2-fluorine is converted to ^{18}O- which gains a proton from its aqueous environment becoming glucose-6-phosphate labeled with ^{18}O which is harmless and can be metabolized in the same manner as ordinary glucose. Because tumor cells have a higher glycolytic rate, they will take up FDG more rapidly than normal cells and so ^{18}F-FDG-PET is used as a diagnostic tool and is also used to evaluate a patient's response to chemotherapy [58, 59]. ^{18}F-FDH-PET is also routinely used to diagnose reduced glucose metabolism which occurs in a

wide range of diseases including Alzheimer's disease, and epilepsy [60]. The design and synthesis of other ^{18}F labeled radiotracers will allow a variety of other conditions to be studied by PET.

1.2. Stereoselective Synthesis of α-Fluoro-β-Hydroxy Esters via KREDs

Having established the relevance of organofluoro compounds in medicinal chemistry, it's no surprise that the field of asymmetric fluorination has received a lot of interest due to the increasing demand for enantiopure fluorinated pharmaceuticals and intermediates. This thesis deals with the stereoselective synthesis of fluoro-hydroxy esters. α-Fluoro-β-hydroxy esters and α-fluoro-β-keto esters are important structural building blocks in the synthesis and preparation of fluorinated derivatives of amino acids, carbohydrates, and other medicinally relevant compounds [61-63].

For example, Huber et al. synthesized α-Fluoro-α-hydrazino β-keto esters as possible precursors for α-fluoro- α-amino acids. Monofluorination of β-keto esters with N-Chloromethyl-N-fluorotriethylenediammonium bis(tetrafluoroborate)-1-Chloromethyl-4-fluoro-1,4-diazoniabicyclo[2.2.2]octane bis(tetrafluoroborate) (Selectfluor®) using $CpTiCl_3$ as a catalyst followed by amination with diazodicarboxylates afforded α-fluoro-α-hydrazino-β-keto esters in good yields (Figure 1.24) [62].

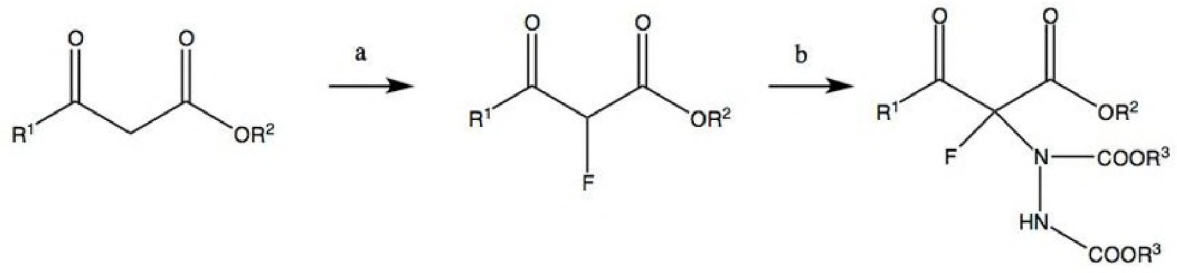

Figure 1.24. Monofluorination of β-keto esters followed by amination to produce α-fluoro-α-hydrazino β-keto esters as possible precursors towards α-fluoro-α-amino-β-keto esters and eventual α-fluoro-α-amino acids. (a) F-TEDA, $CpTiCl_3$, MeCN; (b) DEAD or DBnAD, Cu/Ph-Box, solvent [62].

The classic Reformatsky reaction is a commonly employed synthetic route to making β-hydroxy esters and has some significant benefits over other routes such as base catalyzed aldol reactions because of its high tolerance towards various functional groups and milder reaction conditions [64]. One of the most efficient methods for producing α-fluoro-β-hydroxy esters is the Reformatsky reaction using ethyl bromofluoroacetate [65].

Enantioselective Reformatsky type reactions have been reported using 1,1′-Bi-2-naphthol (BINOL) derivatives, chiral bisoxazolidine, and chiral aminoalcohols [66-73]. However, there are few reports of enantioselective Reformatsky type reactions using fluorinated Reformasky reagents.

A paper published in 2012 describes the enantioselective synthesis α-fluoro-β-hydroxy esters with a Reformatsky reaction using ethyl iodofluoroacetate and (1R,2S)-1-phenyl-2-(pyrrolidin-1-yl)propan-1-ol as a chiral catalyst [74]. The substrates studied included a variety of ketones and two aldehydes. Diastereoselectivites varied but were as high as 92:8 in the case of one substrate (Figure 1.25, entry 3) and enantioselectivties for the major diastereomer were as high as 95% [74].

Here, the enantioselective synthesis of α-fluoro-β-hydroxy esters is described utilizing commercially available ketoreductase enzymes (KREDs) in a 3-step reaction scheme (Figure 1.26). We employed a Reformatsky reaction to synthesize the racemic α-fluoro-β-hydroxy esters which are then oxidized to their corresponding β-keto esters and reduced stereoselectively using a KRED enzyme system from Codexis®. The aldo/keto reductase family of enzymes are found in a variety of different types of organisms and catalyze the reduction of carbonyl compounds such as sugar aldehydes, keto steroids, keto prostaglandins, quinones, lipid peroxidation products, etc [75]. As such they are primarily involved in biosynthesis and metabolic processes.

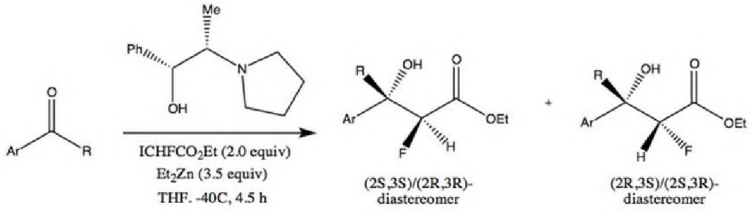

Entry	Ar	R	RR/SS (%)[a]	RS/ SR (%)[a]	ee (%) RR/SS[b]	ee (%) RS/SR[b]	SS (%)[c]	RR (%)[c]	RS (%)[c]	SR (%)[c]
1	Ph	Et	87.0	13.0	95.0	56.0	84.8	2.2	10.1	2.9
2	Ph	Pr	89.0	11.0	93.0	65.0	85.9	3.1	9.1	1.9
3	Ph	*Iso*-Bu	92.0	8.0	94.0	61.0	89.2	2.8	6.4	1.6
4	1-indanone	-	38.0	62.0	86.0	80.0	35.3	2.7	55.8	6.2
5	1-tetralone	-	40.0	60.0	88.0	94.0	37.6	2.4	58.2	1.8
6	4-ClC_6H_4	Me	71.0	29.0	88.0	79.0	66.7	4.3	26.0	3.0
7	2-$MeOC_6H_4$	Me	58.0	42.0	84.0	85.0	53.4	4.6	38.9	3.2

Figure 1.25. Stereoselective synthesis of α-fluoro-β-hydroxy esters via Reformatsky reaction between iodofluoroacetate and various ketones and aldehydes using (1*R*,2*S*)-1-phenyl-2-(pyrrolidin-1-yl)propan-1-ol as a chiral catalyst reported by Fornalczyk et al. [a] percent of *syn* (*R*,*R* / *S*,*S*) diastereomer and *anti* (*R*,*S* / *S*,*R*) diastereomer as determined by ^{19}F NMR spectroscopy. [b] Enantiomeric excess of each diastereomer as determined by chiral HPLC. [c] Overall percentage of each stereoisomer. Absolute configuration was determined by X-ray crystallographic analysis of the product between the reaction of the α-fluoro-β-hydroxy ester with the lithium salt of (*S*)-(1-phenylethyl)amine [74].

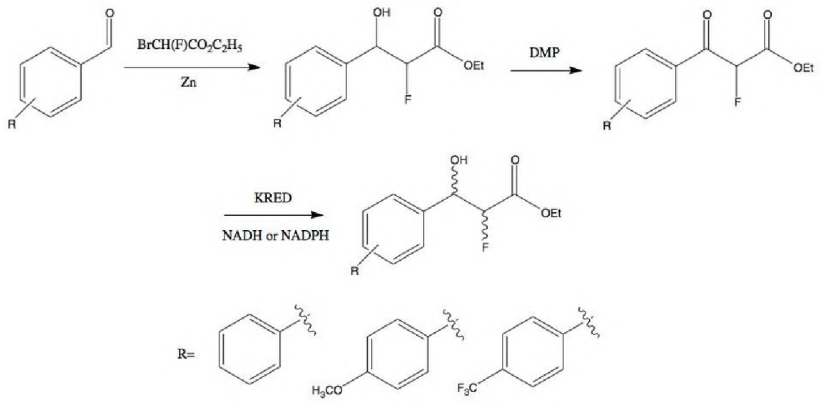

Figure 1.26. Overall reaction scheme for the research presented in this thesis. Three benzaldehyde derivatives were reacted with ethyl bromofluoroacetate in a Reformatsky reaction to form their corresponding racemic α-fluoro-β-hydroxy esters which were then oxidized to their β-keto esters in a Dess-Martin (DMP) oxidation reaction. Ketoreductase enzymes (KREDs) were then used to reduce the β-keto esters back to α-fluoro-β-hydroxy esters stereoselectively using either NADH or NADPH as reducing agents.

KREDs and other enzymes are becoming increasingly popular biocatalysts in synthetic chemistry due to their potentially high stereoselectivity, broad substrate acceptance, mild and environmentally friendly reaction conditions, etc. A variety of KRED enzymes, both wild type and genetically engineered, are commercially available from manufacturers such as Codexis®.

There are many reports in the literature that describe KRED catalyzed reductions of β-keto esters in an enantioselective manner [76-80]. Prior work has shown that the structural variety in substituents at the β and α position strongly affect the activity and stereoselectivity of the various enzymes [81].

Previous work by Green et al. screened 24 of the commercially available KREDs from Codexis for enantioselectivity on a variety of aryl γ,δ-unsaturated β-hydroxy esters [82]. Drawing on their previous work we examined two of the enzymes which gave the highest yields and provided the highest degree of stereoselectivity on several substituted aromatic α-fluoro-β-keto ester substrates.

The process by which a given enantiomer is preferentially formed through KRED reduction is termed dynamic reductive kinetic resolution (DYRKR) [83]. The acidic hydrogen on the α carbon stereocenter of the α-fluoro-β-keto ester substrate allows for interconversion of enantiomers via an enol intermediate in a keto enol tautomerization equilibrium (Figure 1.27).

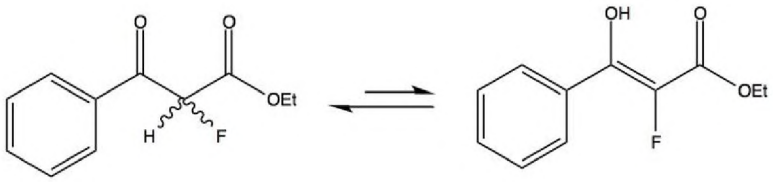

Figure 1.27. Keto-enol tautomerization which allows for interconversion of enantiomers of the α-fluoro-β-keto esters.

Because of the nature of the KRED enzyme and the shape and properties of its active site, the two enantiomers of the substrate will have different rates of reduction. A given enantiomer of

the α-fluoro-β-hydroxy ester is preferentially produced when the rate of racemization exceeds the rate of reduction of the less reactive enantiomer and thus the reduction sets the stereochemistry at the α carbon stereocenter and newly formed β carbon stereocenter (Figure 1.28). In the example in Figure 1.28, the (*S*) enantiomer has a slower rate of reduction with the given KRED enzyme than the (*R*) enantiomer of the keto ester. The rate of racemization of the (*S*) enantiomer is faster than its rate of reduction, so it racemizes to give the (*R*) enantiomer which is then reduced by the KRED enzyme. If the reductant, either NADPH or NADH, attacks preferentially on one side of the pro-chiral face of the (*R*) enantiomer (due to the position of the substrate and cofactor in the active site of the KRED enzyme), then a single stereoisomer of four is possible, in this case yielding the *syn* (2*R*,3*S*) stereoisomer.

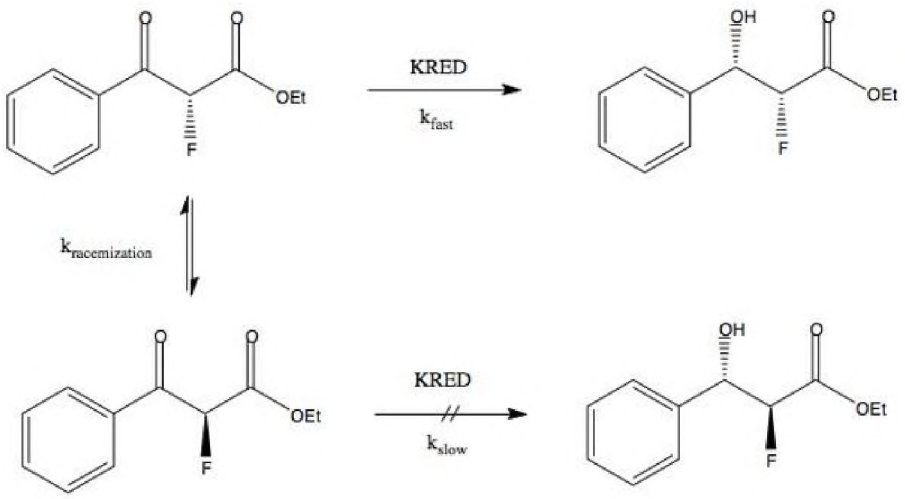

Figure 1.28. The process by which both stereocenters of the α-fluoro-β-hydroxy ester product are set in the KRED reactions, termed DYRKR, occurs because α-fluoro-β-keto ester reactant can tautomerize to form its corresponding enol. Through this interconversion the keto ester racemizes. A given stereoisomer of the α-fluoro-β-hydroxy ester product is produced when the rate of racemization exceeds the rate of reduction of the less reactive keto ester enantiomer.

It is our hypothesis that using KRED enzymes will prove to be a useful method for accessing optically pure α-fluoro-β-hydroxy esters. Accessing this moiety by using KREDs is interesting in that, through the mechanism of DYRKR, the stereochemistry can be manipulated

at both the α and β carbon atoms in the same reaction. The two enzymes selected for study in this research were found to produce opposite diastereomers with high diastereomeric excess. Using Mosher Ester analysis, the absolute stereochemistry of the enzyme products can be assigned. Ideally the KREDs will yield products with high enantiospecificity. If so, these reactions could be applied toward the synthesis of optically pure α amino acids and other medicinally relevant structures [61-63].

Chapter 2. Results & Discussion

2.1. Reformatsky Reaction

The aim of this research was to assess the use of ketoreductase enzymes in the synthesis of enantiopure α-fluoro-β-hydroxy esters. This entailed synthesizing a variety of racemic α-fluoro-β-hydroxy ester derivatives, oxidizing them to their corresponding α-fluoro-β-keto esters, stereoselectively reducing them back to α-fluoro-β-hydroxy esters via ketoreductase enzymes, and using Mosher ester analysis to determine the stereospecificity of the enzymes. The overall reaction scheme is shown in the introduction section in Figure 1.26.

In order to synthesize the enantiopure α-fluoro-β-hydroxy esters, we first synthesized the racemic versions of these compounds. Three different benzaldehydes were selected as precursors in this study: benzaldehyde (1a), 4-methoxybenzaldehyde (1b), and 4-(trifluoromethyl)benzaldehyde (1c) (Figure 2.1). These precursors were chosen to broaden the scope of the reaction. They are all aromatic and similar in size but two of them have functional groups with distinctly different properties with $-OCH_3$ being an electron donating group and $-CF_3$ being an electron withdrawing group. Additionally, the highly fluorinated $-CF_3$ functional group is particularly relevant to drug design as discussed in the introduction.

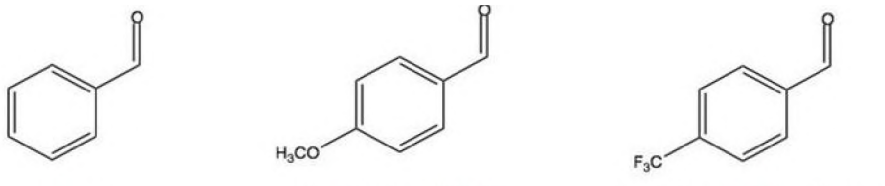

Figure 2.1. Structures of starting materials used in study.

These compounds were converted to their corresponding α-fluoro-β-hydroxy esters via Reformatsky reactions between bromofluoroethylacetate and the respective benzaldehydes. The general outline for this first reaction is shown in Figure 2.2.

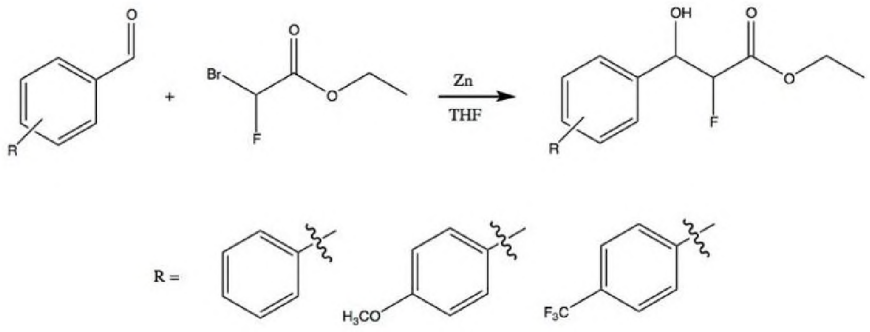

Figure 2.2. General Reformatsky reaction scheme.

The Reformatsky reaction, first reported in the late 1800s, involves the condensation of aldehydes or ketones with α-halo esters to yield β-hydroxy esters using metallic zinc [84]. The mechanism for the generalized reaction is shown in Figure 2.3.

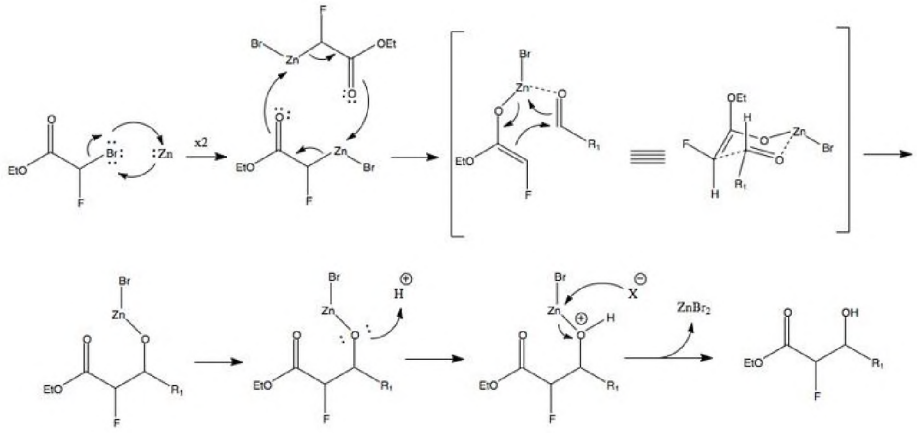

Figure 2.3. General Reformatsky reaction mechanism.

Here, a zinc atom is inserted into the carbon-halogen bond of the α-haloester via oxidative addition. The reaction between two organozinc molecules results in the formation of two zinc enolates. Coordination between the aldehyde/ketone oxygen atom and zinc forms a six

membered transition state, which rearranges causing zinc to attach to the oxygen atom and a new carbon-carbon bond to form. Protonation during acidic workup removes zinc, forming zinc(II) salts and the resulting β-hydroxy ester [85].

The Reformatsky reactions employed here were conducted via one of two possible methods. The first method was under the traditional Reformatsky conditions which involved refluxing the aldehyde, the acetate, and activated zinc in THF [86]. The other method performed was a newer approach in which the same reagents (without any solvent) and solid ammonium chloride were mixed and microwaved in a conventional microwave oven for several minutes [87]. The reaction was then treated with a solution of saturated ammonium chloride and the product extracted with ether. The microwave reaction was generally favored due to the speed of the reaction where a product could be isolated in under an hour as opposed the standard reflux reaction which took numerous hours to complete. While the microwave reactions afforded good yields (excess of 80%) they were limited in scale. Reactions involving more than a couple grams of reagent resulted in messy workups and low yields - likely due to the amount of metallic zinc, which when microwaved caused excess arcing and degradation of the reaction materials.

Both reaction methods produced the racemic α-fluoro-β-hydroxy esters shown in Figure 2.4. The α-fluoro-β-hydroxy ester products contain two stereocenters which allows for four possible stereoisomers. The racemic products comprise a mixture of the *syn* (both fluorine and hydroxyl groups are on the same face of the molecule) and *anti* (fluorine and hydroxyl groups are on opposite faces of the molecule) diastereomers in roughly equal amounts and for each compound, all four stereoisomers are present as evidenced by Mosher ester analysis which is discussed later in the chapter. Figure 2.5 shows the structures of the four possible stereoisomers for a generalized substituted aromatic α-fluoro-β-hydroxy ester.

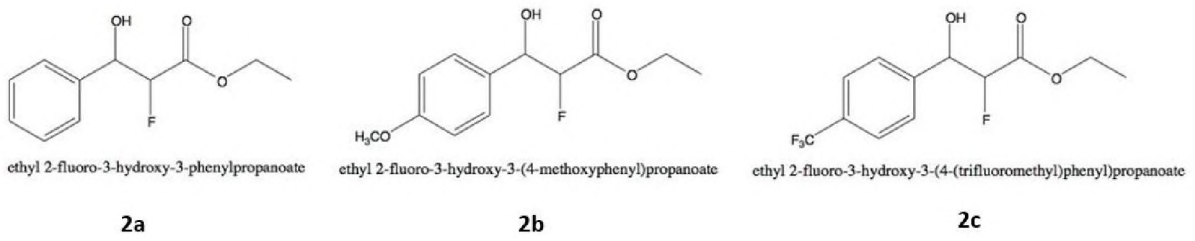

Figure 2.4. Racemic α-fluoro-β-hydroxy ester products of Reformatsky reaction.

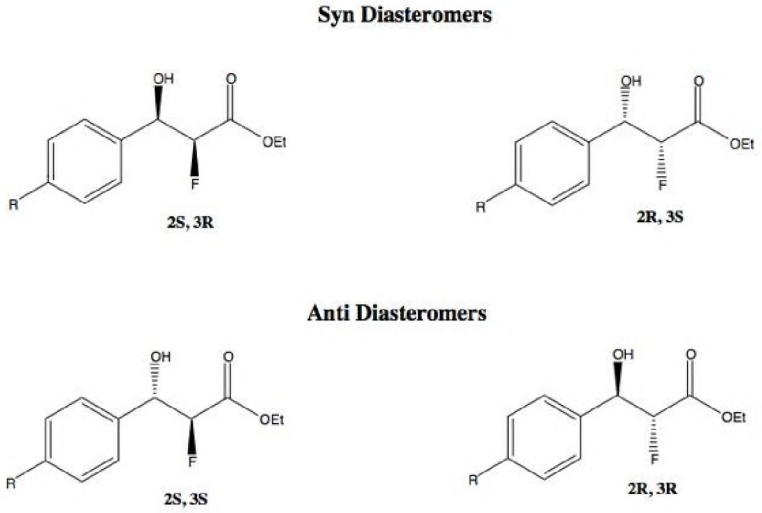

Figure 2.5. The four possible stereoisomers of a generalized α-fluoro-β-hydroxy ester. The racemic product contains a roughly equal mixture of *syn* and *anti* diastereomers. Within each pair of diastereomers, both enantiomers are present.

^{1}H NMR spectra for the Reformatsky products are shown in the Appendix in Figures A.1 - A.3, ^{19}F NMR spectra in Figures A.4 - A.6, and ^{13}C NMR spectra in Figures A.7 - A.9.

2.2. Dess Martin Periodinane Oxidation

The goal of this project was to produce not racemic, but enantio- and diastereomerically pure α-fluoro-β-hydroxy esters. This was ultimately accomplished via enzyme reductions which required that the racemic α-fluoro-β-hydroxy esters be first oxidized to their corresponding α-fluoro-β-keto esters. This was achieved via Dess-Martin periodinane (DMP) oxidation. The general reaction scheme is shown in Figure 2.6.

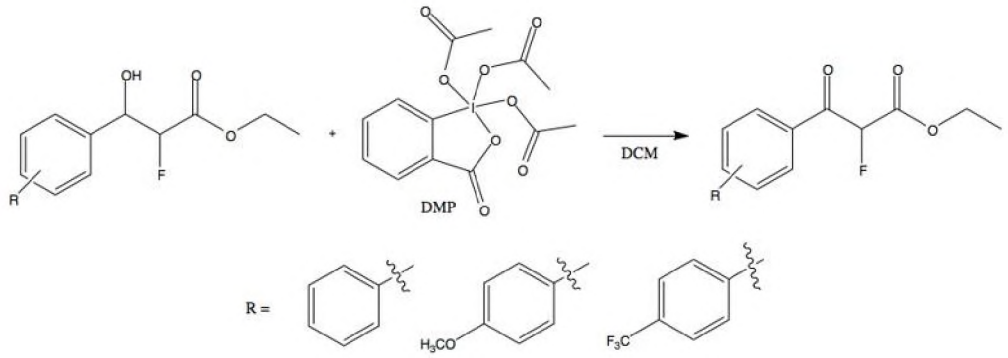

Figure 2.6. DMP oxidation reaction scheme.

This reaction, developed by Daniel Benjamin Dess and James Cullen Martin in 1983 [88], has some advantages over other oxidative methods including milder conditions (the reaction is conducted at room temperature and at neutral pH), simple workup, and high chemo selectivity allowing for oxidation of alcohols to aldehydes or ketones without affecting other functional groups. The reagent is also stable with a long shelf life making it widely available and easy to store [88, 89]. The general mechanism for the oxidation of a secondary alcohol to a ketone with DMP is shown in Figure 2.7 which illustrates that the alcohol displaces the acetate from iodine to form the periodinane ester intermediate followed by proton abstraction from the acetate anion and rearrangement to yield ketone.

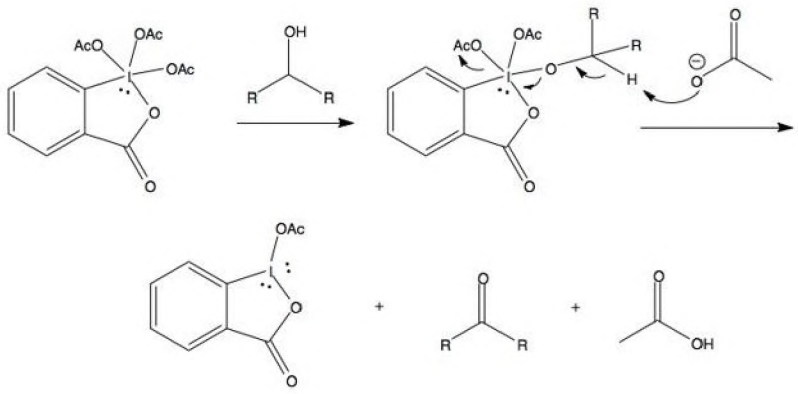

Figure 2.7. Mechanism of DMP oxidation of a secondary alcohol.

A typical reaction procedure consisted of stirring the racemic α-fluoro-β-hydroxy ester with DMP in dichloromethane (DCM) for 24 hours at room temperature. Yields were generally in excess of 80%. Structures of the resulting α-fluoro-β-keto esters are shown in Figure 2.8.

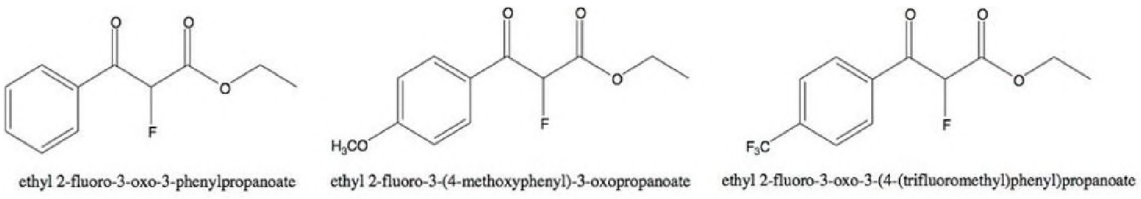

Figure 2.8. α-fluoro-β-keto ester products of DMP reactions.

^{1}H NMR spectra for the α-fluoro-β-keto esters are shown in Figures A.10 - A.12, ^{19}F NMR spectra in Figures A.13-A.15, and ^{13}C NMR spectra in Figures A.16-A.18.

2.3. Ketoreductase Enzyme Reactions

The α-fluoro-β-keto esters were then reduced back to α-fluoro-β-hydroxy esters stereoselectively via the use of ketoreductase enzymes. A variety of ketoreductase enzymes, consisting of 5 wild type and 19 genetically engineered variants, acquired from Codexis®, were previously evaluated for stereoselectivity on (non-fluorinated) β-keto esters [82]. The majority of the enzymes used an NADPH recycling system, while others instead used an NADH recycling system. The general reaction is shown in Figure 2.9. The mechanism by which the KRED enzymes reduce the β-keto esters stereoselectively, termed dynamic reductive kinetic resolution (DYRKR) was discussed in further detail in the introductions section. To summarize, the β-keto ester, due to its acidic α hydrogen atom, interconverts between its keto and enol forms. A given enantiomer of the α-fluoro-β-keto ester is preferentially reduced when the rate of racemization exceeds the rate of reduction of the less reactive enantiomer. If the reductant, either NADPH or NADH, attacks preferentially on one side of the pro-chiral face of the more reactive enantiomer

(due to the position of the substrate and cofactor in the active site of the KRED enzyme), then a single stereoisomer of four is possible [83].

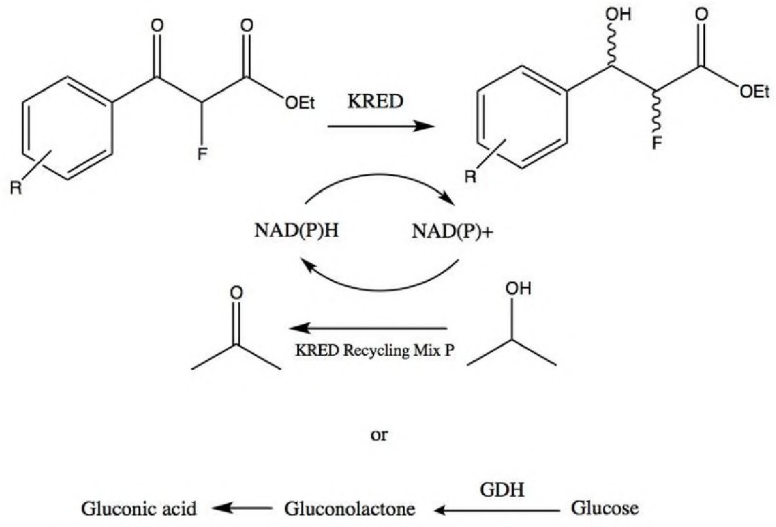

Figure 2.9. General KRED mechanism.

Based on the previously mentioned study by Green et al., several enzymes that gave high enantiomeric excess were selected for use in this study [82]. The enzymes selected were KRED 130 and KRED 110, both wild type variants which gave over 99% enantiomeric excess and a high rate of conversion of β-keto esters to β-keto alcohols [82].

Typical conditions for the KRED reactions consisted of 25 µmol of the β-keto ester to 1 mg of KRED enzyme. The β-keto ester was dissolved in methanol to which was added the ketoreductase and KRED Recycle Mix N dissolved in deionized water. KRED Recycle Mix N, a component of the Codexis® KRED screening kit, contains the nicotinamide cofactor (NADH or NADPH), which is used as the hydride source, as well as glucose and glucose dehydrogenase (GDH). Glucose is used as a reductant to convert the oxidized cofactor back to its reduced form, a reaction that is catalyzed by GDH. Typical reaction conditions consisted of 57.4 mg of KRED Recycle Mix N per 25 µmol of the β-keto ester. KRED Recycle Mix N is comprised of

magnesium sulfate (1.6 mM), $NADP^+$ (1.0 mM), NAD^+ (1.0 mM), D-glucose (76 mM), GDH (4.1 units/mL), and sodium phosphate (250 mM).

2.4. Diastereomer Assignment

Figures 2.10 - 2.12 show ^{19}F NMR spectra overlays of the racemic α-fluoro-β-hydroxy esters (2d, 2e, and 2f) and the enzyme products 4a (KRED 110), 4a (KRED 130), 4b (KRED 110), 4b (KRED 130), 4c (KRED 110), and 4c (KRED 130). By integrating the resonances in the ^{19}F NMR spectra, the diastereomeric excess of the enzyme products was determined. For all the substrates, KRED 110 gave a product with >99% diastereomeric excess, always yielding the diastereomer corresponding to the more downfield (left most) resonance. KRED 130 gave products with a lower degree of diastereomeric excess (though still relatively high, between 85 and >99%). The dominant diastereomer produced from reactions with KRED 130 was always the one corresponding to the more upfield (right most) resonance - opposite of that produced by KRED 110.

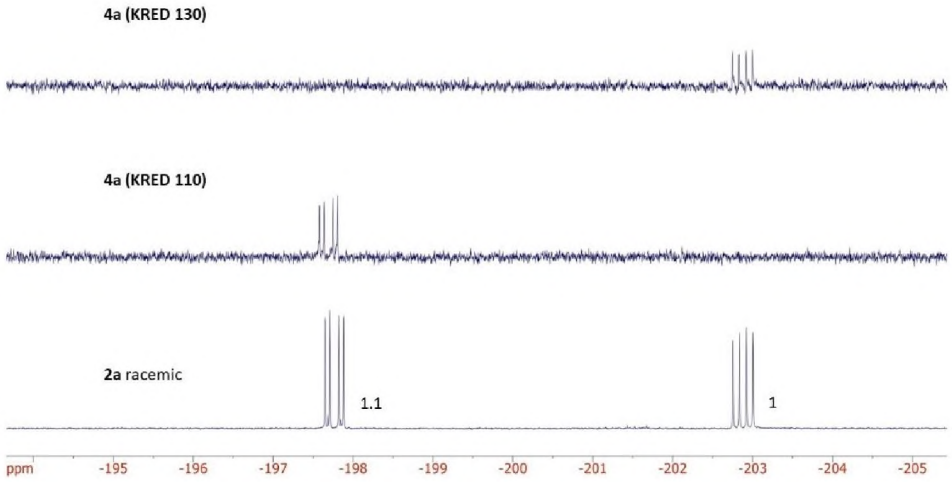

Figure 2.10. Overlay of ^{19}F NMR spectra comparing the racemic phenyl α-fluoro-β-hydroxy ester, 2a (bottom), 4a (KRED 110) (middle), and 4a (KRED 130) (top). Integral values are shown to the right of each set of peaks in the racemic compound. The reduction of 3a with KREDs 110 and 130 each gave >99% diastereomeric excess but the two enzymes yielded different diastereomers.

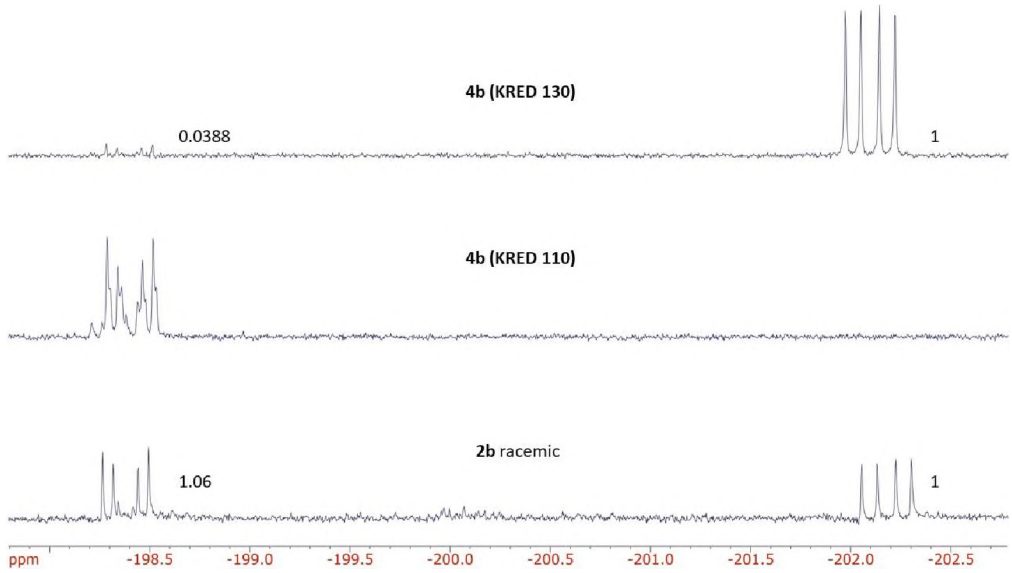

Figure 2.11. Overlay of ^{19}F NMR spectra comparing the racemic 4-methoxy α-fluoro-β-hydroxy ester, 2b, (bottom), 4b (KRED 110) (middle) and 4b (KRED 130) (top). Integral values shown to the right of each set of peaks. KRED 110 yielded a single diastereomer while 130 yielded both diastereomers with a diastereomeric excess of 96%.

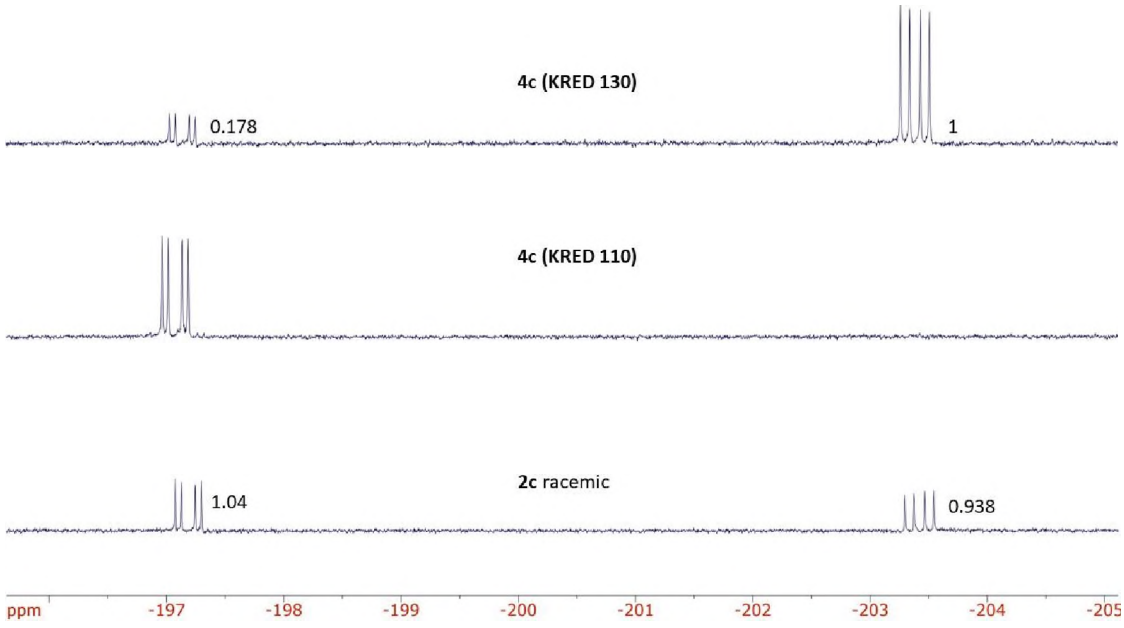

Figure 2.12. Overlay of ^{19}F NMR spectra comparing the racemic 4-trifluoromethyl α-fluoro-β-hydroxy ester, 2c (bottom), 4c (KRED 110) (middle), and 4c (KRED 130) (top). Integral values shown to the right of each set of peaks. KRED 110 yielded a single diastereomer while 130 yielded both diastereomers with a diastereomeric excess of 85%.

In order to determine which diastereomer (*syn* or *anti*) the enzymes produced, an analysis of coupling constants was required. In a study that looked at a different method for the

diastereoselective synthesis of α-fluoro-β-hydroxy esters, Mima et al. synthesized ethyl 2-fluoro-3-hydroxy-3-phenylpropanoate (2a). In order to determine the specific stereochemistry, they reduced the ester with lithium aluminum deuteride and reacted the resulting diol with 2,2-dimethoxypropane in the presence of a catalytic amount of para toluene sulfonic acid which yielded a diastereomeric mixture of the corresponding acetonide (Figure 2.13) [90].

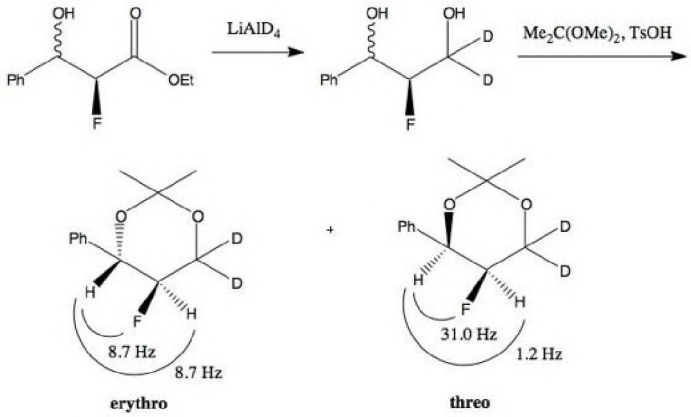

Figure 2.13. Method for the stereochemical assignment of 2a by Mima et al [90].

Through the restriction of free rotation in the acetonide derivative, they were able to assign stereochemistry of the parent compound through coupling constant measurements. In the *anti* diastereomer, the 3 bond F-H, $^{3}J_{FH}$, coupling should have a smaller hertz value than in the *syn* diastereomer since the dihedral angle between F and H is smaller [91]. They measured a $^{3}J_{FH}$ of 8.7Hz for one of the acetonide isomers and a $^{3}J_{FH}$ of 31.0 Hz for the other. They then extrapolated to assign the stereochemistry of the parent α-fluoro-β-hydroxy ester (2a). For the more downfield resonance occurring at about -198 ppm, Mima et al. measured a $^{3}J_{FH}$ of 16.89 Hz corresponding to the *anti* diastereomer and for the upfield resonance occurring at about -203 ppm they measured a $^{3}J_{FH}$ of 22.40 Hz corresponding to the *syn* diastereomer [90].

The ^{19}F NMR spectrum of the racemic phenyl α-fluoro-β-hydroxy ester (2a) that was synthesized via the Reformatsky reaction is shown again in Figure 2.14 along with the

experimentally measured coupling constants. The measured coupling constants were $^{3}J_{FH}$ = 16.98 Hz and $^{1}J_{FH}$ = 47.73 for the more downfield resonance (*anti*) and $^{3}J_{FH}$ = 22.60 Hz and $^{1}J_{FH}$ = 47.96 Hz for the more upfield resonance (*syn*), which closely matched the results of Mima et al [90]. Similarly for the other derivatives, the more downfield resonance in the ^{19}F NMR spectrum always corresponded to that with the smaller $^{3}J_{FH}$ coupling constant.

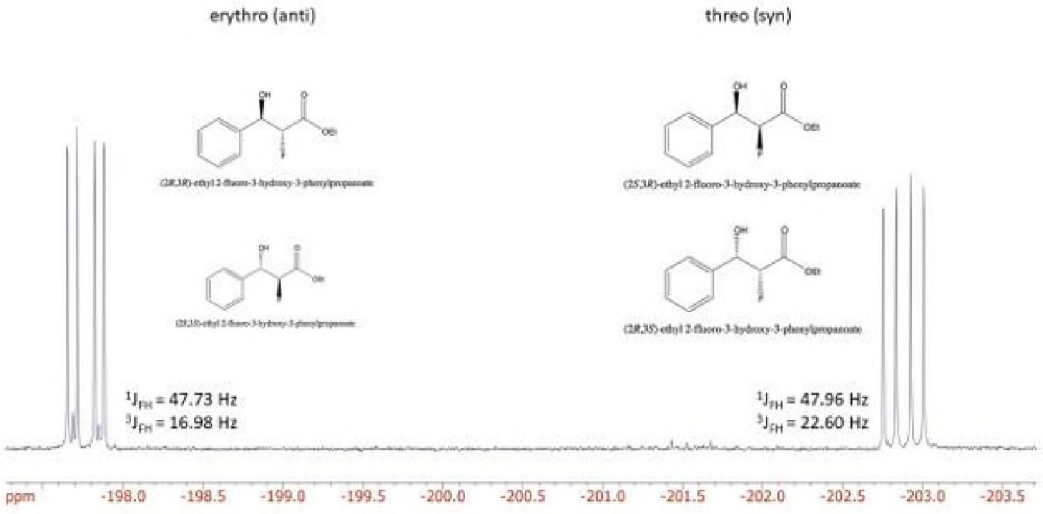

Figure 2.14. ^{19}F NMR spectrum of the racemic phenyl α-fluoro-β-hydroxy ester, 2a. Experimentally determined coupling constants are shown next to each resonance. The more downfield resonance (leftmost) corresponds to the *anti* diastereomer while the more upfield (rightmost) resonance corresponds to the *syn* diastereomer. This pattern is consistent for the other α-fluoro-β-hydroxy ester derivatives (the 4-methoxy and 4-trifluoromethyl compounds).

Having determined that for the racemic α-fluoro-β-hydroxy esters, the *anti* diastereomer resonance in the ^{19}F NMR spectrum is downfield to that of the *syn* diastereomer resonance, the diastereomeric excess of the KRED enzyme products could be measured and structural assignments made through integration of NMR resonances. These assignments are shown in Figure 2.15 for the phenyl, 4-methoxy, and 4-trifluoromethyl derivatives respectively. For the compounds reported here, KRED 110 consistency yielded >99% *anti* diastereomer and KRED 130 yielded a high excess, although not always 100% of the *syn* diastereomer. For the phenyl

derivative KRED 130 gave >99% *syn* diastereomer, but for the 4-methoxy and 4-trifluoromethyl derivatives KRED 130 gave 96.3% and 84.9% *syn* diastereomer respectively.

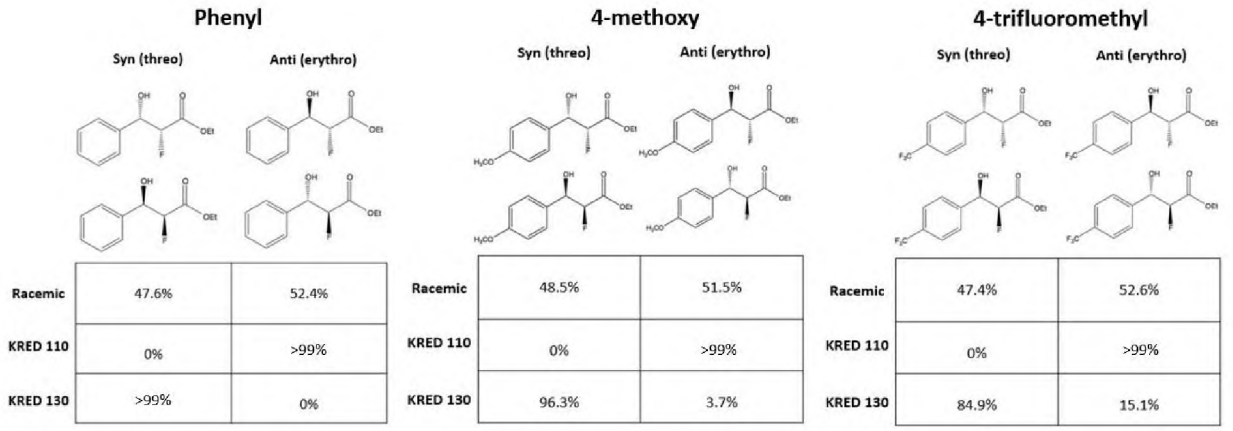

Racemic	47.6%	52.4%
KRED 110	0%	>99%
KRED 130	>99%	0%

Racemic	48.5%	51.5%
KRED 110	0%	>99%
KRED 130	96.3%	3.7%

Racemic	47.4%	52.6%
KRED 110	0%	>99%
KRED 130	84.9%	15.1%

Figure 2.15. Diastereomeric excess of the three derivatives as a racemic product of Reformatsky reaction and as a product from the reduction with KREDs 110 and 130. KRED 110 yielded the *anti* diastereomer with >99% excess and KRED 130 predominantly yielded the *syn* diastereomer with an excess ranging between 84.9% and >99%. Diastereomeric excess was determined by integrating the two resonances in the ^{19}F NMR spectra.

Individual NMR spectra (^{19}F and ^{1}H) for the enzyme products are shown in the Appendix in Figures A.19 - A.24. The absolute stereochemistry (*R* and *S* configuration) of these products could not be determined from their NMR spectra alone but were determined later via Mosher ester NMR analysis which is discussed in the next section.

2.5. Mosher Ester Analysis and Absolute Stereochemistry Assignment

Unlike diastereomers, enantiomers cannot be directly distinguished via NMR spectroscopy because two given enantiomers will have identical resonances. To determine the enantiomeric excess and absolute stereochemistry of the enzyme products, Mosher ester analysis was employed. Mosher ester analysis is a commonly used NMR based procedure for determining the absolute configuration of a non-racemic sample of a chiral molecule. Dale and Mosher first reported the method in 1973 in regard to their work on determining absolute configuration of the stereogenic carbon in secondary alcohols [92]. The method involves the derivatization of the

compound (usually an alcohol) with unknown stereochemistry with both the (*R*) and (*S*) isomers of α-methoxy-α-trifluoromethylphenylacetic acid (MTPA) also known as Mosher's acid. In two analogous but separate reactions, the hydroxyl group of the alcohol is coupled to the carboxylic acid of both the (*R*) and (*S*) isomers of MTPA in an acylation reaction forming the corresponding (*R*) and (*S*) Mosher esters (Figure 2.16) [93].

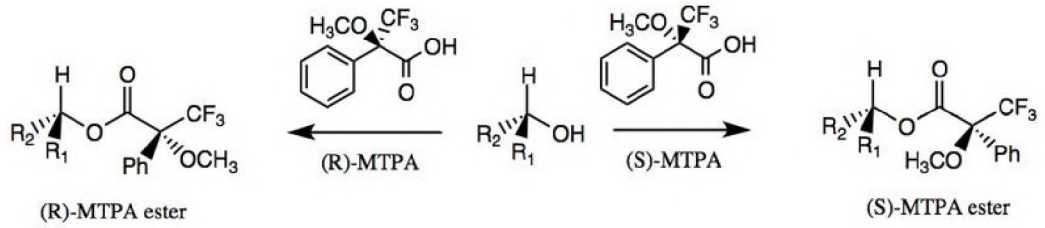

Figure 2.16. Schematic showing the generalized reaction used in Mosher ester analysis. The alcohol with unknown stereochemistry is reacted with both the (*R*)- and (*S*)-isomers of MTPA in two separate reactions resulting in both the (*R*)- and (*S*)-MTPA esters which are then analyzed with NMR spectroscopy [93].

The acid chloride of Mosher's acid is often used directly as an acylating agent, but another route uses Mosher's acid and N,N′-Dicyclohexylcarbodiimide (DCC) or another carboxylic activating agent [93].

The method employed here conducted the derivatization reaction in an NMR tube - a so called "in-tube" reaction based on the previously reported protocol by Gao et al [94]. Here the alcohol, Mosher's acid (either the *R* or *S* isomer), 4-Dimethylaminopyridine (DMAP), and DCC were dissolved in $CDCl_3$ and transferred to an NMR tube, to which was added a small amount of 3Å molecular sieves and allowed to react overnight at 37 °C (Figure 2.17). By conducting two reactions with the (*R*) and (*S*) isomers of MTPA both the (*R*) and (*S*) isomers of the resulting Mosher ester are formed.

The basis of Mosher ester analysis relies on the fact the dominant conformation of the Mosher ester is the *s-trans* arrangement about the O-CO bond with the trifluoromethyl (CF_3)

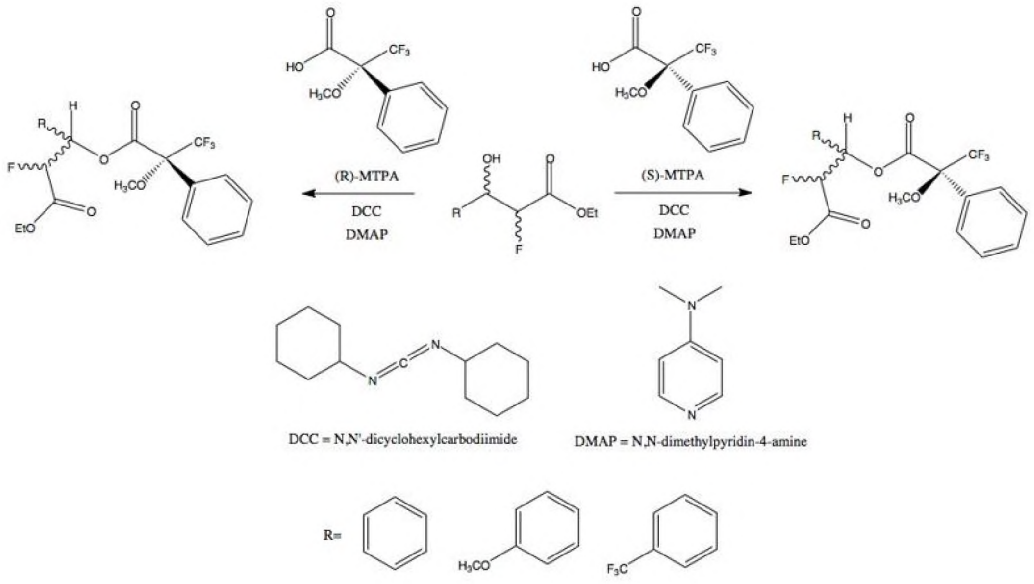

Figure 2.17. More detailed reaction scheme for the Mosher esterification reactions of the α-fluoro-β-hydroxy esters examined in this study. Absolute stereochemistry of Mosher ester products depends on the absolute stereochemistry of the parent α-fluoro-β-hydroxy ester which is what this study aims to determine.

group of the MTPA moiety and the methine proton of the secondary alcohol moiety *syn*-coplanar with the carbonyl group [93]. This results in one of the substituent R groups of the secondary alcohol moiety being in the shielding region of the phenyl group in the MTPA moiety. Figure 2.18 shows a general representation of this effect. In the case of derivatization with *S*-MTPA, R_2 of the secondary alcohol is in the shielding region of the phenyl group. In the case of derivatization with *R*-MTPA, R_1 of the secondary alcohol is in the shielding region of the phenyl group. Because of the shielding effect, the NMR resonance of the atoms in the shielding region will occur upfield relative to the same atoms that are not in the shielding region allowing for the deduction of the absolute stereochemistry of the secondary alcohol [95].

The ^{19}F NMR spectra for the Mosher ester products of the phenyl derivative are shown in Figures A.26 - A.30, the ^{19}F NMR spectra for Mosher ester products of the 4-methoxy derivative

are shown in Figures A.31 - A.35, and the ^{19}F NMR spectra for Mosher ester products of the 4-trifluoromethyl derivative are shown in Figures A.36 - A.40.

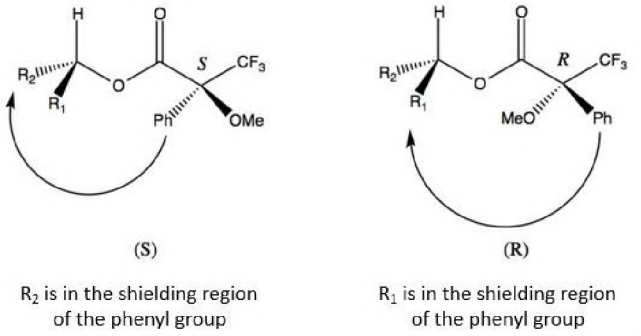

Figure 2.18. Here, the shielding effect of the phenyl group is represented by the curved arrow. In the case of the (*S*)-MTPA ester, R_2 is in the shielding region of the phenyl group and in the case of the (*R*)-MTPA ester, R_1 is in the shielding region of the phenyl group. This is the case because the most important conformation of the Mosher ester is an s-trans arrangement about the O-CO bond with the CF_3 group, methine proton, and carbonyl in the same plane [93].

When the racemic α-fluoro-β-hydroxy esters are esterified with MTPA, four distinct (although sometimes overlapping) resonances are visible in each of their ^{19}F NMR spectra, each corresponding to one of the four possible stereoisomers for that derivative. The structures of the possible isomers of the parent phenyl α-fluoro-β-hydroxy ester derivative and their IUAPC names are shown in Figure 2.19 as well as for the 4-methoxy and 4-trifluoromethyl derivatives in Figure 2.20 and Figure 2.21 respectively.

Figures 2.22 - 2.24 show a condensed representation of the ^{19}F NMR spectra for each derivative's Mosher ester using overlays. For convenience, these figures will be referred to when referencing the Mosher ester product spectra. A detailed examination of the ^{19}F NMR spectra of the Mosher ester products of the phenyl derivative will serve as an example of how absolute stereochemistry was assigned for the enzyme products of all the derivatives.

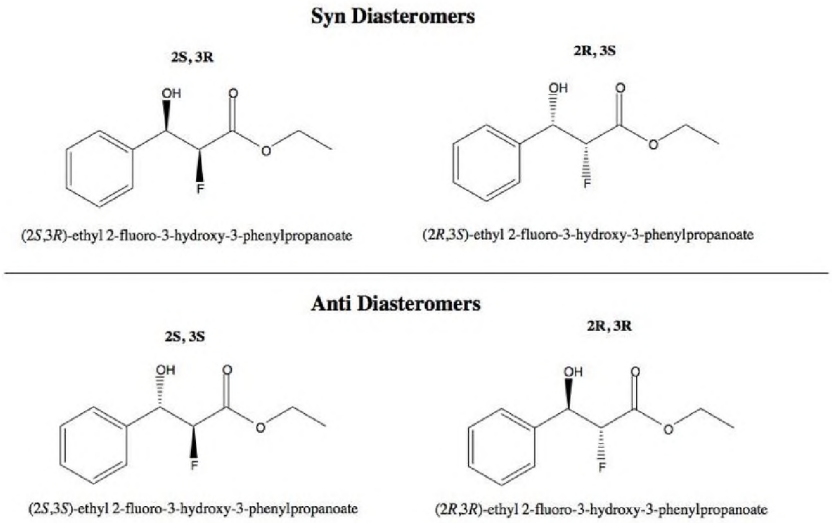

Figure 2.19. Structures and names of the four possible stereoisomers (two possible diastereomers each with two possible enantiomers) of the phenyl α-fluoro-β-hydroxy ester derivative. In this case, KRED 110 produces >99% of the *anti* diastereomer, so the KRED 110 reduction product may consist of the (2S, 3S) and/or (2R, 3R) isomers. KRED 130 gave >99% of the *syn* diastereomer so the KRED 130 product may consist of the (2S, 3R) and/or the (2R,3S) isomer.

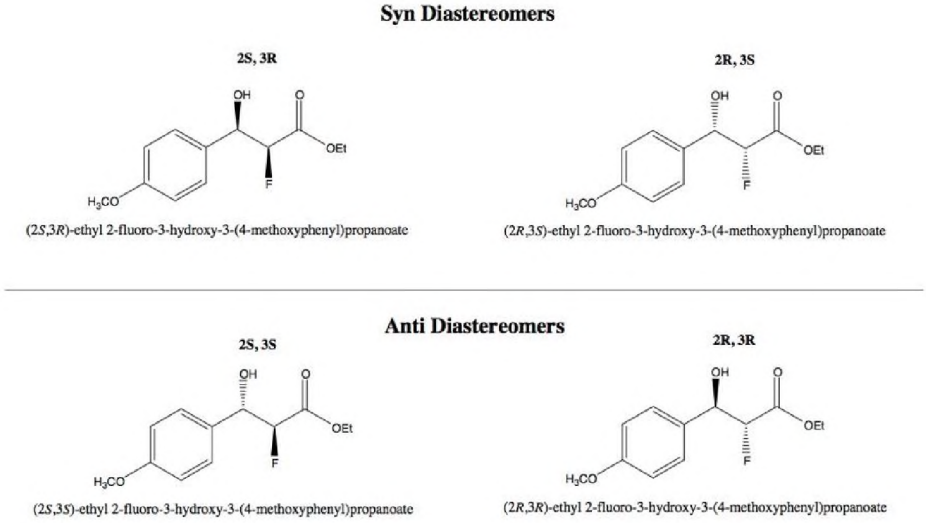

Figure 2.20. Structures and names of the four possible stereoisomers (two possible diastereomers each with two possible enantiomers) of the 4-methoxy α-fluoro-β-hydroxy ester derivative. In this case, KRED 110 produces >99% of the *anti* diastereomer, so the KRED 110 reduction product may consist of the (2S, 3S) and/or (2R, 3R) isomers. KRED 130 gave 96.3% of the *syn* diastereomer with 3.7% *anti* diastereomer. So, the KRED 130 product will consist of predominantly the (2S, 3R) and/or the (2R,3S) isomers with much smaller amounts of the (2S,3S) and/or the (2R,3R) isomers.

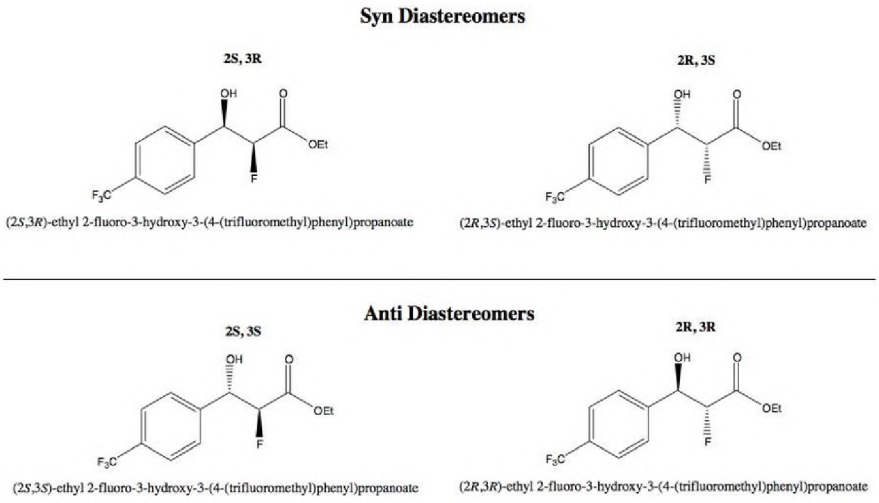

Figure 2.21. Structures and names of the four possible stereoisomers (two possible diastereomers each with two possible enantiomers) of the 4-trifluoromethyl α-fluoro-β-hydroxy ester derivative. In this case, KRED 110 produces 100% of the *anti* diastereomer, so the KRED 110 reduction product may consist of the (2S, 3S) and/or (2R, 3R) isomers. KRED 130 gave 84.9% of the *syn* diastereomer and 15.1% of the *anti* diastereomer. So, the KRED 130 product may consist of predominantly the (2S, 3R) and/or the (2R,3S) isomer with smaller amounts of the (2S,3S) and/or (2R,3R) isomers.

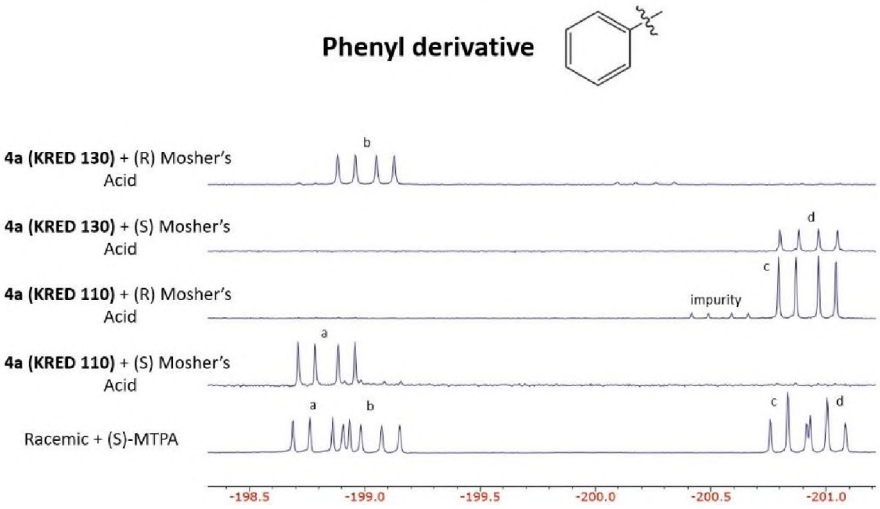

Figure 2.22. Overlay of the ^{19}F NMR spectra of phenyl derivative Mosher ester products. From bottom to top: racemic compound + (*S*)-MTPA, KRED 110 product + (*S*)-MTPA, KRED 110 product + (*R*)-MTPA, KRED 130 product + (*S*)-MTPA, and KRED 130 product + (*R*)-MTPA. The bottom most, racemic overlay contains the resonances of the four possible stereoisomers identified with arbitrary letters (a, b, c, d). The corresponding resonances in the Mosher esters of the enzyme products are identified with matching letters.

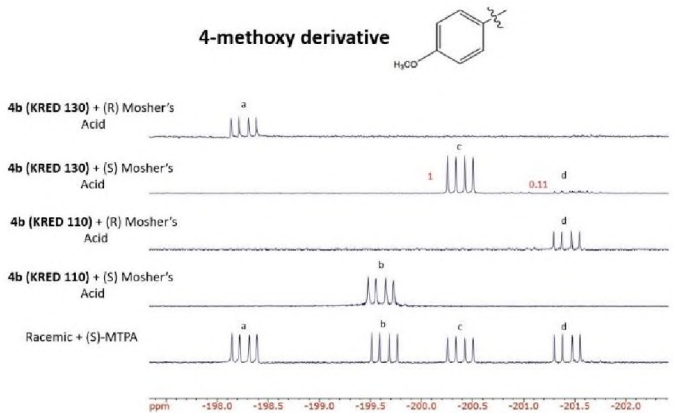

Figure 2.23. Overlay of the ^{19}F NMR spectra of 4-methoxy derivative Mosher ester products. From bottom to top: racemic compound + (*S*)-MTPA, KRED 110 product + (*S*)-MTPA, KRED 110 product + (*R*)-MTPA, KRED 130 product + (*S*)-MTPA, and KRED 130 product + (*R*)-MTPA. The bottom most, racemic overlay contains the resonances of the four possible stereoisomers identified with arbitrary letters (a, b, c, d). The corresponding resonances in the Mosher esters of the enzyme products are identified with matching letters. The KRED 130 product + (*S*)-MTPA spectrum shows two resonances. Integral values for each resonance is shown to the left of each resonance in red.

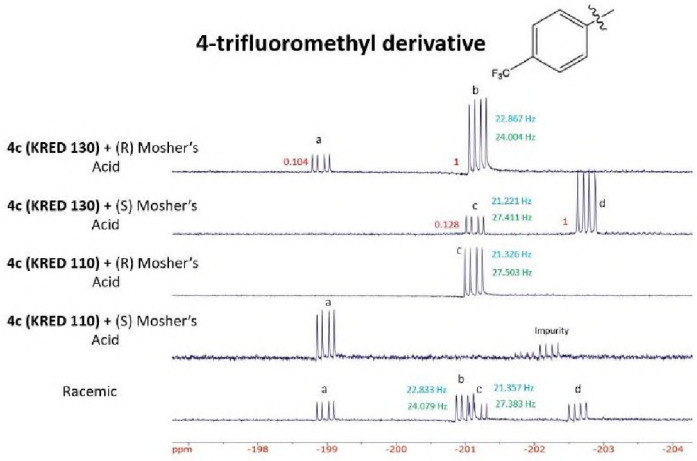

Figure 2.24. Overlay of the ^{19}F NMR spectra of 4-trifluoromethyl derivative Mosher ester products. From bottom to top: racemic compound + (*S*)-MTPA, KRED 110 product + (*S*)-MTPA, KRED 110 product + (*R*)-MTPA, KRED 130 product + (*S*)-MTPA, and KRED 130 product + (*R*)-MTPA. The bottom most, racemic overlay contains the resonances of the four possible stereoisomers identified with arbitrary letters (a, b, c, d). The corresponding resonances in the Mosher esters of the enzyme products are identified with matching letters. For the KRED 130 spectra which contain more than one resonance, integral values of each resonance are shown to the left of each resonance in red. Additionally because of the overlap in chemical shift observed for resonances b and c, coupling constants are shown next to each resonance. The separation between peaks 1 and 2 (reading the 4 peaks from left to right) are shown in blue. The separation between peaks 2 and 3 are shown in green. These values were used to help label the peaks in the Mosher ester spectra.

The ^{19}F NMR spectra of the Mosher ester of 4a (KRED 110) (overlays 2 and 3 counting from the bottom in Figure 2.22) shows a single resonance indicating that only a single enantiomer is present in the product. That resonance is more downfield when 4a (KRED 110) is esterified with (*S*)-MTPA and more upfield when 4a (KRED 110) is esterified with (*R*)-MTPA. Figure 2.25 shows a diagram of the structures of the possible Mosher esters produced from 4a (KRED 110).

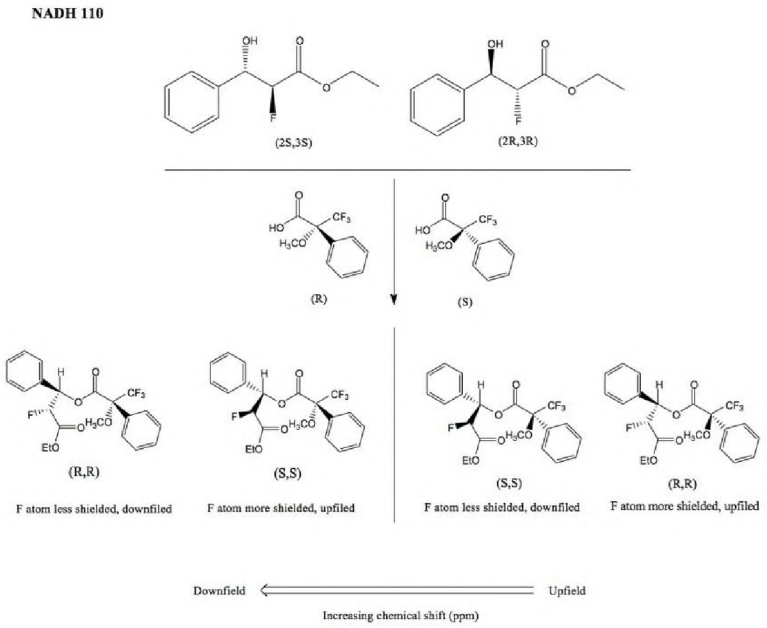

Figure 2.25. Possible stereoisomers produced via Mosher esterification of 4a (KRED 110). Knowing that KRED 110 produced the *anti* diastereomer with >99% diastereomeric excess, two stereoisomers are possible. In the case of esterification with (*R*)-MTPA, Mosher ester analysis using ^{19}F NMR would predict that the (*R*,*R*) isomer's resonance would occur more downfield because in this case the fluorine atom of the α-fluoro-β-hydroxy ester moiety is *anti* to, and therefore less shielded by, the phenyl group of the (*R*)-MTPA moiety. When the (*S*,*S*) α-fluoro-β-hydroxy ester is esterified with (*R*)-MTPA the opposite would be expected. In this case the fluorine atom of the α-fluoro-β-hydroxy ester moiety is *syn* to the phenyl moiety of (*R*)-MTPA, and therefore more shielded by it. The resonance in this case would be expected to occur more upfield in the ^{19}F NMR spectrum relative to that of the (*R*,*R*) Mosher ester. The opposite effect would be expected to occur when each α-fluoro-β-hydroxy esters, the (*S*,*S*) and (*R*,*R*) isomers, are esterified with (*S*)-MTPA. In the case of the (*S*,*S*) α-fluoro-β-hydroxy ester the fluorine atom is *anti* to the phenyl group and therefore less shielded and its resonance would be expected to occur more downfield relative to that of the (*R*,*R*) isomer.

Because it was previously determined that when the phenyl derivative 3a is reduced with KRED 110 the *anti* diastereomer is produced with >99% diastereomeric excess, there can be two possible enantiomers. The single resonance in the ^{19}F NMR spectrum of the Mosher ester product indicates that only one of the two possible enantiomers is present in 4a (KRED 110). Which enantiomer was present in 4a (KRED 110) was determined by comparing the relative positions of the (*R*)- and (*S*)- Mosher ester product resonances.

When 4a (KRED 110) was esterified with (*R*)-MTPA, resonance C (as indicated in Figure 2.22) was observed. When 4a (KRED 110) was esterified with (*S*)-MTPA, resonance A was observed. Because KRED 110 produces only the *anti* diastereomer, in this case, resonances A and C represent the one of the two possible *anti*-enantiomers of the parent α-fluoro-β-hydroxy ester - the (2*S*, 3*S*) or (2*R*,3*R*)-isomers (Figure 2.19).

Which resonance corresponds to which specific enantiomer was determined by the relative positions of the resonances. Depending on which enantiomer of MTPA is used, the resonance of the resulting Mosher ester will be either downfield or upfield relative to one another based on whether the fluorine atom of the α-fluoro-β-hydroxy ester moiety is or isn't in the shielding region of the MTPA phenyl moiety.

For example, as depicted in Figure 2.25, if 4a (KRED 110) consists solely of the (2*S*,3*S*) enantiomer then the resonance of the resulting Mosher ester product when esterified with (*R*)-MTPA will occur more upfield relative to the resonance of the Mosher ester resulting from esterification with (*S*)-MTPA which will occur more downfield. In the case of esterification of the (2*S*,3*S*) enantiomer with (*R*)-MTPA, the fluorine atom and phenyl group are more *syn* to each other, with the fluorine atom more within the shielding region of the phenyl group. On the other hand, when the (2*S*,3*S*) enantiomer is esterified with (*S*)-MTPA, the fluorine atom and phenyl

group are more *anti* to each other with the fluorine atom more outside the shielding region of the phenyl group. As such, the resonance of the former (*R*)- Mosher ester would occur more upfield relative to the latter (*S*)-Mosher ester.

Looking back at the spectra of the Mosher ester products of 4a (KRED 110) (Figure 2.22), we see that resonance A (observed when 4a (KRED 110) is esterified with (*S*)-MTPA) is more downfield relative to resonance C (observed when 4a (KRED 110) is esterified with (*R*)-MTPA). Again, looking at the Mosher ester stereoisomer possibility diagram in Figure 2.25 we see that when the possible *anti* enantiomers, (2*S*,3*S*) and (2*R*,3*R*), are esterified with (*S*)-MTPA, we should expect the (2*S*,3*S*) resonance to be more downfield relative to that of the (2*R*,3*R*) isomer. Similarly, when the two *anti* enantiomers are esterified with (*R*)-MTPA we expect, in this case, the (2*R*,3*R*) resonance to be more downfield relative to the (2*S*,3*S*) resonance. From this it can be determined that KRED 110 yields the (2*S*,3*S*) enantiomer since resonance A (observed when 4a (KRED 110) is esterified with (*S*)-MTPA) is downfield relative to resonance C (observed when 4a (KRED 110) is esterified with (*R*)-MTPA). If KRED 110 instead yielded the (2*R*,3*R*) isomer, we would expect the resonance of the (*S*)-MTPA ester to occur upfield relative to the resonance of the (*R*)-MTPA ester - which is not the case.

The same analysis is applied to assigning the absolute stereochemistry of 4a (KRED 130). Again Figure 2.22 shows a single resonance in the 4a (KRED 130) Mosher ester products. In the case of esterification with (*S*)-MTPA resonance D is observed and in the case of esterification with (*R*)-MTPA, resonance B is observed. Figure 2.26 contains a diagram of the stereoisomers possible from derivatization of 4a (KRED 130) with either (*S*)- or (*R*)-MTPA.

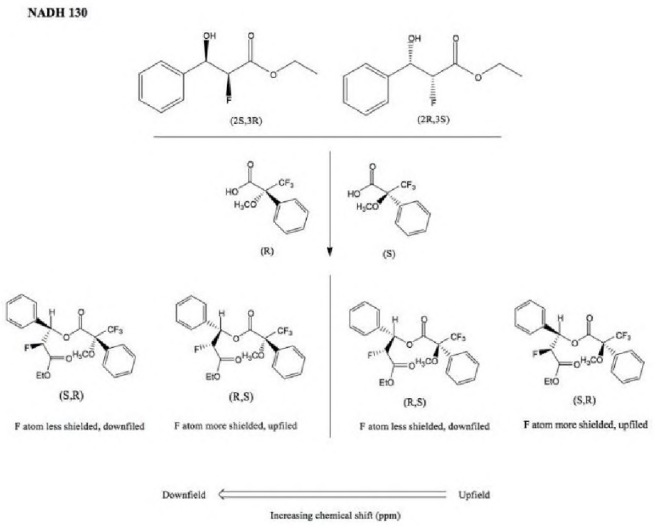

Figure 2.26. Similar to the previous figure (Figure 2.25) the possible stereoisomers and the relative position of their ^{19}F NMR resonances are shown. Because KRED 130 produced the *syn* diastereomer with >99% diastereomeric excess, there are two possible stereoisomers - the (2*S*, 3*R*) and the (2*R*, 3*S*) enantiomers. When the (2*S*, 3*R*) enantiomer is esterified with (*R*)-MTPA, the product's ^{19}F NMR resonance would be expected to occur downfield relative to that of the (2*R*, 3*S*) (*R*)-Mosher ester because the fluorine atom in the (2*S*,3*R*) isomer is less shielded by the phenyl group of (*R*)-MTPA while the fluorine atom of the (2*R*, 3*S*) isomer is more shielded by the phenyl group of (*R*)-MTPA. The opposite effect would be expected to occur when each isomer is esterified with (*S*)-MTPA.

Because it was previously determined that 4a (KRED 130) consists of the *syn* diastereomer in >99% diastereomeric excess, the KRED 130 product can contain either the (2*S*,3*R*) or (2*R*,3*S*) enantiomers. Resonance B (observed in the 4a (KRED 130) + (*R*)-MTPA Mosher ester spectrum) is downfield relative to resonance D (observed in the 4a (KRED 130) + (*S*)-MTPA Mosher ester spectrum). This indicates that 4a (KRED 130) consists entirely of the (2*S*,3*R*) enantiomer.

Using this same analysis, the absolute stereochemistry of 4b (KRED 110), 4b (KRED 130), 4c (KRED 110), and 4c (KRED 130) was determined. In the case of the 4-methoxy α-fluoro-β-hydroxy ester (4b), KRED 110 produced the (2*S*,3*S*) enantiomer and KRED 130 produced the (2*S*,3*R*) enantiomer. The ^{19}F NMR spectrum of 4b (KRED 130) (Figure 2.12) showed 2 resonances - a dominant resonance representing the *syn* diastereomer (integral value of

1) and a minor resonance representing the *anti* diastereomer (integral value of 0.0388). This indicates that for the 4-methoxy derivative KRED 130 yields both diastereomers, *syn* (96.3%) and the *anti* (3.7%). However, in only one of the Mosher ester product spectra (4b (KRED 130) + (*S*)-MTPA) are there two visible resonances - the dominant resonance, labeled C, corresponding to (2*S*,3*R*) isomer, and a minor resonance, labeled D, corresponding to the (2*R*,3*R*) isomer (Figure 2.23). The integral values for these two resonances are 1 for resonance C and 0.11 for resonance D giving a ratio of 90.1% of the *syn* (2*S*,3*R*) isomer to 9.9% of the *anti* (2*R*,3*R*). Given this, one would expect to also find two resonances in the 4b (KRED 130) + (*R*)-MTPA spectrum, but only the single resonance (labeled A in Figure 2.23) is visible. This could be due to a difference in purity between the (*R*)- and (*S*)-MTPA reagents used. Additionally, there is a discrepancy in the two methods for calculating diastereomeric excess. The ^{19}F NMR spectrum for 4b (KRED 130) the 4-methoxy KRED 130 product (Figure 2.13) shows two resonances, one for each diastereomer. Integration of the resonances gives a diastereomeric excess of 96.3% *syn* and 3.7% *anti*. However, integrating the resonances in the 4b (KRED 130) 4-methoxy KRED 130 product + (*S*)-MTPA Mosher ester product spectrum gives a diastereomeric excess of 90.1% *syn* and 9.9% *anti* - a 6.65% difference.

In the case of the 4-trifluoromethyl α-fluoro-β-hydroxy ester derivative, the racemic Mosher ester spectrum contained overlapping resonances (B and C in Figure 2.24). Because of this, assigning these resonances in the enzyme product Mosher ester spectra was more difficult. To assist in these assignments, the coupling constants of each multiplet were measured (Hz). Each resonance is split into a doublet of doublets resulting in four distinct peaks. If the peaks in the resonance are numbered 1-4 starting from the left to the right, the separation between peaks 1 and 2 was measured as well as the separation between peaks 2 and 3. These values are shown in

Figure 2.24 with the separation of peaks 1 and 2 in blue and the separation between peaks 2 and 3 in green. Resonance B had coupling constants of ~22.8 Hz and ~24.0 Hz respectively. Resonance C had coupling constants of ~21.3 Hz and ~27.4 Hz. The more upfield resonance in the 4c (KRED 130) + (*R*)-MTPA Mosher ester spectrum (topmost spectrum in Figure 2.24) had coupling constants of 22.87 HZ and 24.0 Hz and as such was assigned resonance B. The more downfield resonance in the 4c (KRED 130) + (*S*)-MTPA Mosher ester spectrum (second from the top in Figure 2.24) had coupling constants of 21.2 Hz and 27.4 Hz and as such was assigned resonance C. Similarly, the only visible resonance in the 4c (KRED 110) + (*R*)-MTPA Mosher ester spectrum (third from the top in Figure 2.24) had coupling constants of 21.3 Hz and 27.5 Hz and was assigned resonance C.

With this information it was determined that, for the 4-trifluoromethyl derivative, KRED 110 produced the (2*S*,3*S*) enantiomer. The 4c (KRED 130) Mosher ester spectra (Figure 2.24) each show two resonances as opposed to just one. In the case of the esterification with the (*R*)-Mosher ester, the ratio of the two peaks was 1 to 0.104 or 90.6% to 9.4%. In the case of esterification with (*S*)-Mosher ester, the ratio of the two peaks was 1 to 0.128 or 88.7% to 11.3%. Or if averaged, 89.7% to 10.3%. The dominant peak corresponded to the (2*S*,3*R*) isomer and the minor peak corresponded to the (2*R*, 3*R*) isomer. In this case, the calculated ratio of isomers between the two Mosher ester spectra had a difference of 2.12% which again may be due to a difference in purity between the (*R*)- and (*S*)-MTPA reagents used.

Similar to 4b (KRED 130), there is also a discrepancy in the diastereomeric excess as determined by integrating resonances in the 4c (KRED 130) spectrum vs. integrating the resonances in the 4c (KRED 130) Mosher ester spectrum. The diastereomeric excess of 4c (KRED 130) for the KRED 130 product determined by integrating the two resonances in the ^{19}F

NMR spectrum (Figure 2.12) was 84.9% *syn*. Taking the average value for diastereomeric excess determined through integrating the resonances in the Mosher ester spectra of 89.7%, the percent difference is 5.5%.

Figures 2.27 and 2.28 show the stereochemistry and relative percentages, of the KRED 110 and KRED 130 enzyme products for the three derivatives. Overall KRED 110 consistently produced >99% of the *anti* (2S,3S) isomer. KRED 130 predominantly produced the *syn* (2S,3R) isomer with up to 10% of the product containing the *anti* (2R,3R) isomer.

KRED 110

	Anti/Syn	2R,3R	2S,3S	2S,3R	2R,3S
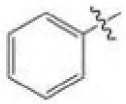	99/1	nd	>99	nd	nd
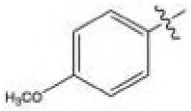	99/1	nd	>99	nd	nd
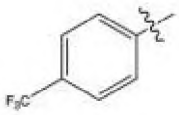	99/1	nd	>99	nd	nd

Figure 2.27. Stereochemistry assignments for the KRED 110 products. Diastereomeric excess (*anti*/*syn*) determined by integration of resonances in respective Mosher ester spectra.

Figure 2.29 contains another representation of these results highlighting the structures of the enzyme products with their absolute stereochemistry assigned.

KRED 130

	Anti/Syn	2R,3R	2S,3S	2S,3R	2R,3S
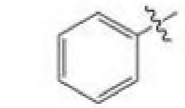	1/99	nd	nd	>99	nd
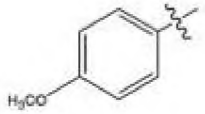	10/90	10	nd	90	nd
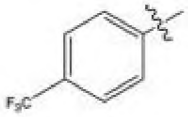	10/90	10	nd	90	nd

Figure 2.28. Stereochemistry assignments for the KRED 130 products. Diastereomeric excess (*anti*/*syn*) determined by integration of resonances in respective Mosher ester spectra.

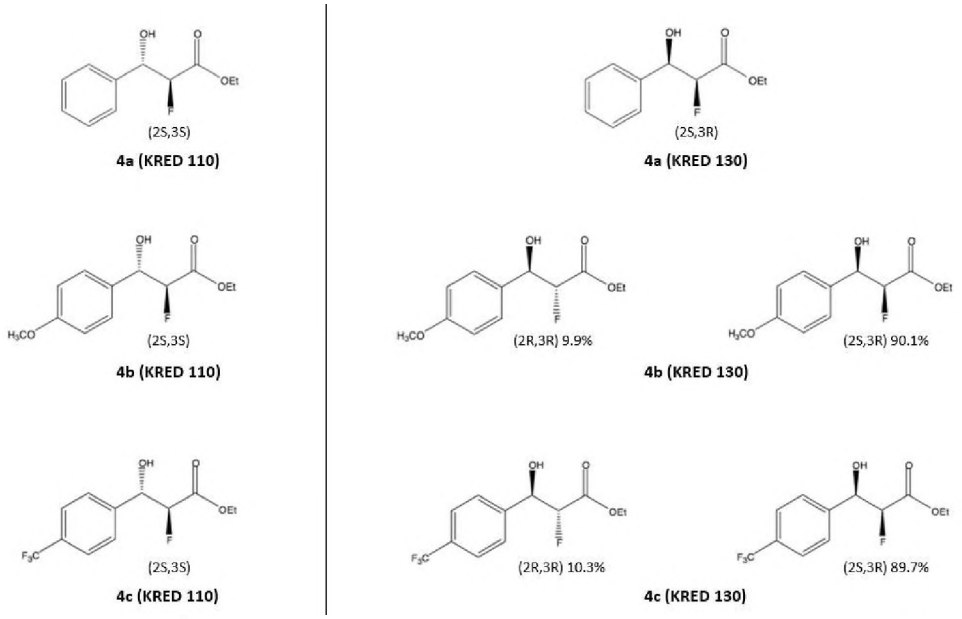

Figure 2.29. Structures of the enzyme products showing their absolute stereochemistry.

Chapter 3. Conclusions

The work presented here describes a new method for the synthesis of enantiopure α-fluoro-β-hydroxy esters and is the first description in the literature of enzymatic reduction to produce α-fluoro-β-hydroxy in a highly stereoselective manner. Starting with a benzaldehyde derivative, its corresponding α-fluoro-β- hydroxy ester can be produced in both a diastero- and enatiomerically pure fashion in only three reactions - a Reformatsky reaction to form the racemic α-fluoro-β-hydroxy ester, DMP oxidation to form the corresponding α-fluoro-β-keto ester, and subsequent reduction to the enantiopure α-fluoro-β-hydroxy ester using the KRED enzyme system.

While this work only examined three benzaldehyde derivatives as substrates, previous works showed that the methods reported here can be applied to a variety of other substrates. Several non-aromatic, simple alkyl substituted and other α-fluoro-β-hydroxy esters were synthesized enantioselectively using these methods [96].

The data collected in this study shows that, for the substrates examined here, KRED 110 selects for *anti* 2S,3S enantiomer with a high degree of enantiomeric and diastereomeric excess. KRED 130 on the other hand selects for the *syn* 2S,3R enantiomer with a high degree of enantiomeric excess and with a slightly lower degree of diastereomeric excess. While this was true for the three substrates examined here, it is still unknown to what extent this pattern is universal across other aromatic and non-aromatic α-fluoro-β-keto esters generally. Experiments with a broader range of substrates would be needed to confirm this pattern.

Additionally, the scope of the work presented here is limited to the synthesis of those two configurations (2S,3S and 2S,3R). Of the number of KRED enzymes commercially available from Codexis, several were found to yield the 2R,3R configuration upon the reduction of ethyl-

α-fluoroacetate - primarily KREDs P1-A04, P1-H10, and P2-H07. In the case of some substrates, the 2R,3S configuration can be accessed with the enzymes P2-C02 and P1-B02 [96].

The optically pure α-fluoro-β-hydroxy esters reported here may serve as useful intermediates in the synthesis of 2-fluorinated D-erythro sphingosine analogues. Attempts at α amination of the α-fluoro-β-hydroxy esters via the method described by Dai and Green were however unsuccessful [97]. These compounds may also serve as useful intermediates in the synthesis of α-fluoro-α-amino acids [62, 63].

References

1. Paul, E. A., and P. M. Huang. "Chemical aspects of soil." Handbook of environmental chemistry 1.Part A (1980): 69-86.

2. Harpere, D.B and D.O'Hagan. "The Fluorinated Natural Products." Natural Product Reports 11 (1994): 123-133.

3. Emsley, John. Nature's Building Blocks: An A-Z Guide to the Elements. Oxford : Oxford University Press, 2011.

4. Taplin, C. E., Cowell, C. T., Silink, M., & Ambler, G. R. "Fludrocortisone therapy in cerebral salt wasting." Pediatrics (2006): 1904–1908.

5. Heidelberger, C., et al. "Fluorinated pyrimidines, a new class of tumour-inhibitory compounds ." Nature (1957): 663-666.

6. Ahmad, S. I., S. H. Kirk and A. Eisenstark. "Thymine Metabolism and Thyminless Death in Prokaryotes and Eukaryotes." Annual Review of Microbiology (1998): 591-625.

7. Aldred, K. J., Kerns, R. J., & Osheroff, N. "Mechanism of quinolone action and resistance." Biochemistry (2014): 1565–1574.

8. Lesher, George Y., et al. "1, 8-Naphthyridine derivatives. A new class of chemotherapeutic agents." Journal of Medicinal Chemistry 5.5 (1962): 1063-1065.

9. Takahashi, Hisashi, Isao Hayakawa, and Takeshi Akimoto. "The history of the development and changes of quinolone antibacterial agents." Yakushigaku zasshi 38.2 (2003): 161-179.

10. Hiroshi Koga, Akira Itoh, Satoshi Murayama, Seigo Suzue, and Tsutomu Irikura. "Structure-activity relationships of antibacterial 6,7- and 7,8-disubstituted 1-alkyl-1,4-dihydro-4-oxoquinoline-3-carboxylic acids." Journal of Medicinal Chemistry (1980): 1358–1363.

11. Kocsis, B., Domokos, J., & Szabo, D. "Chemical structure and pharmacokinetics of novel quinolone agents represented by avarofloxacin, delafloxacin, finafloxacin, zabofloxacin and nemonoxacin." Annals of clinical microbiology and antimicrobials (2016).

12. Chambers, R. D. Fluorine in Organic Chemistry. Oxford: Blackwell Publishing, 2000.

13. Morgenthaler, M., Schweizer, E., Hoffmann-Röder, A., Benini, F., Martin, R. E., Jaeschke, G., Wagner, B., Fischer, H., Bendels, S., Zimmerli, D., Schneider, J., Diederich, F., Kansy, M., & Müller, K. "Predicting and tuning physicochemical properties in lead optimization: amine basicities." ChemMedChem (2007): 1100–1115.

14. Gillis, E. P., Eastman, K. J., Hill, M. D., Donnelly, D. J., & Meanwell, N. A. "Applications of Fluorine in Medicinal Chemistry." Journal of medicinal chemistry (2015): 8315–8359.

15. van Niel, M. B., Collins, I., Beer, M. S., Broughton, H. B., Cheng, S. K., Goodacre, S. C., Heald, A., Locker, K. L., MacLeod, A. M., Morrison, D., Moyes, C. R., O'Connor, D., Pike, A., Rowley, M., Russell, M. G., Sohal, B., Stanton, J. A., Thomas, S., Ve. "Fluorination of 3-(3-(piperidin-1-yl)propyl)indoles and 3-(3-(piperazin-1-yl)propyl)indoles gives selective human 5-HT1D receptor ligands with improved pharmacokinetic profiles." Journal of medicinal chemistry (1999): 2087–2104.

16. Cox, C. D., Coleman, P. J., Breslin, M. J., Whitman, D. B., Garbaccio, R. M., Fraley, M. E., Buser, C. A., Walsh, E. S., Hamilton, K., Schaber, M. D., Lobell, R. B., Tao, W., Davide, J. P., Diehl, R. E., Abrams, M. T., South, V. J., Huber, H. E., Torrent,. "Kinesin spindle protein (KSP) inhibitors. 9. Discovery of (2S)-4-(2,5-difluorophenyl)-n-[(3R,4S)-3-fluoro-1-methylpiperidin-4-yl]-2-(hydroxymethyl)-N-methyl-2-phenyl-2,5-dihydro-1H-pyrrole-1-carboxamide (MK-0731) for the treatment of taxane-refractory can." Journal of medicinal chemistry (2008): 4239–4252.

17. Goncharov, N. V., Jenkins, R. O., & Radilov, A. S. "Toxicology of fluoroacetate: a review, with possible directions for therapy research." Journal of applied toxicology (2006): 148–161.

18. Rowley, M., Hallett, D. J., Goodacre, S., Moyes, C., Crawforth, J., Sparey, T. J., Patel, S., Marwood, R., Patel, S., Thomas, S., Hitzel, L., O'Connor, D., Szeto, N., Castro, J. L., Hutson, P. H., & MacLeod, A. M. "3-(4-Fluoropiperidin-3-yl)-2-phenylindoles as high affinity, selective, and orally bioavailable h5-HT(2A) receptor antagonists." Journal of medicinal chemistry (2001): 1603–1614.

19. Purser, Sophie, Moore, Peter R., Swallow, Steeve, Gouverneur, Veronique. "Fluorine in medicinal chemistry." Chemical Society Reviews (2007): 320-330.

20. David F.V Lewis, Maruice Dickins. "Baseline lipophilicity relationships in human cytochromes P450 associated with drug metabolism." Drug Metab Rev. (2003): 1-18.

21. Park, B. K., Kitteringham, N. R., & O'Neill, P. M. "Metabolism of fluorine-containing drugs." Annual review of pharmacology and toxicology (2001): 443–470.

22. Park, B. K., & Kitteringham, N. R. "Effects of fluorine substitution on drug metabolism: pharmacological and toxicological implications." Drug metabolism reviews (1994): 605–643.

23. Dugar, S., Yumibe, N., Clader, J., Vizziano, M., Huie, K., Heek, M.V., Compton, D., & Davis, H.R. "Metabolism and structure activity data based drug design: discovery of (−) SCH 53079 an analog of the potent cholesterol absorption inhibitor (−) SCH 48461." Bioorganic & Medicinal Chemistry Letters (1996): 1271-1274.

24. Rosenblum, S. B., Huynh, T., Afonso, A., Davis, H. R., Jr, Yumibe, N., Clader, J. W., & Burnett, D. A. "Discovery of 1-(4-fluorophenyl)-(3R)-[3-(4-fluorophenyl)-(3S)-hydroxypropyl]-(4S)-(4 -hydroxyphenyl)-2-azetidinone (SCH 58235): a designed, potent, orally active inhibitor of cholesterol absorption." Journal of medicinal chemistry (1998): 973–980.

25. Shah, P., & Westwell, A. D. "The role of fluorine in medicinal chemistry." Journal of enzyme inhibition and medicinal chemistry (2007): 527–540.

26. Zaccara, G., Franciotta, D., & Perucca, E. "Idiosyncratic adverse reactions to antiepileptic drugs." Epilepsia (2007): 1223–1244.

27. Uetrecht, Jack. "Idiosyncratic drug reactions: current understanding." Annu. Rev. Pharmacol. Toxicol. 47 (2007): 513-539.

28. Evans, D. C., Watt, A. P., Nicoll-Griffith, D. A., & Baillie, T. A. "Drug-protein adducts: an industry perspective on minimizing the potential for drug bioactivation in drug discovery and development." Chemical research in toxicology (2004): 3–16.

29. Hop, Cornelis ECA, Amit S. Kalgutkar, and John R. Soglia. "Importance of early assessment of bioactivation in drug discovery." Annual Reports in Medicinal Chemistry 41 (2006): 369-381.

30. Lin, L. S., Lanza, T. J., Jr, Jewell, J. P., Liu, P., Shah, S. K., Qi, H., Tong, X., Wang, J., Xu, S. S., Fong, T. M., Shen, C. P., Lao, J., Xiao, J. C., Shearman, L. P., Stribling, D. S., Rosko, K., Strack, A., Marsh, D. J., Feng, Y., Kumar, S., … Hagman. "Discovery of N-[(1S,2S)-3-(4-Chlorophenyl)-2- (3-cyanophenyl)-1-methylpropyl]-2-methyl-2- {[5-(trifluoromethyl)pyridin-2-yl]oxy}propanamide (MK-0364), a novel, acyclic cannabinoid-1 receptor inverse agonist for the treatment of obesity." Journal of medicinal chemistry (2006): 7584–7587.

31. Hagmann, W.K. "The many roles for fluorine in medicinal chemistry." Journal of medicinal chemistry (2008): 4359–4369.

32. Samuel, K., Yin, W., Stearns, R. A., Tang, Y. S., Chaudhary, A. G., Jewell, J. P., Lanza, T., Jr, Lin, L. S., Hagmann, W. K., Evans, D. C., & Kumar, S. "Addressing the metabolic activation potential of new leads in drug discovery: a case study using ion trap mass spectrometry and tritium labeling techniques." Journal of mass spectrometry (2003): 211–221.

33. Addy, C., Wright, H., Van Laere, K., Gantz, I., Erondu, N., Musser, B. J., Lu, K., Yuan, J., Sanabria-Bohórquez, S. M., Stoch, A., Stevens, C., Fong, T. M., De Lepeleire, I., Cilissen, C., Cote, J., Rosko, K., Gendrano, I. N., 3rd, Nguyen, A. M., Gumbiner. "The acyclic CB1R inverse agonist taranabant mediates weight loss by increasing energy expenditure and decreasing caloric intake." Cell metabolism (2008): 68–78.

34. Proietto, J., Rissanen, A., Harp, J. B., Erondu, N., Yu, Q., Suryawanshi, S., Jones, M. E., Johnson-Levonas, A. O., Heymsfield, S. B., Kaufman, K. D., & Amatruda, J. M. "A clinical trial assessing the safety and efficacy of the CB1R inverse agonist taranabant in obese and overweight patients: low-dose study." International journal of obesity (2010): 1243–1254.

35. Spurgeon, M. E., Chung, S. H., & Lambert, P. F. "Recurrence of cervical cancer in mice after selective estrogen receptor modulator therapy." The American journal of pathology (2014): 530–540.

36. G., Liehr J. "2-Fluoroestradiol. Separation of estrogenicity from carcinogenicity." Molecular Pharmacology (1983): 278–281.

37. Fried J, John V, Szwedo MJ, Chen C, O'Yang C. "Synthesis of 10,10-difluorothromboxane A2, a potent and chemically stable thromboxane agonist." Journal of the American Chemical Society (1989): 4510-4511.

38. Cho, M. J., & Allen, M. A. "Chemical stability of prostacyclin (PGI2) in aqueous solutions." Prostaglandins (1978): 943–954.

39. Bartmann, W., Beck, G., Knolle, J., Rupp, R. H., Schölkens, B. A., & Weithmann, U. "Synthesis of stable prostacyclin analogs." Advances in prostaglandin, thromboxane, and leukotriene research (1983): 287–292.

40. Chang, C. S., Negishi, M., Nakano, T., Morizawa, Y., Matsumura, Y., & Ichikawa, A. "7,7-Difluoroprostacyclin derivative, AFP-07, a highly selective and potent agonist for the prostacyclin receptor." Prostaglandins (1997): 83–90.

41. Penning, T. D., Talley, J. J., Bertenshaw, S. R., Carter, J. S., Collins, P. W., Docter, S., Graneto, M. J., Lee, L. F., Malecha, J. W., Miyashiro, J. M., Rogers, R. S., Rogier, D. J., Yu, S. S., AndersonGD, Burton, E. G., Cogburn, J. N., Gregory, S. A.,. "Synthesis and biological evaluation of the 1,5-diarylpyrazole class of cyclooxygenase-2 inhibitors: identification of 4-[5-(4-methylphenyl)-3-(trifluoromethyl)-1H-pyrazol-1-yl]benze nesulfonamide (SC-58635, celecoxib)." Journal of medicinal chemistry (1997): 1347–1365.

42. Tanaka, H., & Shishido, Y. "Synthesis of aromatic compounds containing a 1,1-dialkyl-2-trifluoromethyl group, a bioisostere of the tert-alkyl moiety." Bioorganic & medicinal chemistry letters (2007): 6079–6085.

43. Gauthier, J. Y., Chauret, N., Cromlish, W., Desmarais, S., Duong, L. T., Falgueyret, J. P., Kimmel, D. B., Lamontagne, S., Léger, S., LeRiche, T., Li, C. S., Massé, F., McKay, D. J., Nicoll-Griffith, D. A., Oballa, R. M., Palmer, J. T., Percival, M. D., R. "The discovery of odanacatib (MK-0822), a selective inhibitor of cathepsin K." Bioorganic & medicinal chemistry letters (2008): 923–928.

44. McClung, M. R., O'Donoghue, M. L., Papapoulos, S. E., Bone, H., Langdahl, B., Saag, K. G., Reid, I. R., Kiel, D. P., Cavallari, I., Bonaca, M. P., Wiviott, S. D., de Villiers, T., Ling, X., Lippuner, K., Nakamura, T., Reginster, J. Y., Rodriguez-Portales,. "Odanacatib for the treatment of postmenopausal osteoporosis: results of the LOFT multicentre, randomised, double-blind, placebo-controlled trial and LOFT Extension study." The lancet. Diabetes & endocrinology (2019): 899–911.

45. Black, W. C., Bayly, C. I., Davis, D. E., Desmarais, S., Falgueyret, J. P., Léger, S., Li, C. S., Massé, F., McKay, D. J., Palmer, J. T., Percival, M. D., Robichaud, J., Tsou, N., & Zamboni, R. "Trifluoroethylamines as amide isosteres in inhibitors of cathepsin K." Bioorganic & medicinal chemistry letters (2005): 4741–4744.

46. Isabel, E., Mellon, C., Boyd, M. J., Chauret, N., Deschênes, D., Desmarais, S., Falgueyret, J. P., Gauthier, J. Y., Khougaz, K., Lau, C. K., Léger, S., Levorse, D. A., Li, C. S., Massé, F., Percival, M. D., Roy, B., Scheigetz, J., Thérien, M., Truong, V. "Difluoroethylamines as an amide isostere in inhibitors of cathepsin K." Bioorganic & medicinal chemistry letters (2011): 920–923.

47. Smart, Bruce E. "Fluorine substituent effects (on bioactivity)." Journal of Fluorine Chemistry 109.1 (2001): 3-11.

48. Huchet, Quentin & Kuhn, Bernd & Wagner, Björn & Fischer, Holger & Kansy, Manfred & Zimmerli, Daniel & Carreira, Erick & Müller, Klaus. "On the polarity of partially fluorinated methyl groups." Journal of Fluorine Chemistry (2013): 119-128.

49. Jacobs, R. T., Bernstein, P. R., Cronk, L. A., Vacek, E. P., Newcomb, L. F., Aharony, D., Buckner, C. K., & Kusner, E. J. "Synthesis, structure-activity relationships, and pharmacological evaluation of a series of fluorinated 3-benzyl-5-indolecarboxamides: identification of 4-[[5-[((2R)-2-methyl-4,4,4-trifluorobutyl)carbamoyl]-1-methyl indol-3-yl]methyl]-3-methoxy-N-[(2-meth." Journal of medicinal chemistry (1994): 1282–1297.

50. Ettorre, A., D'Andrea, P., Mauro, S., Porcelloni, M., Rossi, C., Altamura, M., Catalioto, R. M., Giuliani, S., Maggi, C. A., & Fattori, D. "hNK2 receptor antagonists. The use of intramolecular hydrogen bonding to increase solubility and membrane permeability." Bioorganic & medicinal chemistry letters (2011): 1807–1809.

51. Massa, M. A., Spangler, D. P., Durley, R. C., Hickory, B. S., Connolly, D. T., Witherbee, B. J., Smith, M. E., & Sikorski, J. A. "Novel heteroaryl replacements of aromatic 3-tetrafluoroethoxy substituents in trifluoro-3-(tertiaryamino)-2-propanols as potent inhibitors of cholesteryl ester transfer protein." Bioorganic & medicinal chemistry letters (2001): 1625–1628.

52. L., Hunter. "The C-F bond as a conformational tool in organic and biological chemistry." Beilstein journal of organic chemistry (2010).

53. Kim C-Y, Chang JS, Doyon JB, Baird TT, Fierke CA, Jain A, Christianson DW. "Contribution of Fluorine to Protein−Ligand Affinity in the Binding of Fluoroaromatic Inhibitors to Carbonic Anhydrase II." Journal of the American Chemical Society (2000): 12125-12134.

54. Abeles, R. H., & Alston, T. A. "Enzyme inhibition by fluoro compounds." The Journal of biological chemistry (1990): 16705–16708.

55. Riley, K. E., & Merz, K. M., Jr. "Effects of fluorine substitution on the edge-to-face interaction of the benzene dimer." The journal of physical chemistry (2005): 17752–17756.

56. Abbate, F., Casini, A., Scozzafava, A., & Supuran, C. T. "Carbonic anhydrase inhibitors: X-ray crystallographic structure of the adduct of human isozyme II with the perfluorobenzoyl analogue of methazolamide. Implications for the drug design of fluorinated inhibitors." Journal of enzyme inhibition and medicinal chemistry (2003): 303–308.

57. Böhm, H. J., Banner, D., Bendels, S., Kansy, M., Kuhn, B., Müller, K., Obst-Sander, U., & Stahl, M. "Fluorine in medicinal chemistry." Chembiochem : a European journal of chemical biology (2004): 637–643.

58. Glasspool RM, Evans T.R.J. "Clinical imaging of cancer metastasis." European Journal of Cancer (2000): 1661-1670.

59. Westera, G., & Schubiger, P. A. "Functional imaging of physiological processes by positron emission tomography." News in physiological sciences : an international journal of physiology produced jointly by the International Union of Physiological Sciences and the American Physiological Society (2003): 175–178.

60. Herholz, K., & Heiss, W. D. "Positron emission tomography in clinical neurology." Molecular imaging and biology (2004): 239–269.

61. Haufe, Günter. "Regio- and stereoselective synthesis of vicinal fluorohydrins." Journal of Fluorine Chemistry (2004): 875-894.

62. Huber, Dominique Pascal, Kyrill Stanek, and Antonio Togni. "Consecutive catalytic electrophilic fluorination/amination of β-keto esters: toward α-fluoro-α-amino acids?." Tetrahedron: Asymmetry 17.4 (2006): 658-664.

63. Tarui, A., Sato, K., Omote, M., Kumadaki, I. and Ando, A. "Stereoselective Synthesis of α-Fluorinated Amino Acid Derivatives." Adv. Synth. Catal. (2010): 2733-2744.

64. Shriner, Ralph L. "The Reformatsky Reaction." Organic reactions 1 (2004): 1-37.

65. McBee, E. T., O. R. Pierce, and D. L. Christman. "The Reformatsky Reaction with Ethyl Bromofluoroacetate1." Journal of the American Chemical Society 77.6 (1955): 1581-1583.

66. Wolf, Christian, and Max Moskowitz. "Bisoxazolidine-catalyzed enantioselective Reformatsky reaction." The Journal of Organic Chemistry 76.15 (2011): 6372-6376.

67. Cozzi, Pier Giorgio, et al. "Me2Zn mediated, tert-butylhydroperoxide promoted, catalytic enantioselective Reformatsky reaction with aldehydes." Chemical communications 28 (2008): 3317-3318.

68. Cozzi, Pier Giorgio, Alessandro Mignogna, and Paola Vicennati. "Dimethylzinc-Mediated, Oxidatively Promoted Reformatsky Reaction of Ethyl Iodoacetate with Aldehydes and Ketones." Advanced Synthesis & Catalysis 350.7-8 (2008): 975-978.

69. Fernandez-Ibanez, M. Angeles, et al. "Catalytic enantioselective Reformatsky reaction with ortho-substituted diarylketones." Organic letters 10.18 (2008): 4041-4044.

70. Fernández-Ibáñez, M. Ángeles, et al. "Catalytic enantioselective Reformatsky reaction with ketones." Chemical communications 22 (2008): 2571-2573.

71. Fernandez-Ibanez, M. A., Macia, B., Minnaard, A. J., & Feringa, B. L. "Catalytic enantioselective Reformatsky reaction with aldehydes." Angewandte Chemie-International Edition (2008): 1317 - 1319.

72. Cozzi, Pier Giorgio. "A Catalytic, Me2Zn-Mediated, Enantioselective Reformatsky Reaction With Ketones." Angewandte Chemie 118.18 (2006): 3017-3020.

73. Lin, Ning, et al. "Indolinylmethanol catalyzed enantioselective Reformatsky reaction with ketones." Tetrahedron: Asymmetry 21.23 (2010): 2816-2824.

74. Fornalczyk, Michal, Kuldip Singh, and Alison M. Stuart. "Synthesis of α-fluoro-β-hydroxy esters by an enantioselective Reformatsky-type reaction." Chemical Communications 48.29 (2012): 3500-3502.

75. Penning, Trevor M. "The aldo-keto reductases (AKRs): Overview." Chemico-biological interactions 234 (2015): 236-246.

76. Giannopoulos, Vasileios, and Ioulia Smonou. "Asymmetric Reduction of α, α-Dichloro-β-Keto Esters by NADPH-Dependent Ketoreductases." European Journal of Organic Chemistry 2022.27 (2022): e202200410.

77. González-Granda, Sergio, et al. "Stereoselective Bioreduction of α-diazo-β-keto Esters." Molecules 25.4 (2020): 931.

78. Giannopoulos, Vasileios, et al. "Novel Enzymatic Reduction of α-amido-and α-cyanoalkyl-β-keto Esters Catalyzed by Ketoreductases." Molecular Catalysis 490 (2020): 110952.

79. Huang, Chenming, et al. "Ketoreductase catalyzed (dynamic) kinetic resolution for biomanufacturing of chiral chemicals." Frontiers in Bioengineering and Biotechnology 10 (2022): 929784.

80. Tang, Jiawei, et al. "Structure-guided Evolution of a Ketoreductase for Efficient and Stereoselective Bioreduction of Bulky α-amino β-keto Esters." Catalysis Science & Technology 11.20 (2021): 6755-6769.

81. Zhu, Dunming, et al. "A recombinant ketoreductase tool-box. Assessing the substrate selectivity and stereoselectivity toward the reduction of β-ketoesters." Tetrahedron 62.5 (2006): 901-905.

82. Dai, Zhipeng, Kate Guillemette, and Thomas K. Green. "Stereoselective synthesis of aryl γ, δ-unsaturated β-hydroxyesters by ketoreductases." Journal of Molecular Catalysis B: Enzymatic 97 (2013): 264-269.

83. Applegate, Gregory A., and David B. Berkowitz. "Exploiting enzymatic dynamic reductive kinetic resolution (DYRKR) in stereocontrolled synthesis." Advanced synthesis & catalysis 357.8 (2015): 1619-1632.

84. Reformatsky, Sergius. "Neue Synthese zweiatomiger einbasischer Säuren aus den Ketonen." Berichte der deutschen chemischen Gesellschaft 20.1 (1887): 1210-1211.

85. Kurti, Laszlo, and Barbara Czakó. Strategic applications of named reactions in organic synthesis. Elsevier, 2005.

86. Rathke, M. W. "The Reformatsky Reaction." Organic Reactions (1975): 423–460.

87. Gholap, Atul R., and Abhijit P. Chavan. "Microwave-promoted synthesis of β-hydroxyesters by the Reformatsky reaction in the absence of solvent." Journal of Chemical Research 2003.6 (2003): 374-376.

88. Dess, D. B., and J. C. Martin. "Readily accessible 12-I-5 oxidant for the conversion of primary and secondary alcohols to aldehydes and ketones." The Journal of Organic Chemistry 48.22 (1983): 4155-4156.

89. Meyer, Stephanie D., and Stuart L. Schreiber. "Acceleration of the Dess-Martin oxidation by water." The Journal of Organic Chemistry 59.24 (1994): 7549-7552.

90. Mima, Kazuhide, et al. "An efficient method for the diastereoselective synthesis of α-fluoro-β-hydroxy esters based on the radical reduction of α-bromo-α-fluoro-β-hydroxy esters." Tetrahedron 58.12 (2002): 2369-2376.

91. Minch, Michael J. "Orientational dependence of vicinal proton-proton NMR coupling constants: The Karplus relationship." Concepts in magnetic resonance 6.1 (1994): 41-56.

92. Dale, James A., and Harry S. Mosher. "Nuclear magnetic resonance enantiomer regents. Configurational correlations via nuclear magnetic resonance chemical shifts of diastereomeric mandelate, O-methylmandelate, and. alpha.-methoxy-. alpha.-trifluoromethylphenylacetate (MTPA) esters." Journal of the American Chemical Society 95.2 (1973): 512-519.

93. Hoye, Thomas R., Christopher S. Jeffrey, and Feng Shao. "Mosher ester analysis for the determination of absolute configuration of stereogenic (chiral) carbinol carbons." Nature protocols 2.10 (2007): 2451-2458.

94. Gao, Jinhai, Srinivasan Rajan, and Bing Wang. "In-tube derivatization for determination of absolute configuration and enantiomeric purity of chiral compounds by NMR spectroscopy." Magnetic Resonance in Chemistry 55.4 (2017): 269-273.

95. Hoye, Thomas R., et al. "Long-range shielding effects in the 1H NMR spectra of Mosher-like ester derivatives." Organic letters 12.8 (2010): 1768-1771.

96. Green, T.K., Damarancha, A., Vanagel, M., Showalter, B., Kolberg, S. and Thompson, A. "Stereoselective Reduction of α-Fluoro-β-keto Esters by NADH and NADPH-Dependent Ketoreductases." Eur. J. Org. Chem. (2019): 4080-4084.

97. Dai, Zhipeng, and Thomas K. Green. "Synthesis of Aromatic Sphingosine Analogues by Diastereoselective Amination of Enantioenriched trans-γ, δ-Unsaturated β-Hydroxyesters." The Journal of Organic Chemistry 79.16 (2014): 7778-7784.

Appendices

A1. Experimental

Synthesis of racemic 2-fluoro-3-hydroxyesters (2a-2c). Reformatsky reactions were carried out by either of the two methods described below.

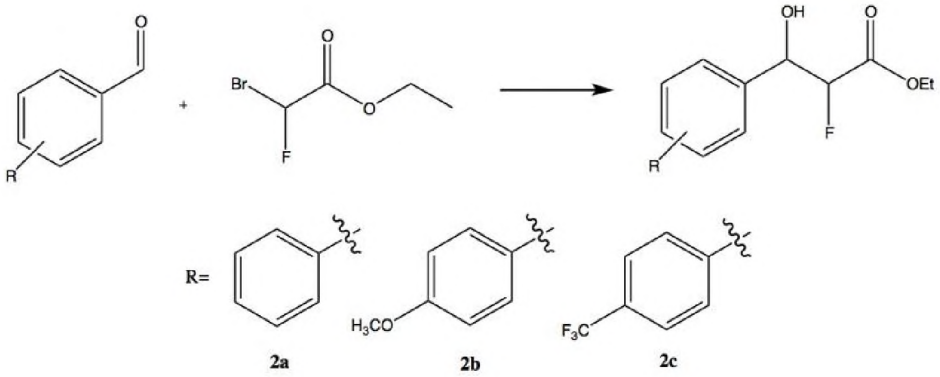

Figure S.1. Reformatsky reaction scheme.

Method 1: The given aldehyde (1 mmol), ethyl bromofluoroacetate (3 mmol), activated 100 mesh zinc (7.6 mmol), and ammonium chloride (19 mmol) were mixed thoroughly in a glass beaker. The reaction mixture was microwaved in a standard domestic microwave oven for 60 seconds in 10 second pulses. After which the reaction mixture was treated with a saturated ammonium chloride solution (25 mL) and diethyl ether (15 mL). The reaction mixture was filtered over celite to remove the remaining zinc. The organic and aqueous phases were separated and the aqueous phase extracted with diethyl ether (2 x 25 mL). The combined organic phases were washed with DI water (2 x 25 mL), brine (2 x 25 mL), and dried with anhydrous sodium sulfate. Solvent was removed under vacuum affording an amber oil. Flash chromatography on silica eluting with a solution of 80% hexane and 20% ethyl acetate gave the pure α-fluoro-β-hydroxy esters with ~70-80% yield (Atul R. Gholap, 2003).

Method 2: Activated 100 mesh zinc (10 mmol), ethyl bromofluoroacetate (5.5 mmol), and the given aldehyde (5 mmol) were combined in THF (15 mL) and heated to reflux. After the completion of the reaction, as monitored by TLC, the reaction was cooled to room temperature and to it was added ethyl acetate (100 mL) and a 1M solution of sodium bisulfate (25 mL). The reaction mixture was filtered over celite and the layers separated. The aqueous layer was extracted with ethyl acetate (2 x 75 mL). The combined organic phases were washed with aqueous sodium bicarbonate (2 x 25 mL), DI water (2 x 25 mL), brine (2 x 25 mL), and then dried over anhydrous magnesium sulfate. Solvent was removed under vacuum affording an amber oil. Flash chromatography on silica eluting with a solution of 80% hexane and 20% ethyl acetate gave the pure α-fluoro-β-hydroxy esters with ~70-80% yield (Graves, 1989).

Zinc Activation: 100 mesh zinc was stirred in 2% HCl solution for 15 minutes after which the zine was transferred to a filtration flask under vacuum and washed successively with DI water, acetone, absolute ethanol, and anhydrous diethyl ether. The zinc was then dried in a vacuum oven at 90°C for 30 minutes.

NMR Spectroscopy: ^{1}H and ^{13}C NMR spectra were recorded with a Varian 300 MHz and Bruker 600 MHz instrument. Chemical shifts are reported in ppm relative to TMS as an internal standard. Ethyl 2-fluoro-3-hydroxy-3-phenylpropanoate (2a): colorless oil, 658 mg, 82%: ^{1}H NMR (300 MHz, $CDCl_3$) δ 7.52 – 7.28 (m, 5H), 5.25 – 4.85 (m, 2H), 4.34 – 4.04 (m, 3H), 2.84 (d, J = 43.2 Hz, 1H), 1.31 – 1.11 (m, 3H); ^{13}C NMR (75 MHz, $CDCl_3$) δ 167.81 (d, J = 24.4 Hz), 167.75 (d, J = 23.3), 138.0 (d, J = 2.9 Hz), 137.6 (d, J = 2.8 Hz), 128.57, 128.54, 128.4, 126.80, 126.78, 126.53, 126.51, 91.54 (d, J = 191.9 Hz), 91.05 (d, J = 190.8 Hz), 73.9 (d, J = 20.1 Hz) 73.6 (d, J = 22.0 Hz), 61.9, 61.8, 13.95, 13.94; ^{19}F NMR (282 MHz, $CDCl_3$) δ -197.8 (dd, J = 47.7, 16.9 Hz), -202.8 (dd, J = 48.0, 22.4 Hz).

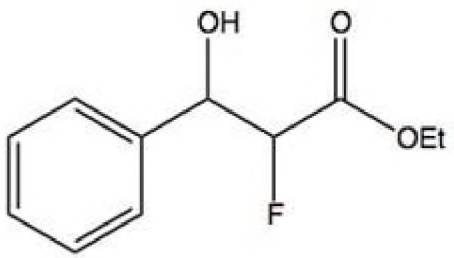

2a

Figure S.2. Ethyl 2-fluoro-3-hydroxy-3-phenylpropanoate (2a) structure.

Ethyl 2-fluoro-3-hydroxy-3-(4-methoxyphenyl)propanoate (2b): colorless oil, 430 mg, 81%; ^{1}H NMR (300 MHz, CDCl3) δ 7.40 – 7.21 (m, 2H), 6.99 – 6.78 (m, 2H), 5.16 – 4.77 (m, 2H), 4.31 –4.12 (m, 2H), 3.80, 3.79 (s, 3H), 2.79 (d, J = 38.8 Hz, 1H), 1.34 – 1.11 (m, 4H); ^{13}C NMR (75MHz, $CDCl_3$) δ 167.94 (d, J = 24.3 Hz), 167.86 (d, J = 23.2 Hz), 159.6, 130.2 (d, J = 2.9 Hz),129.9 (d, J = 2.3 Hz), 128.2 (d, J = 1.3 Hz), 127.9 (d, J = 1.0 Hz), 113.8, 113.7, 91.8 (d, J =191.5), 91.2 (J = 189.8 Hz), 73.4 (d, J = 20.3 Hz), 73.1 (d, J = 22.0 Hz), 61.8, 61.7, 55.21, 55.17,13.94, 13.91; ^{19}F NMR (282 MHz, $CDCl_3$) δ -198.5 (dd, J = 49.9, 15.8 Hz), -202.1 (dd, J = 48.0, 22.0 Hz).

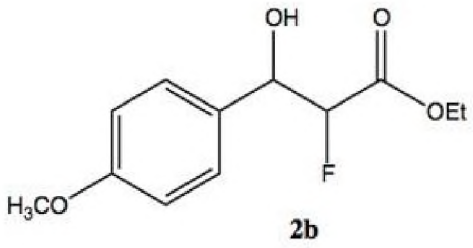

2b

Figure S.3. Ethyl 2-fluoro-3-hydroxy-3-(4-methoxyphenyl)propanoate (2b) structure.

Ethyl 2-fluoro-3-hydroxy-3-(4-(trifluoromethyl)phenyl)propanoate (2c): colorless oil, 71 mg,89%; ^{1}H NMR (300 MHz, $CDCl_3$) δ 7.73 – 7.41 (m, 4H), 5.28 – 5.12 (m, 1H), 5.13 – 4.87 (m,1H), 4.34 – 4.10 (m, 2H), 3.19 (d, J = 48.2 Hz, 1H), 1.31 – 1.08 (m, 3H);); ^{13}C NMR (75 MHz, $CDCl_3$) δ 167.7 (d, J = 24.3 Hz), 167.5 (d, J = 23.4 Hz), 142.1, 141.5, 130.6 (q, J = 32.5

Hz),127.1 (d, J = 1.3 Hz), 126.9 ppm (d, J = 1.1 Hz),125.4 (q, J = 3.8 Hz), 125.2 (q, J = 3.8 Hz),124.0 (q, J = 272.1 Hz), 91.1 (d, J = 192.7 Hz), 90.9, (d, J = 191.2 Hz), 73.2 (d, J = 20.2 Hz), 73.0 (d, J = 22.1 Hz), 62.2, 62.0, 13.81, 13.77; ^{19}F NMR (282 MHz, $CDCl_3$) δ -62.72, -62.74 (s,3F), -197.2 (dd, J = 48.0, 15.5 Hz), -203.6 (dd, J = 47.7, 22.6 Hz)

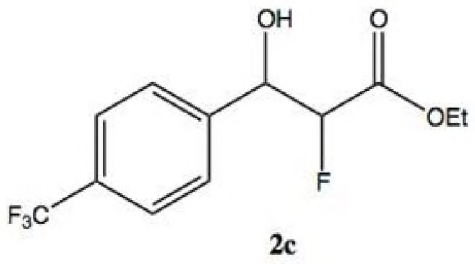

2c

Figure S.4. Ethyl 2-fluoro-3-hydroxy-3-(4-(trifluoromethyl)phenyl)propanoate (**2c**) structure.

Synthesis of 2-fluoro-3-ketoesters (3a-3c)

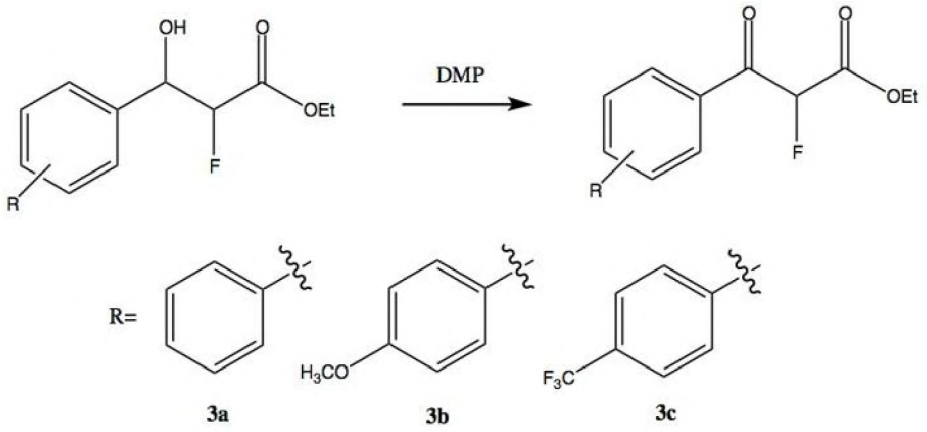

3a **3b** **3c**

Figure S.5. DMP oxidation reaction scheme.

Wet dichloromethane (1 mmol of water was solvated in 30 mL of CH_2Cl_2) was added dropwise to a vigorously stirring solution of 2-fluoro-3-hydroxyester (1 mmol) and Dess-Martin periodinane (0.636 g, 1.5 mmol) in 6 mL of dry CH_2Cl_2. The mixture was stirred at room temperature for 8 hr, then quenched with 1M sodium thiosulphate solution (10mL). The layers were separated, and the organic phase was washed sequentially with saturated aqueous sodium bicarbonate (2 X 30 mL) and water (2 X 30 mL). The combined aqueous washes were then back

extracted with ether (2 X 60 mL). The organic phase was dried with anhydrous $MgSO_4$, filtered, and concentrated. Crude product was purified by flash chromatography (SiO_2, 10% ethyl acetate/hexane) to get pure compound (Graves, 1989).

Ethyl 2-fluoro-3-oxo-3-phenylpropanoate (3a): colorless oil, 89 mg, 92%; ^{1}H NMR (300 MHz, $CDCl_3$) δ 8.17 – 7.93 (m, 2H), 7.73 – 7.44 (m, 3H), 5.86 (d, J = 48.9 Hz, 1H), 4.30 (qd, J = 7.2, 1.1 Hz, 2H), 1.26 (t, J = 7.1 Hz, 3H); ^{13}C NMR (75 MHz, $CDCl_3$) δ 189.5 (d, J = 20.5 Hz), 164.9 (d, J = 24.0 Hz), 133.2 (d, J = 2.2 Hz), 129.5 (d, J = 3.5 Hz), 128.8, 90.0 (d, J = 197.6 Hz), 62.7, 13.9; ^{19}F NMR (282 MHz, $CDCl_3$) δ -190.3 (d, J = 48.9 Hz).

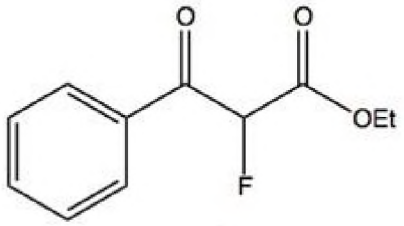

3a

Figure S.6. Ethyl 2-fluoro-3-oxo-3-phenylpropanoate (3a) structure.

Ethyl 2-fluoro-3-(4-methoxyphenyl)-3-oxopropanoate (3b): colorless oil, 116 mg, 85%; ^{1}H NMR (300 MHz, $CDCl_3$) δ 8.13 – 7.93 (m, 2H), 7.05 – 6.85 (m, 2H), 5.81 (d, J = 49.0 Hz, 1H), 4.29 (qd, J = 7.1, 2.0 Hz, 2H), 3.89 (s, 3H), 1.26 (t, J = 7.1 Hz, 3H); ^{13}C NMR (75 MHz, $CDCl_3$) δ 187.8 (d, J = 19.8 Hz), 165.2, (d, J = 24.3 Hz), 164.6, 132.0 (d, J = 3.5 Hz), 126.2 (d, J = 2.1 Hz), 114.0, 89.9 (d, J 196.7 Hz), 62.5, 55.5, 13.9; ^{19}F NMR (282 MHz, $CDCl_3$) δ -189.5 (d, J = 49.0 Hz).

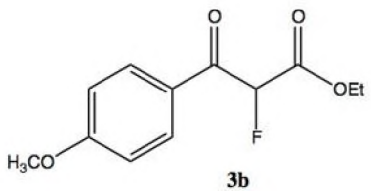

3b

Figure S.7. Ethyl 2-fluoro-3-(4-methoxyphenyl)-3-oxopropanoate (3b) structure.

Ethyl 2-fluoro-3-oxo-3-(4-(trifluoromethyl)phenyl)propanoate (3c): colorless oil, 92 mg, 92%; ^{1}H NMR (300 MHz, $CDCl_3$) δ 8.16 (dt, J = 8.9, 0.9 Hz, 2H), 7.82 – 7.72 (m, 2H), 5.84 (d, J = 48.8 Hz, 1H), 4.32 (qd, J = 7.1, 1.9 Hz, 2H), 1.28 (t, J = 7.2 Hz, 3H); ^{13}C NMR (75 MHz, $CDCl_3$) δ 188.9 (d, J = 21.1 Hz), 164.2 (d, J = 23.9 Hz), 135.9 (m),135.5 (q, J = 33.0 Hz) 129.9 (d, J = 3.8 Hz), 125.8 (q, J = 3.8 Hz), 123.9 (q, J = 273.1 Hz), 90.3 (d, 198.5 Hz), 63.0 , 13.9; ^{19}F NMR (282 MHz, $CDCl_3$) δ -63.43 s, 3F), -190.4 (d, J = 48.9 Hz, 1F).

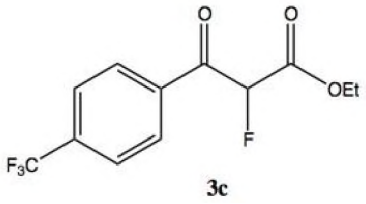

3c

Figure S.8. Ethyl 2-fluoro-3-oxo-3-(4-(trifluoromethyl)phenyl)propanoate (**3c**) structure.

KRED Reactions (4a-4c) NADH system: Into a solution of β-ketoester (50 µmol) in 100 µL methanol, was added KRED Mix N (114.8 mg in 2.0 mL deionized H_2O) and 2.0 mg ketoreductase. The mixture was shaken at 37 ± 1 °C. After 24 hours, the reaction was extracted with ethyl acetate (2 x 1 mL). The combined organic extract was dried over anhydrous sodium sulfate and was subjected to ^{1}H and ^{19}F NMR spectroscopy (Dai, Guillemette, & Green, 2013).

Ethyl-2-fluoro-3-hydroxy-3-phenylpropanoate (4a): ^{1}H NMR (300 MHz, CDCl3) *anti* δ 5.05 (dd,J = 47.7, 5.0, 1H, H-2), *syn* 5.02 (dd, J = 48.0, 3.7, 1H, H-2); ^{19}F NMR (282 MHz, $CDCl_3$) *anti* δ-197.78 (dd, J = 47.7, 16.5 Hz), *syn* δ -202.87 (dd, J = 48.0, 22.2 Hz).

4a (KRED 110) **4a (KRED 130)**

Figure S.9. (2S,3S)-ethyl 2-fluoro-3-hydroxy-3-phenylpropanoate (4a (KRED110)) and (2S,3R)-ethyl 2-fluoro-3-hydroxy-3-phenylpropanoate (4a (KRED130)) structures.

Ethyl-2-fluoro-3-(4-methoxyphenyl)propanoate (4b): ^{1}H NMR (300 MHz, $CDCl_3$) *anti* δ 5.00 (dd, J = 49.9, 5.0 Hz, 1H, H-2), *syn* 4.98 (dd, J = 48.1, 3.9 Hz, 1H, H-2); ^{19}F NMR (282 MHz, $CDCl_3$) *anti* δ -198.4 (dd, J = 49.9, 14.5 Hz), *syn* δ -202.1 (dd, J = 48.1, 21.8 Hz)

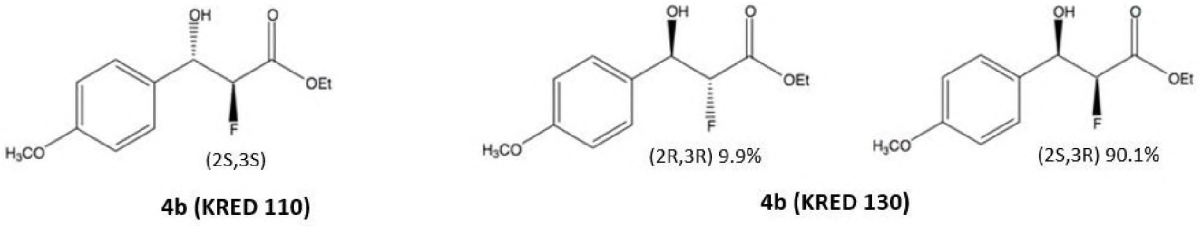

Figure S.10. (2S,3S)-ethyl 2-fluoro-3-hydroxy-3-(4-methoxyphenyl)propanoate (4b (KRED 110)) structure. 4b (KRED 130) contained 9.9% (2R,3R)-ethyl 2-fluoro-3-hydroxy-3-(4-methoxyphenyl)propanoate and 90.1% (2S,3R)-ethyl 2-fluoro-3-hydroxy-3-(4-methoxyphenyl)propanoate.

Ethyl-2-fluoro-3-hydroxy-3-(4-(trifluoromethyl)phenyl)propanoate (4c): ^{1}H NMR (300 MHz, $CDCl_3$) *anti* 5.03 (dd, J = 48.0, 5.1 Hz, 1H), *syn* 5.02 (dd, J = 47.6, 3.6 Hz); ^{19}F NMR (282 MHz, $CDCl_3$) *anti* δ -197.08 (dd, J = 48.0, 14.8 Hz), *syn* δ -203.38 (dd, J = 47.6, 22.0 Hz).

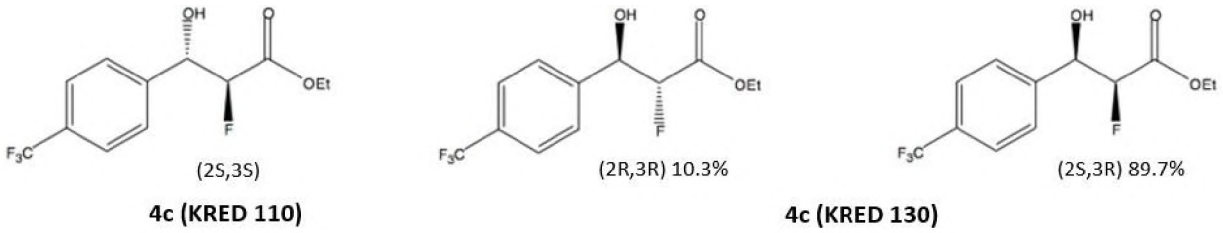

Figure S.11. (2S,3S)-ethyl 2-fluoro-3-hydroxy-3-(4-(trifluoromethyl)phenyl)propanoate (4c (KRED 110)). 4c (KRED 130) contained 10.3% (2R,3R)-ethyl 2-fluoro-3-hydroxy-3-(4-(trifluoromethyl)phenyl)propanoate and 89.7% (2S,3R)-ethyl 2-fluoro-3-hydroxy-3-(4-(trifluoromethyl)phenyl)propanoate.

Mosher Ester Synthesis and Analysis: In-tube derivatization, similar to the method previously described by Gao et al., was used to synthesize α-methoxy-α-trifluoromethylphenylacetic acid (MPTA) esters of the KRED product alcohols (Gao J, 2017). Approximately 50 μmol of KRED reduced product was dissolved in 0.6 mL of $CDCl_3$ in an NMR tube. To which was added a solution of approximately 0.3 mL of $CDCl_3$, either R- or S-

MTPA (0.0176 g, 75 μmol, 3 equivalents), N,N'-dicyclohexylcarbodiimide (DCC) (0.0154 g, 75 μmol, 3 eq), and 4-dimethylaminopyridine (DMAP) (0.00915 g, 75 μmol, 3 eq). A small amount of 3Å molecular sieves was added (0.5 cm in height). The NMR tube and its contents was then allowed to react overnight at 37°C. In some instances, a solid precipitate formed and dissolved upon mixing. The NMR tube contents were then analyzed directly by ^{19}F NMR spectroscopy to assess stereoisomeric ratios. To minimize signal to noise ratio, a minimum of 2000 transients were collected. The typical spectrum yielded the following chemical shift and coupling information:

Phenyl Derivatives: Racemic + (*S*)-MTPA ^{19}F NMR (282 MHz, $CDCl_3$) δ -198.8 (dd, J = 48.69, 20.95 Hz), -199.03 (dd, J = 47.5, 21.73 Hz), -200.91 (dd, J = 44.88, 21.49 Hz), -200.94 (dd, J = 43.09, 20.74 Hz) 4a (KRED 130) + (*R*)-MTPA ^{19}F NMR (282 MHz, $CDCl_3$) δ -199.0 (dd, J = 47.5, 21.8 Hz) 4a (KRED 130) + (*S*)-MTPA ^{19}F NMR (282 MHz, $CDCl_3$) δ -200.9 (dd, J = 47.3, 23.0 Hz) 4a (KRED 110) + (*R*)-MTPA ^{19}F NMR (282 MHz, $CDCl_3$) δ -200.9 (dd, J = 49.0, 21.3 Hz) 4a (KRED 110) + (*S*)-MTPA ^{19}F NMR (282 MHz, $CDCl_3$) δ -198.8 (dd, J = 48.8, 20.8 Hz)

4-methoxy Derivatives: Racemic + (*S*)-MTPA ^{19}F NMR (282 MHz, $CDCl_3$) δ -198.3 (dd, J = 47.8, 21.3 Hz), -199.6 (dd, J = 49.0, 21.5 Hz), -200.4 (dd, J = 47.4, 22.8 Hz), -201.4 (dd, J = 49.1, 21.9 Hz) 4b (KRED 130) + (*R*)-MTPA ^{19}F NMR (282 MHz, $CDCl_3$) δ -198.3 (dd, J = 47.8, 21.3 Hz) 4b (KRED 130) + (*S*)-MTPA ^{19}F NMR (282 MHz, $CDCl_3$) δ -200.4 (dd, J = 47.4, 22.9 Hz) 4b (KRED 110) + (*R*)-MTPA ^{19}F NMR (282 MHz, $CDCl_3$) δ -201.4 (dd, J = 49.1, 21.8 Hz) 4b (KRED 110) + (*S*)-MTPA ^{19}F NMR (282 MHz, $CDCl_3$) δ -199.6 (dd, J = 49.1, 21.5 Hz)

4-trifluoromethly Derivatives: Racemic + (*S*)-MTPA ^{19}F NMR (282 MHz, $CDCl_3$) δ -199.0 (dd, J = 48.5, 20.7 Hz), -201.0 (dd, J = 46.9, 22.8 Hz), -201.2 (dd, J = 48.7, 21.4 Hz), -

202.6 (dd, J = 46.4, 24.0 Hz) 4c (KRED 130) + (*R*)-MTPA ^{19}F NMR (282 MHz, $CDCl_3$) δ -198.9 (dd, J = 48.4, 20.7 Hz), -201.2 (dd, J = 46.9, 22.9 Hz) 4c (KRED 130) + (*S*)-MTPA ^{19}F NMR (282 MHz, $CDCl_3$) δ -201.1 (dd, J = 48.7, 21.2 Hz), -202.8 (dd, J = 46.9, 23.8 Hz) 4c (KRED 110) + (*R*)-MTPA ^{19}F NMR (282 MHz, $CDCl_3$) δ -201.1 (dd, J = 48.8, 21.3 Hz) 4c (KRED 110) + (*S*)-MTPA ^{19}F NMR (282 MHz, $CDCl_3$) δ -199.0 (dd, J = 48.5, 20.8 Hz)

A2. NMR Spectra

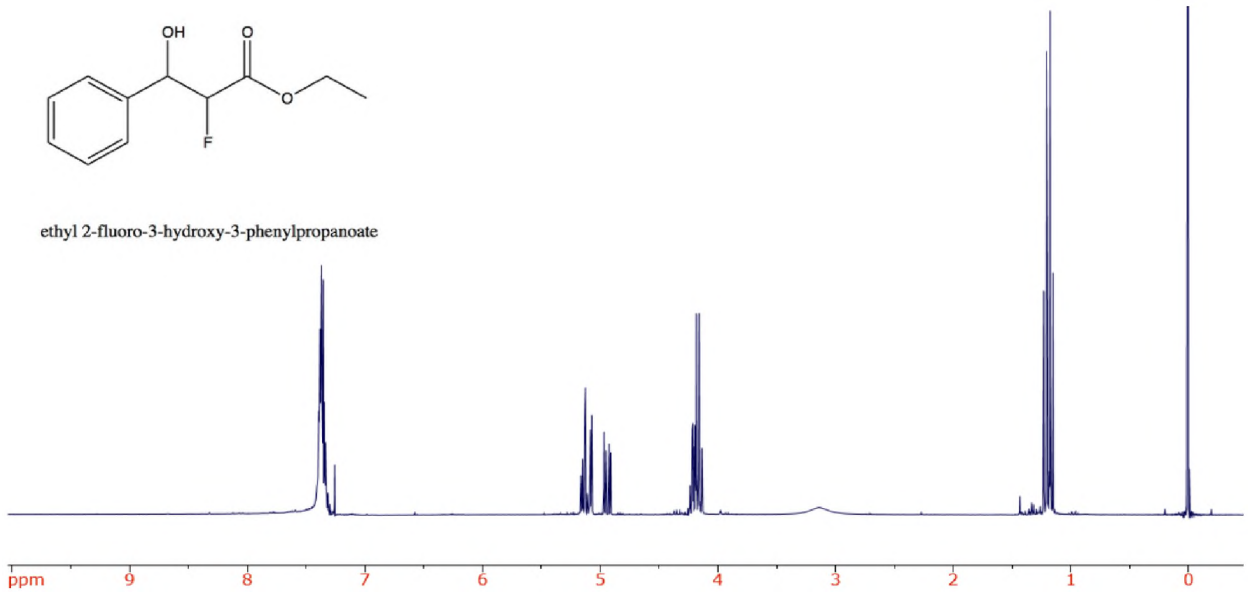

Figure A.1. ^{1}H NMR spectrum of product 2a.

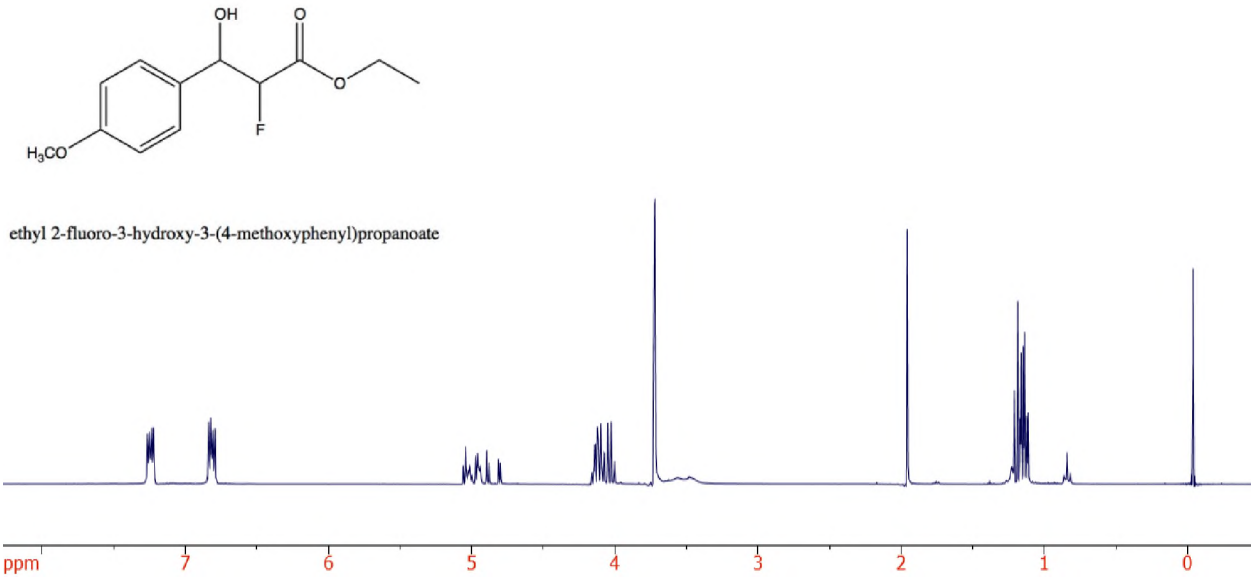

Figure A.2. ^{1}H NMR spectrum of product 2b.

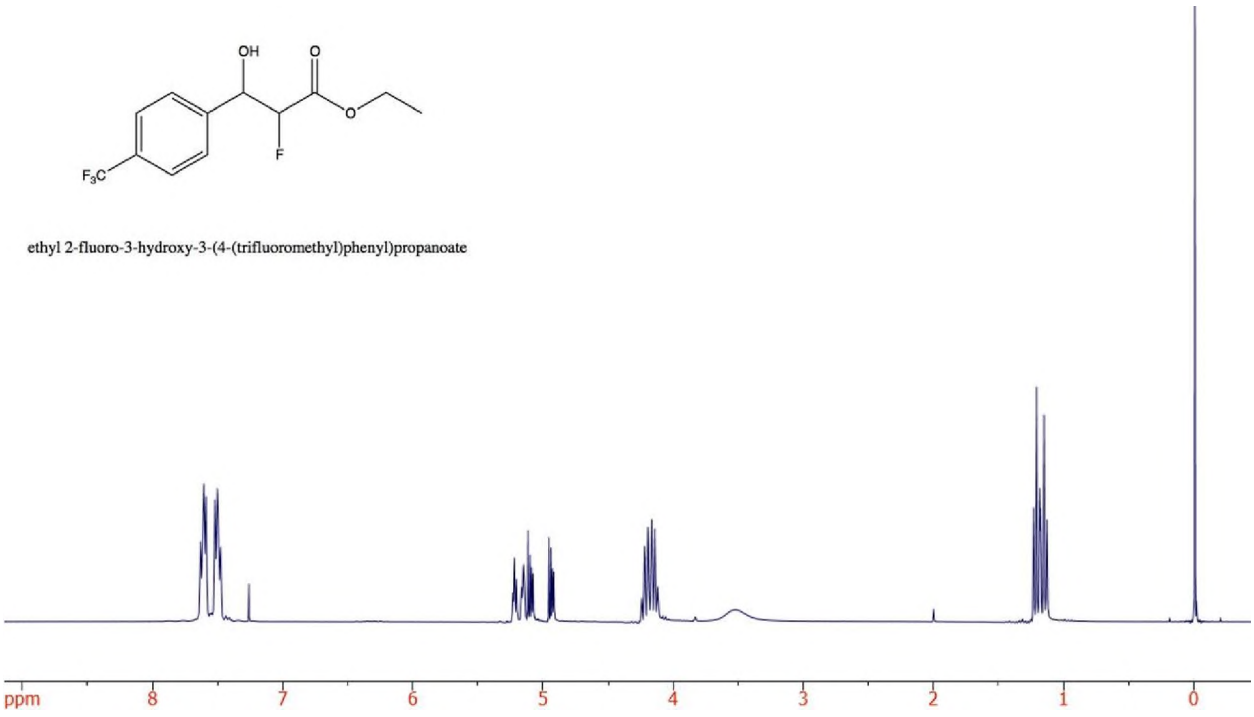

Figure A.3. ^{1}H NMR spectrum of product 2c.

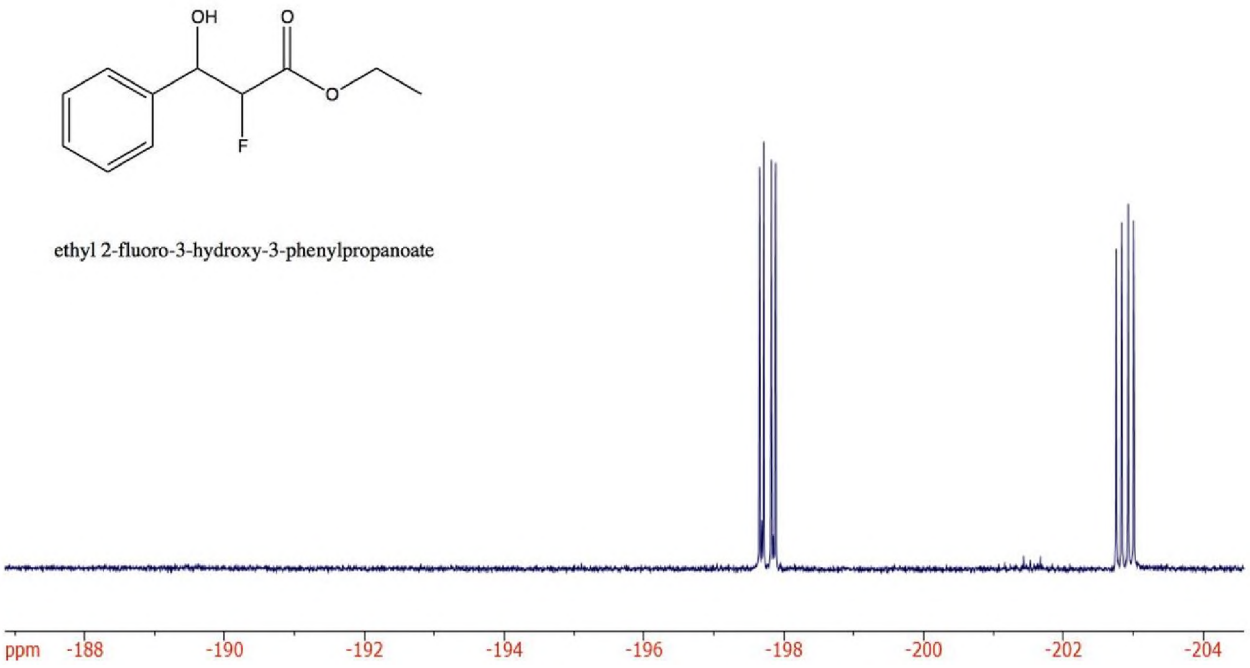

Figure A.4. ^{19}F NMR spectrum of product 2a.

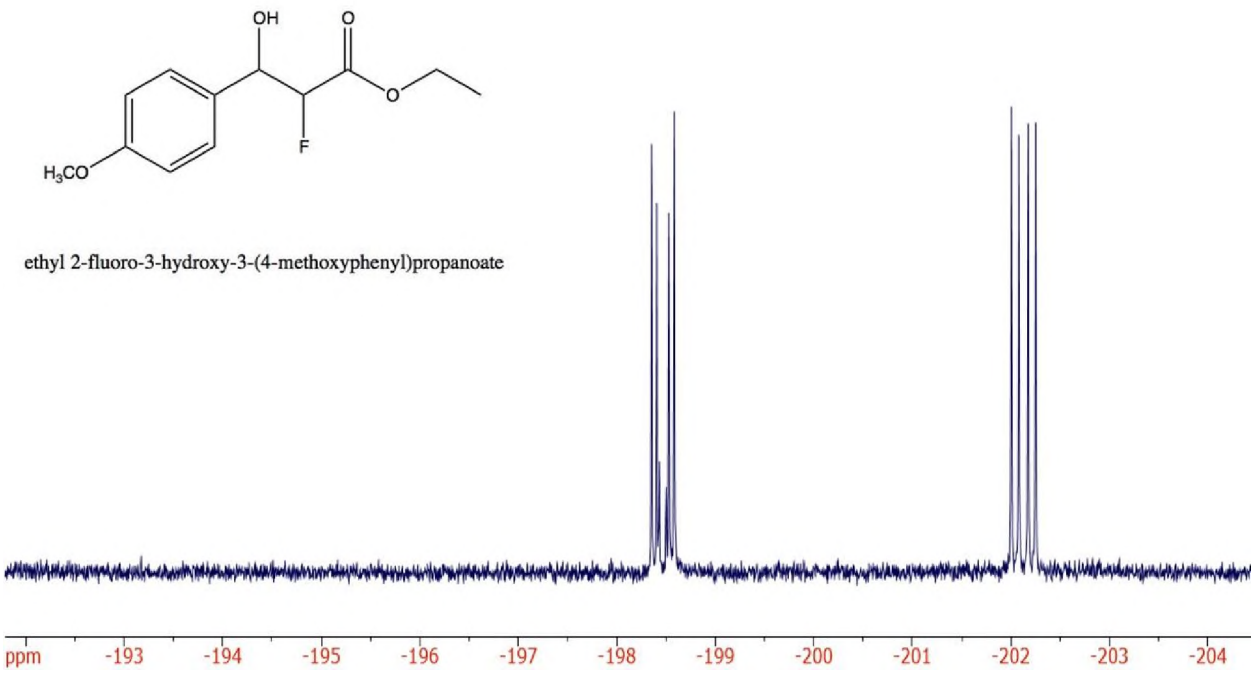

Figure A.5. ^{19}F NMR spectrum of product 2b.

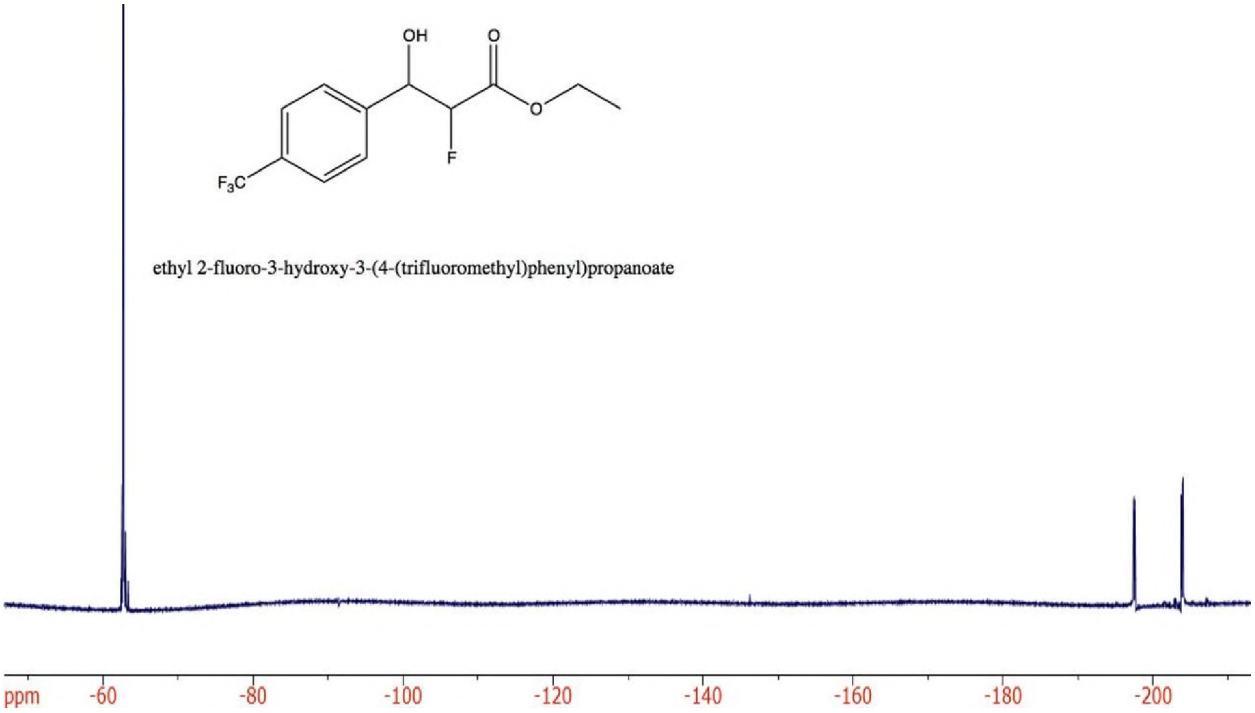

Figure A.6. ^{19}F NMR spectrum of product 2c.

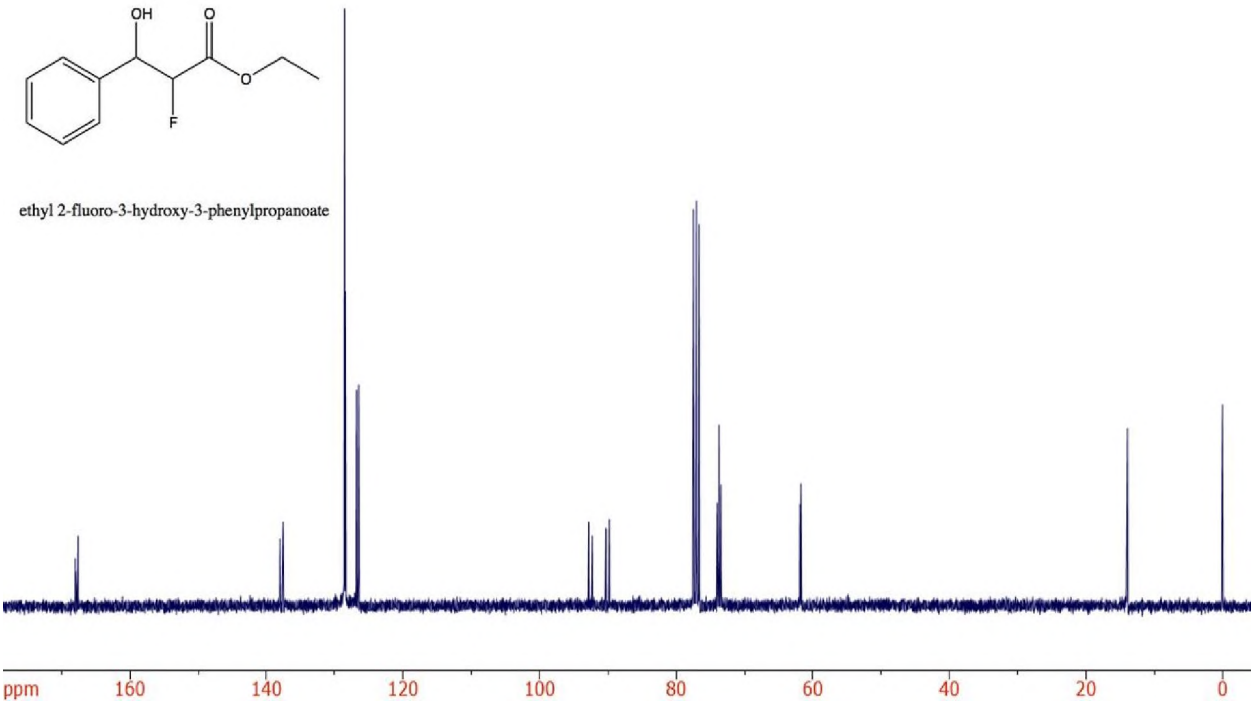

Figure A.7. ^{13}C NMR spectrum of product 2a.

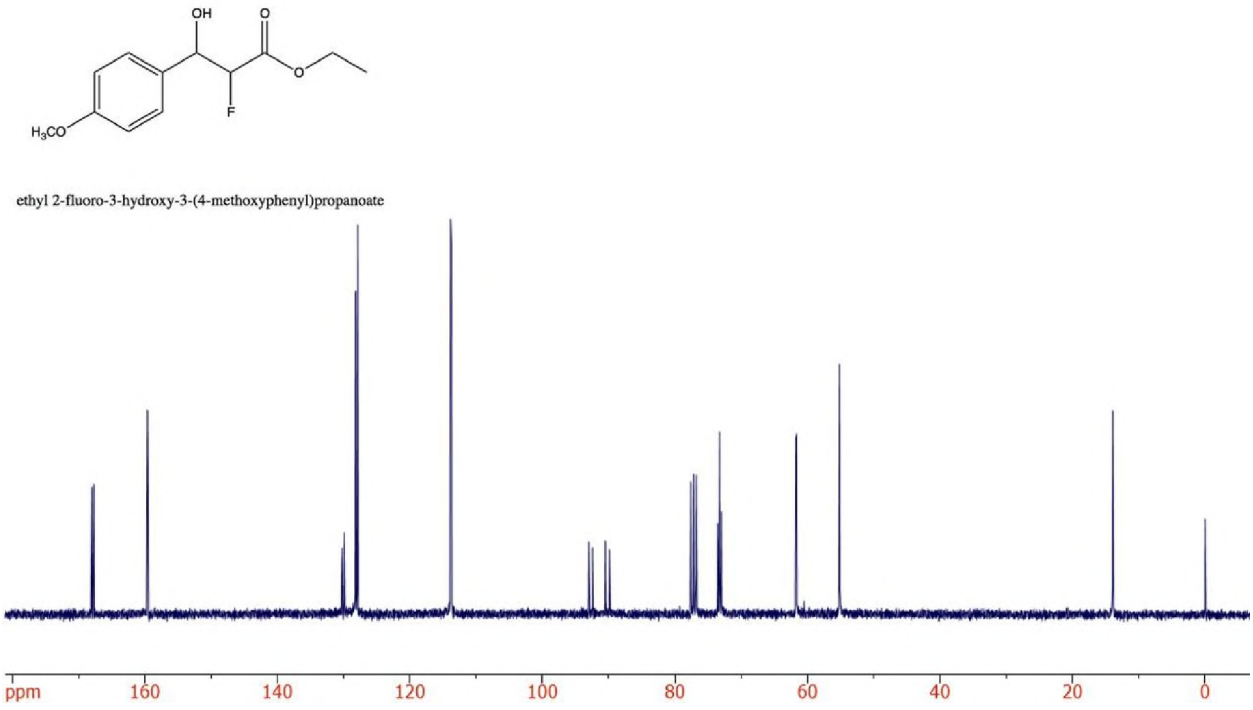

Figure A.8. ^{13}C NMR spectrum of product 2b.

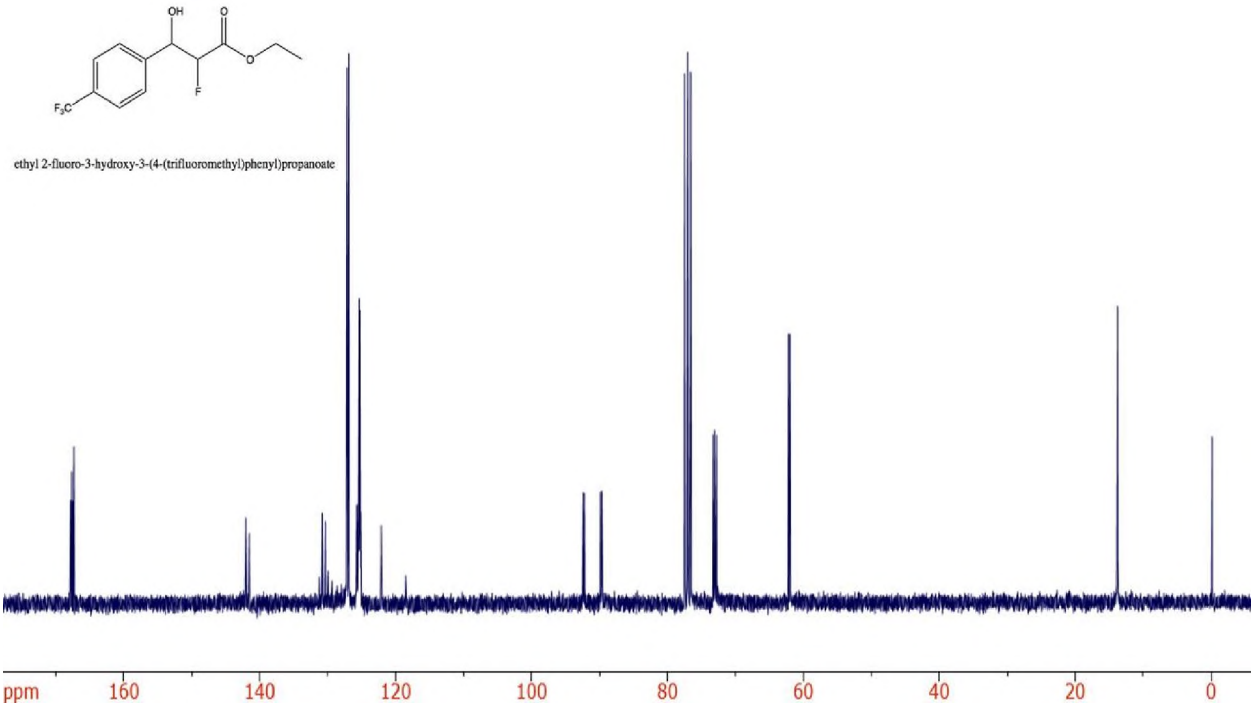

Figure A.9. ^{13}C NMR spectrum of product 2c.

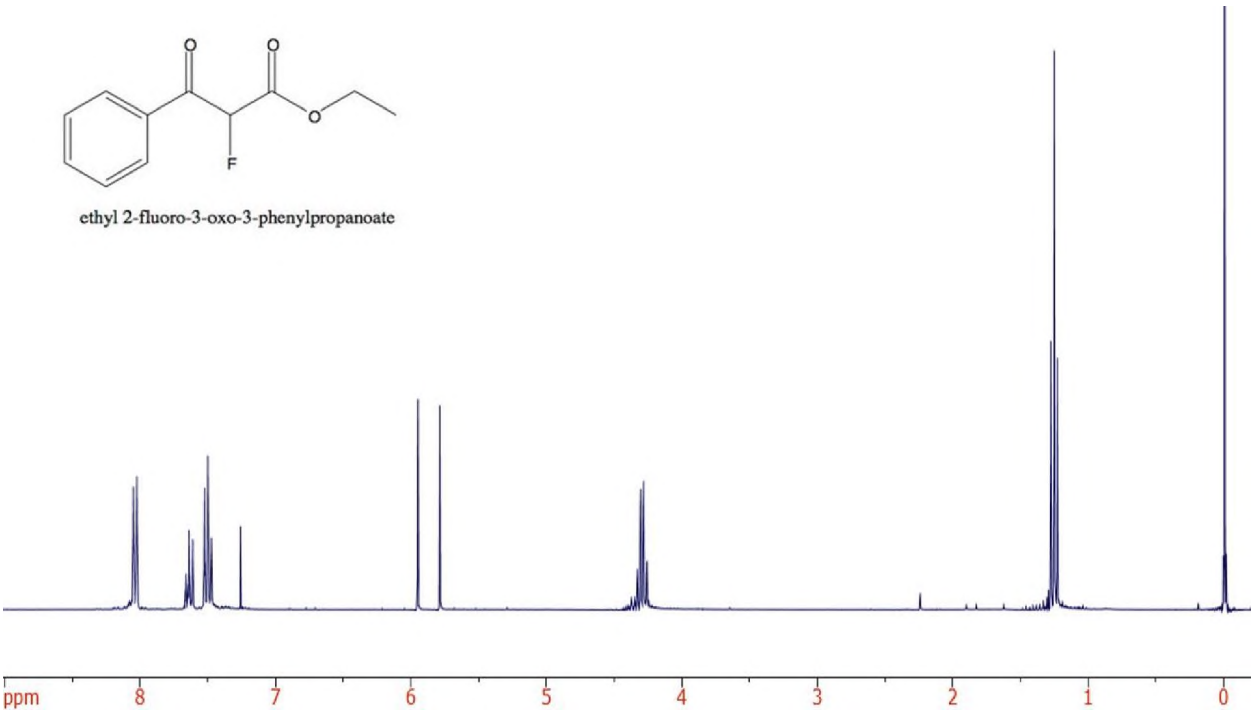

Figure A.10. ^{1}H NMR spectrum of product 3a.

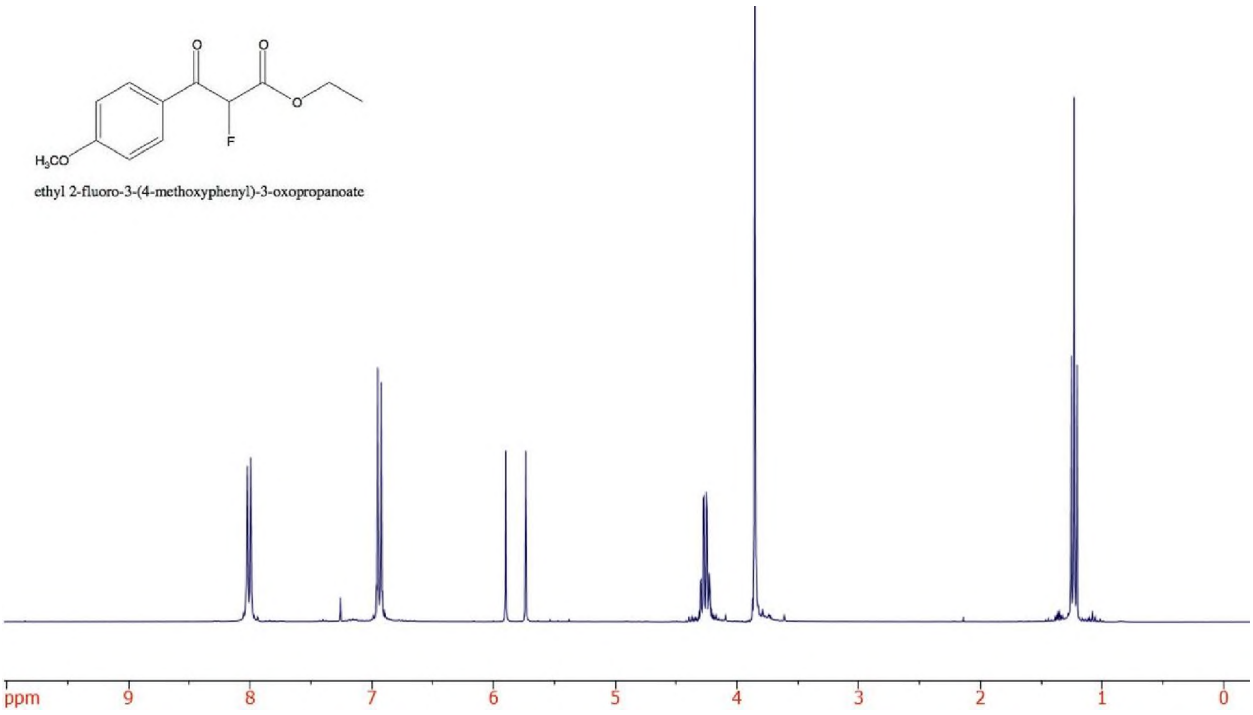

Figure A.11. ^{1}H NMR spectrum of product 3b.

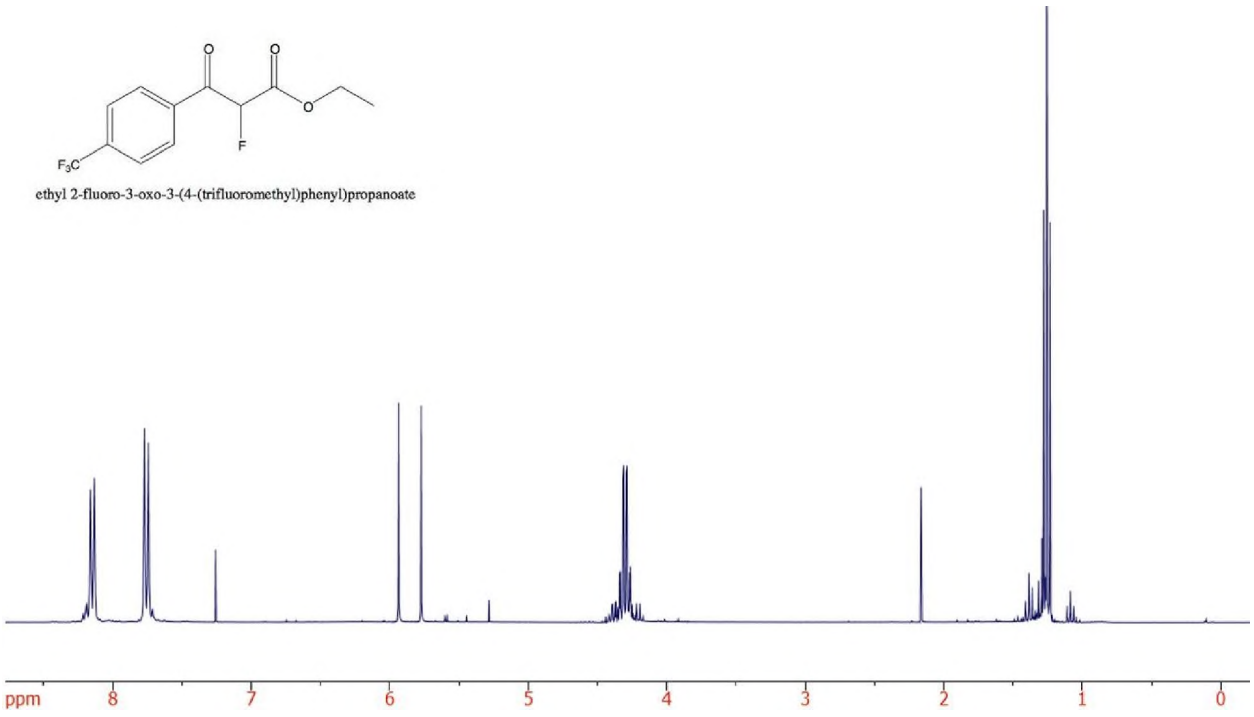

Figure A.12. ^{1}H NMR spectrum of product 3c.

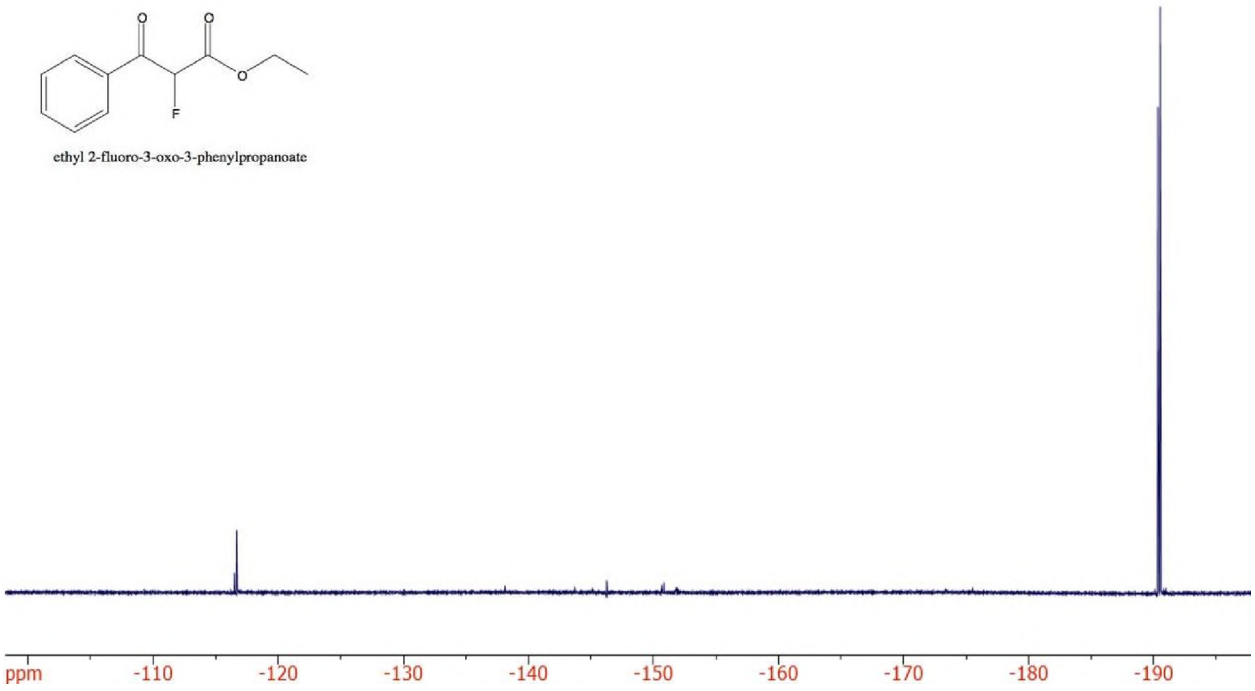

Figure A.13. ^{19}F NMR spectrum of product 3a.

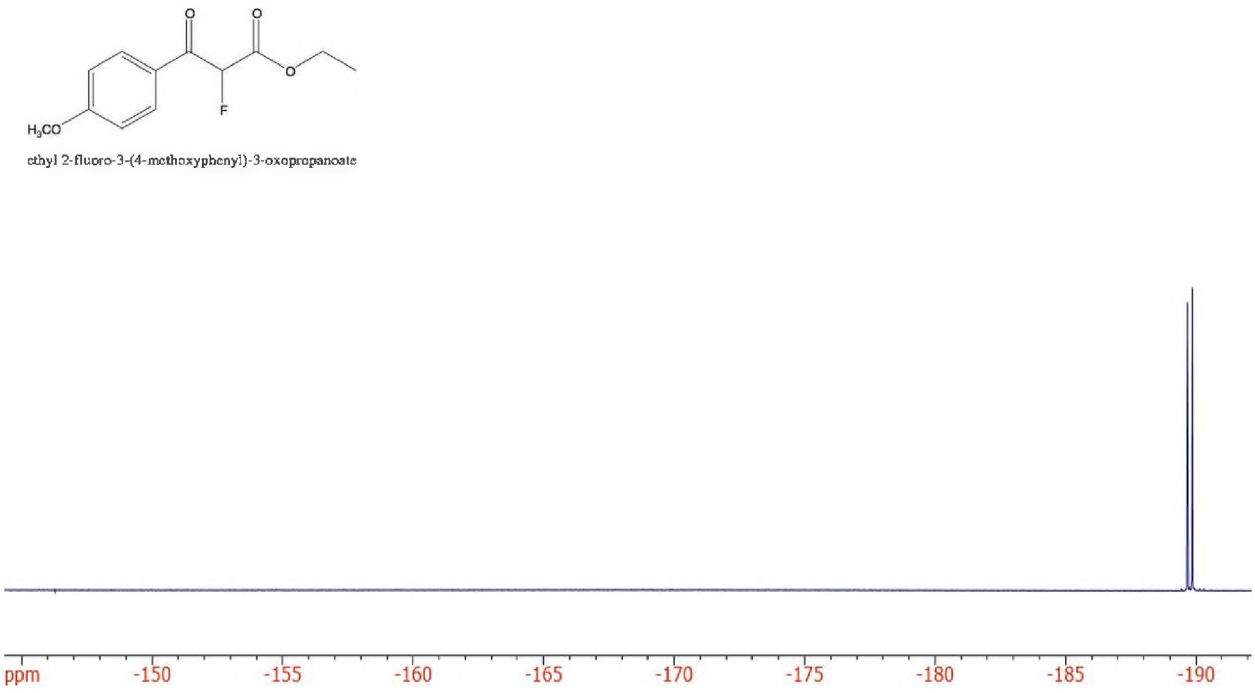

Figure A.14. ^{19}F NMR spectrum of product 3b.

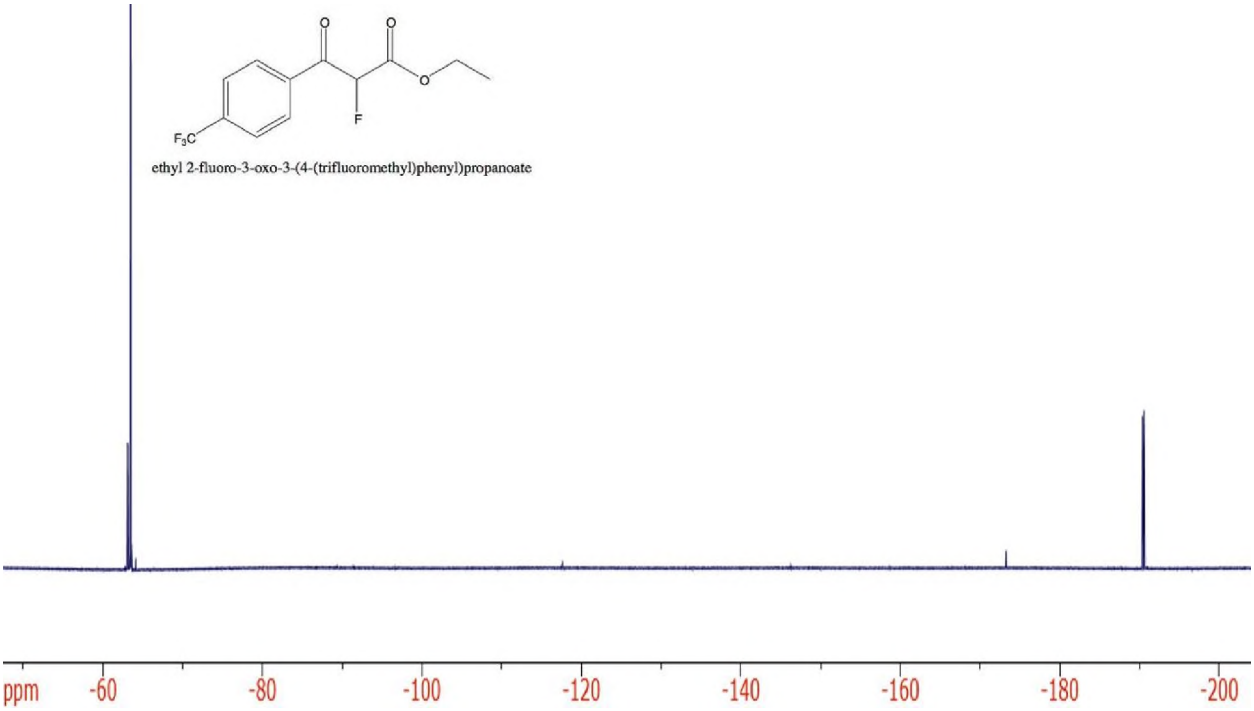

Figure A.15. ^{19}F NMR spectrum of product 3c.

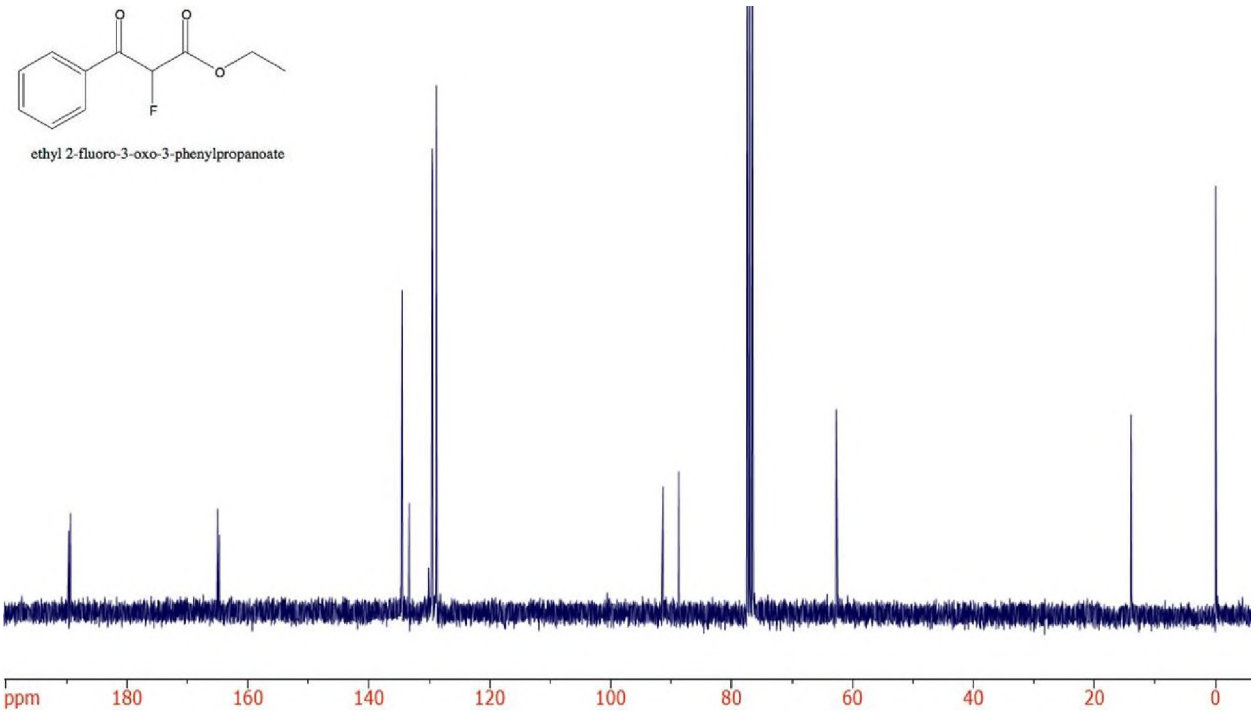

Figure A.16. ^{13}C NMR spectrum of product 3a.

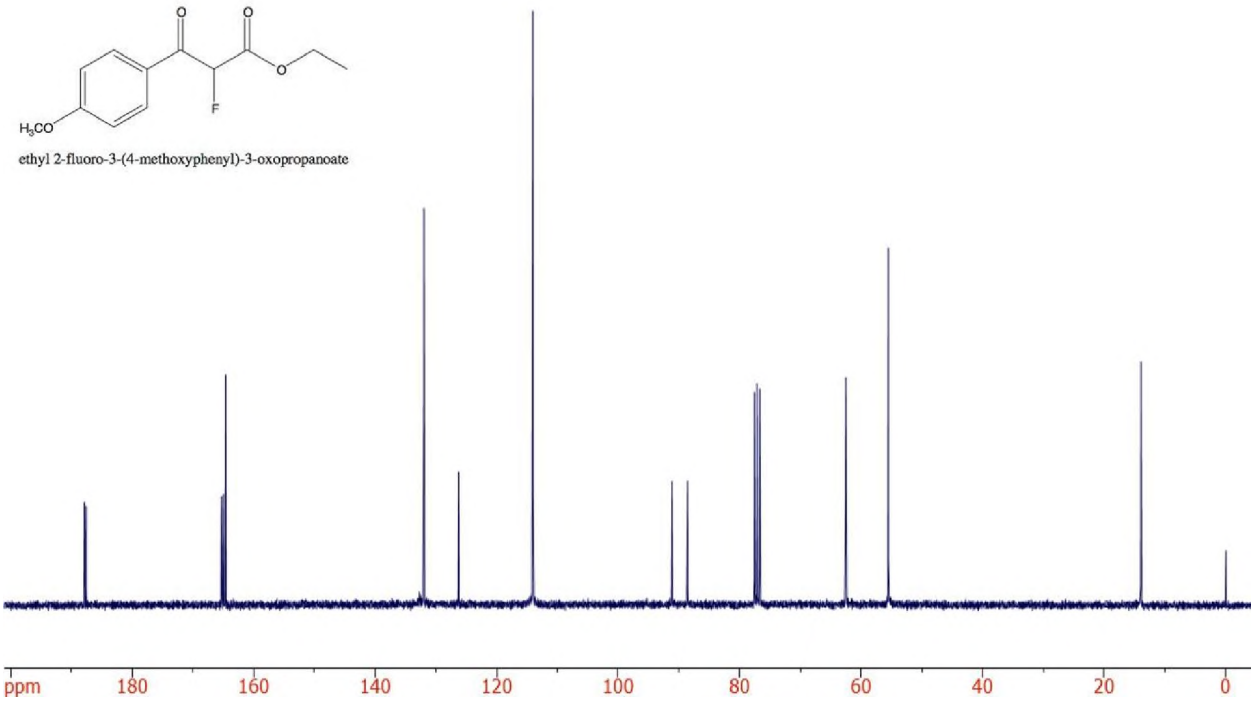

Figure A.17. ^{13}C NMR spectrum of product 3b.

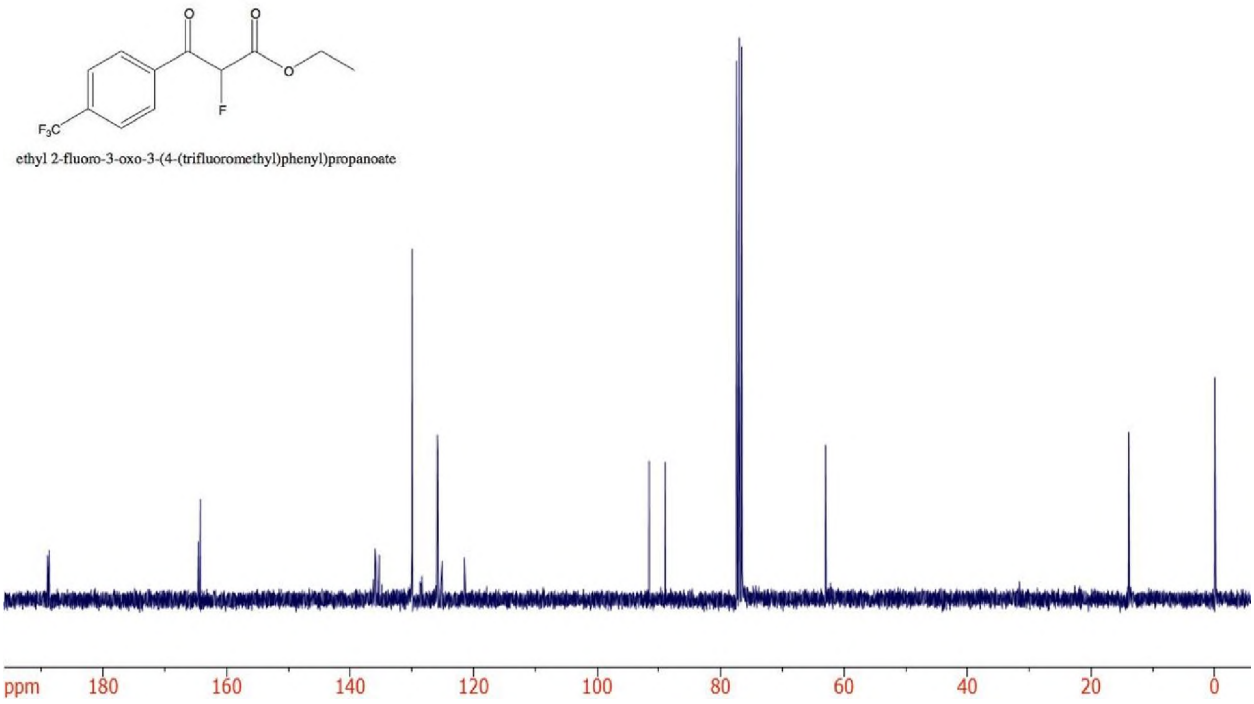

Figure A.18. ^{13}C NMR spectrum of product 3c.

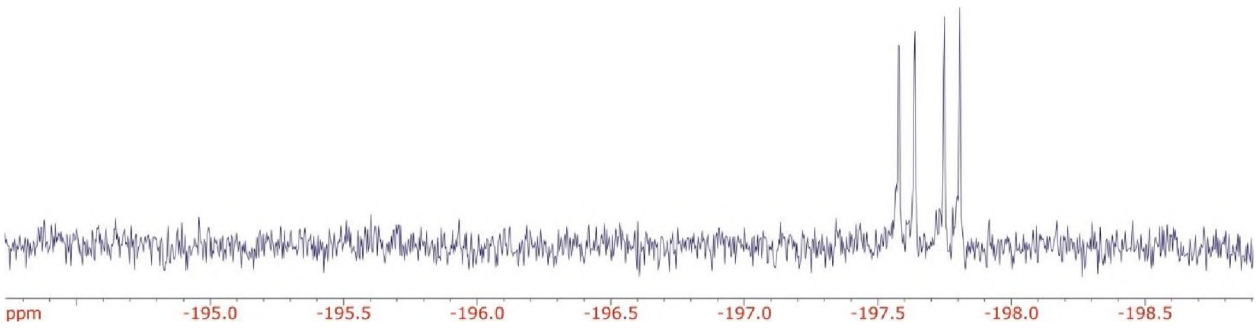

Figure A.19. ^{19}F NMR spectrum of 4a (KRED 110).

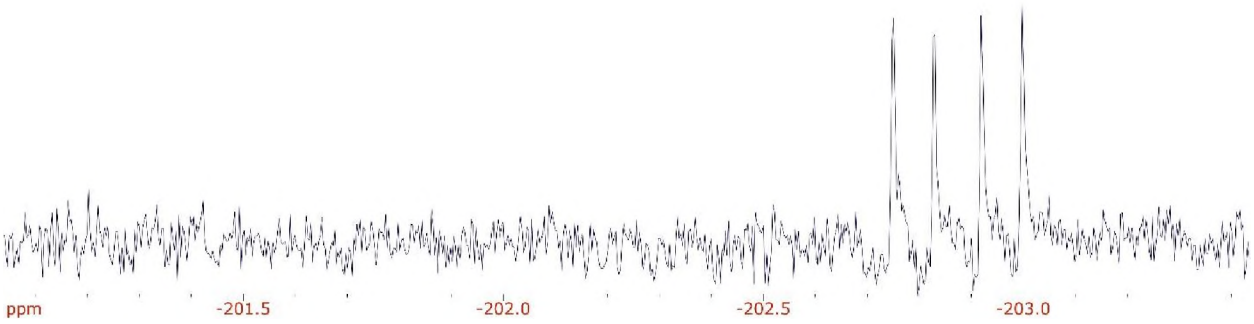

Figure A.20. ^{19}F NMR spectrum of 4a (KRED 130).

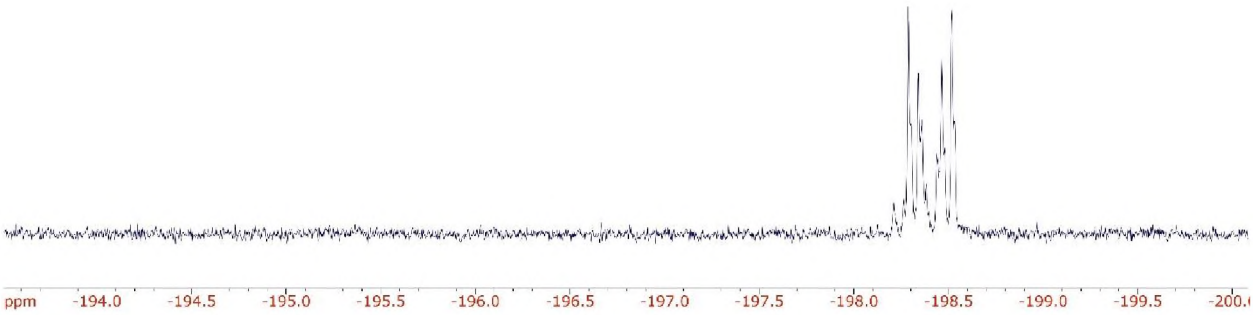

Figure A.21. ^{19}F NMR spectrum of 4b (KRED 110).

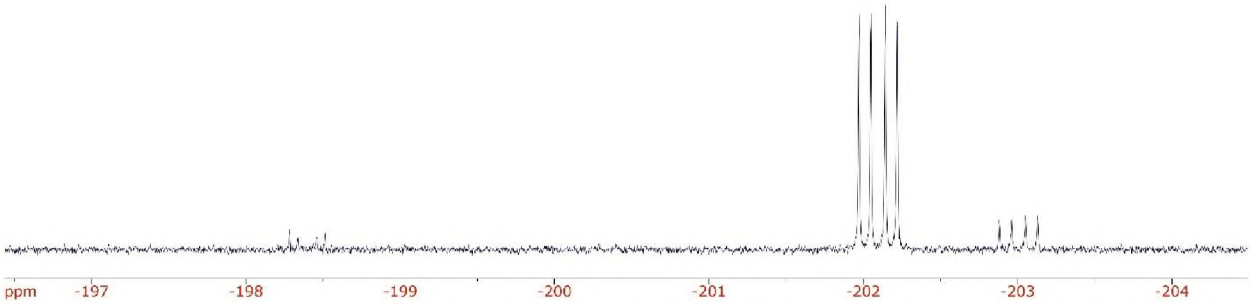

Figure A.22. ^{19}F NMR spectrum of 4b (KRED 130).

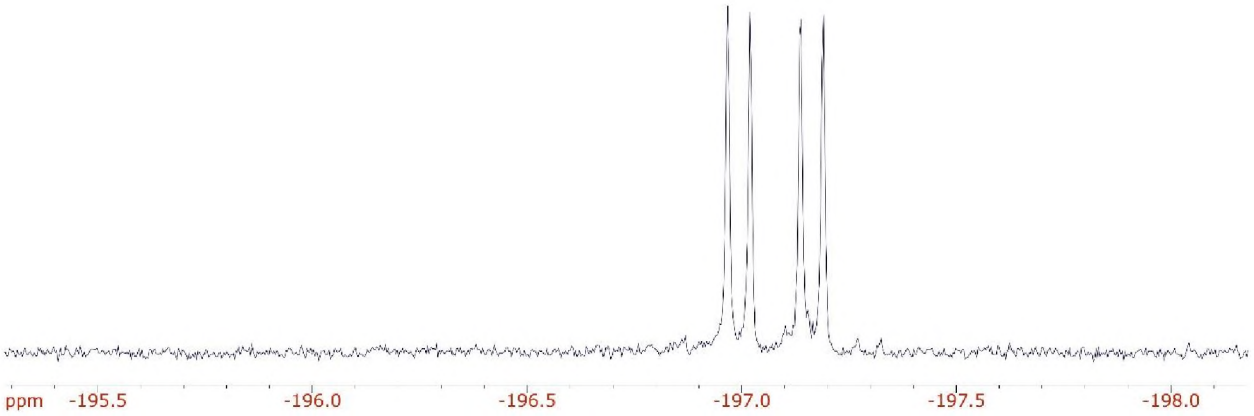

Figure A.23. ^{19}F NMR spectrum of 4c (KRED 110).

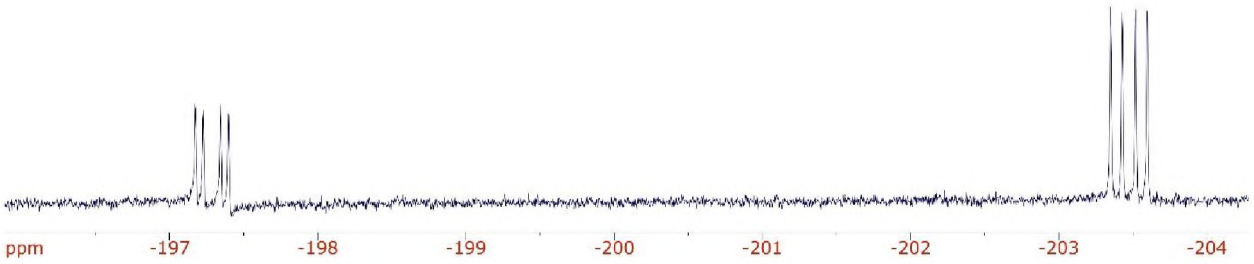

Figure A.24. ^{19}F NMR spectrum of 4c (KRED 130).

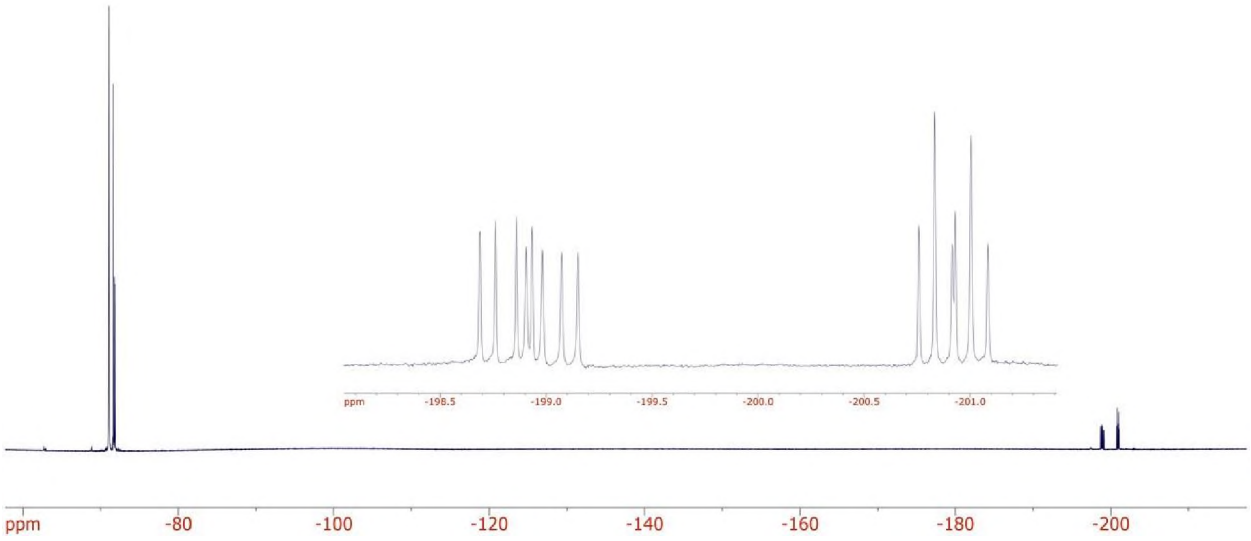

Figure A.25. ^{19}F NMR spectrum of Mosher ester product of racemic phenyl derivative, 2a, and (*S*)-MTPA.

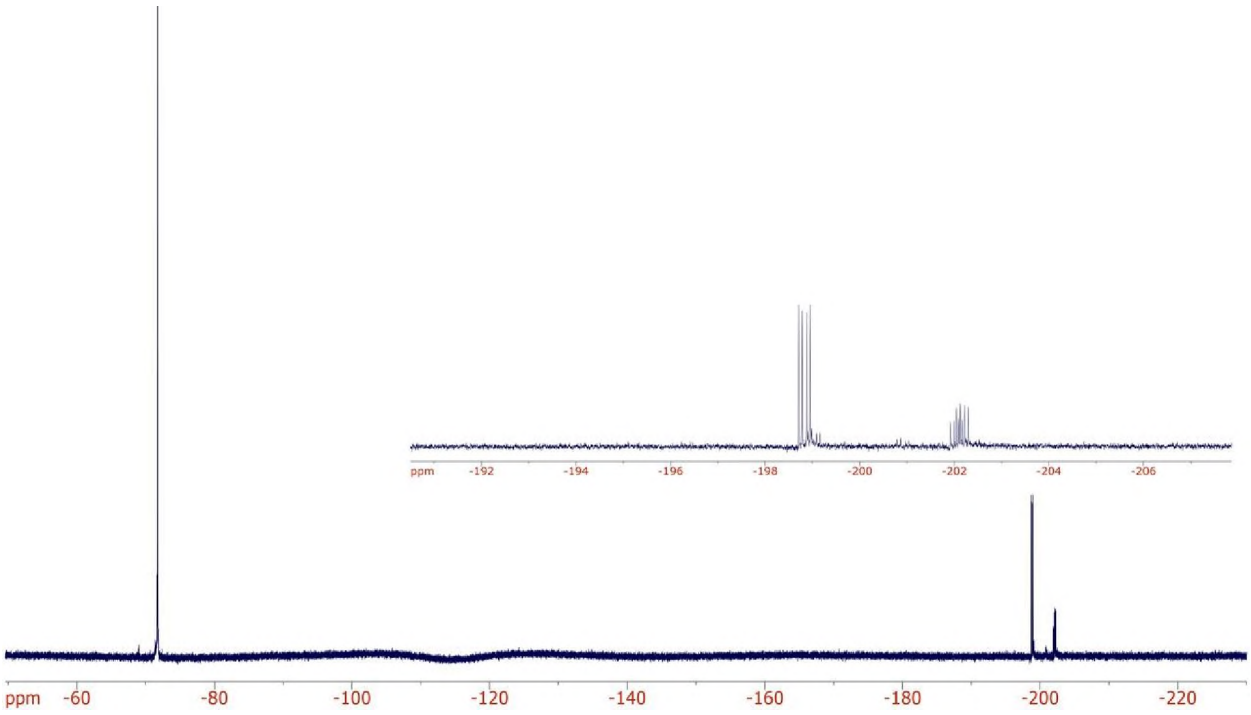

Figure A.26. ^{19}F NMR spectrum of Mosher ester product of 4a (KRED 110) and (*S*)-Mosher's acid.

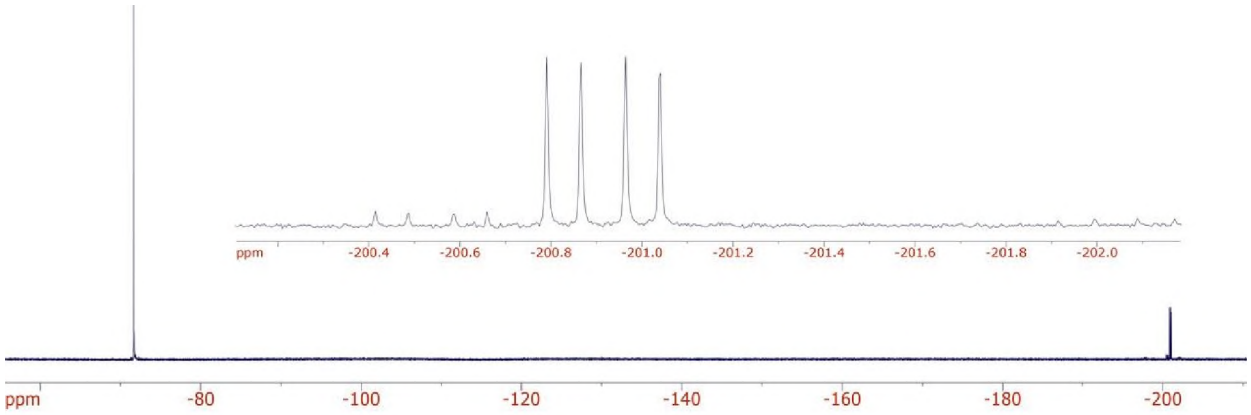

Figure A.27. ^{19}F NMR spectrum of Mosher ester product of 4a (KRED 110) and (*R*)-Mosher's acid.

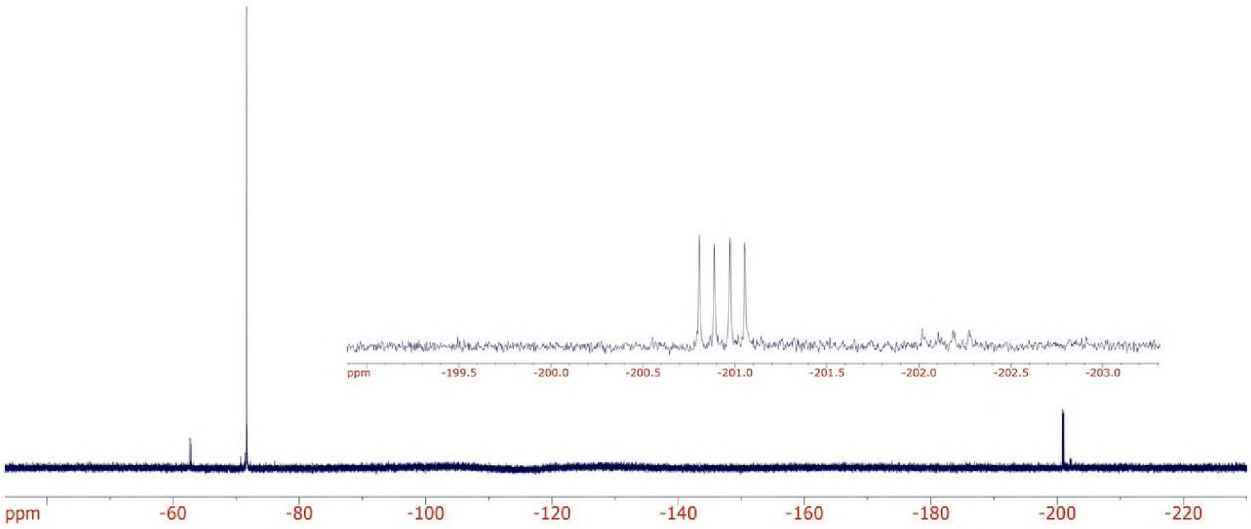

Figure A.28. ^{19}F NMR spectrum of Mosher ester product of 4a (KRED 130) and (*S*)-Mosher's acid.

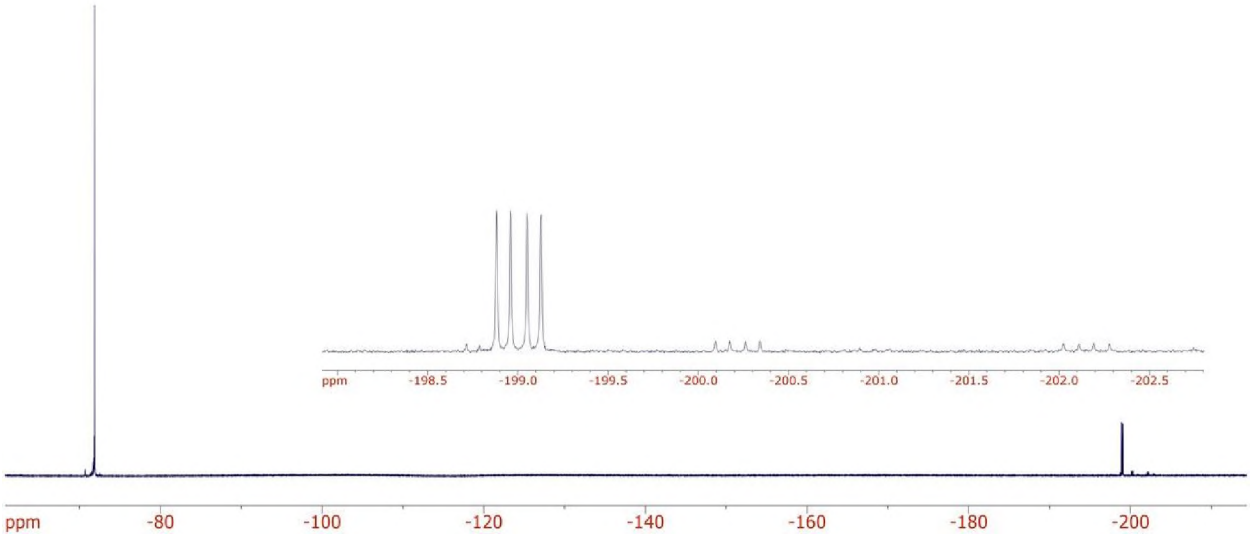

Figure A.29. ^{19}F NMR spectrum of Mosher ester product of 4a (KRED 130) and (*R*)-Mosher's acid.

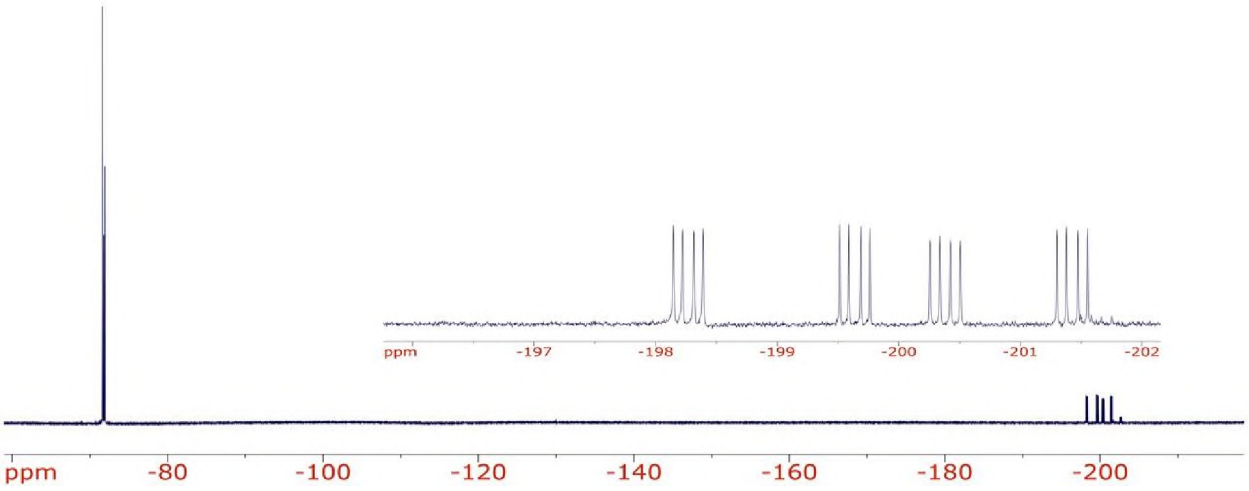

Figure A.30. ^{19}F NMR spectrum of Mosher ester product of racemic 4-methoxy derivative, 2b, and (*S*)-MTPA.

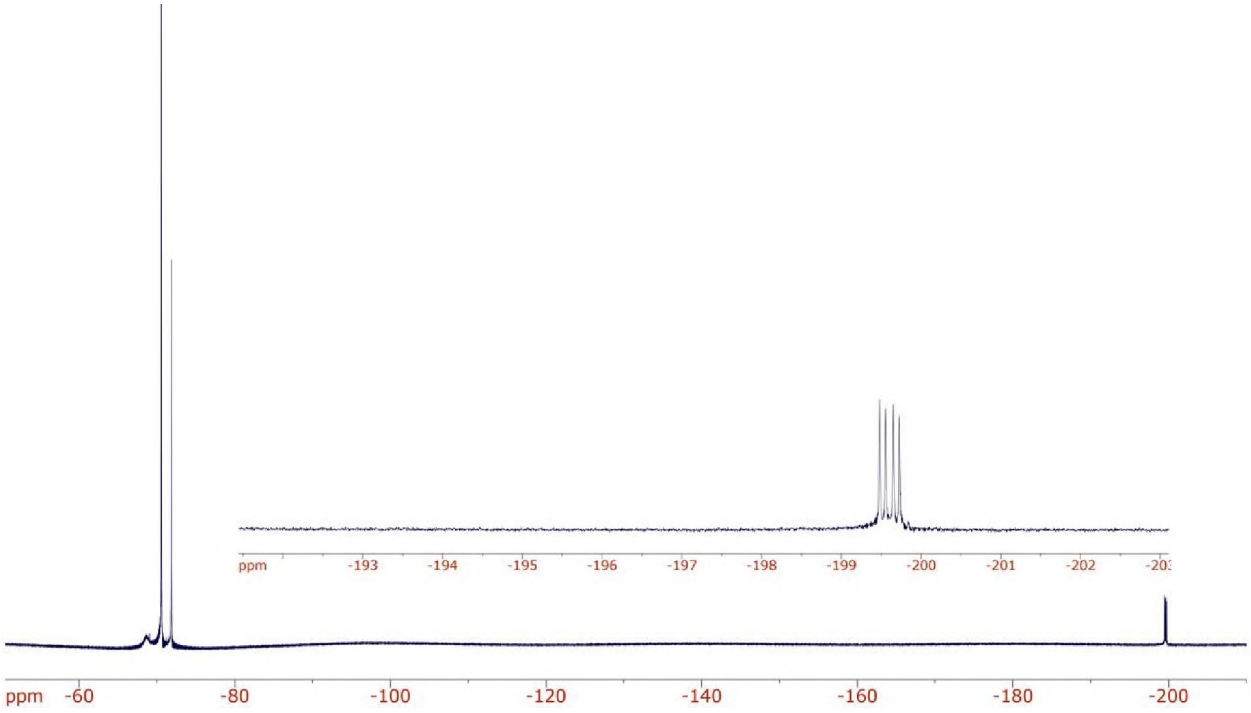

Figure A.31. ^{19}F NMR spectrum of Mosher ester product of 4b (KRED 110) and (*S*)-Mosher's acid.

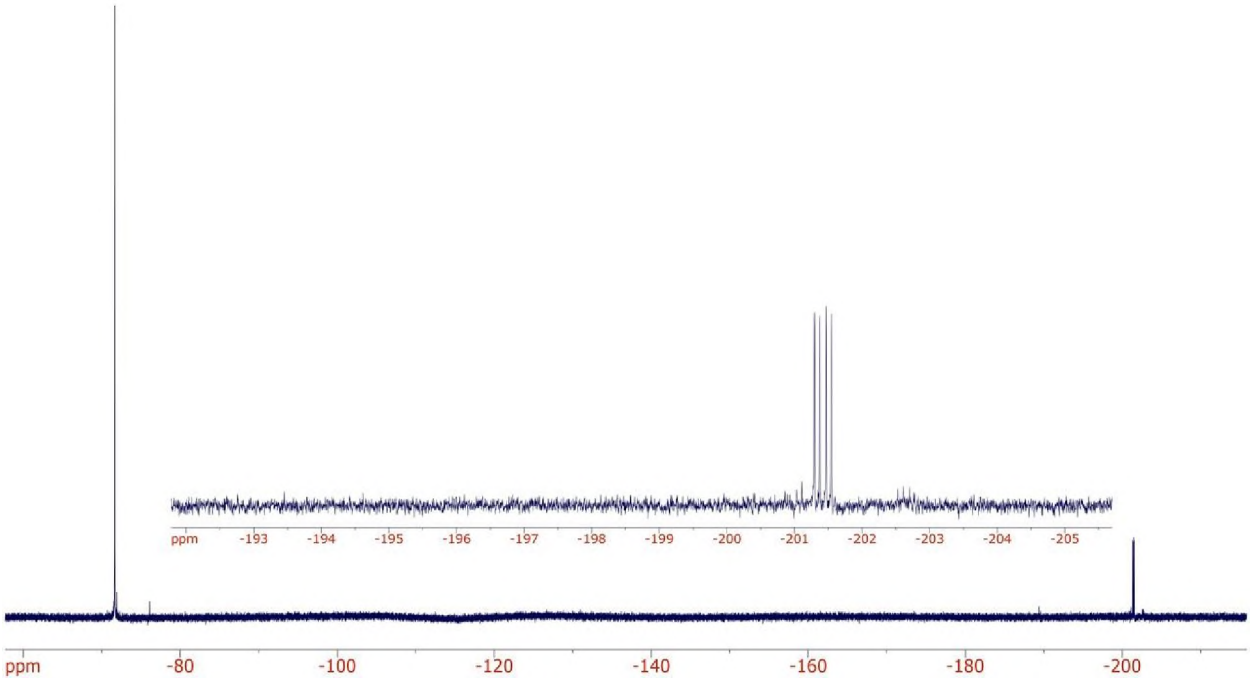

Figure A.32. ^{19}F NMR spectrum of Mosher ester product of 4b (KRED 110) and (*R*)-Mosher's acid.

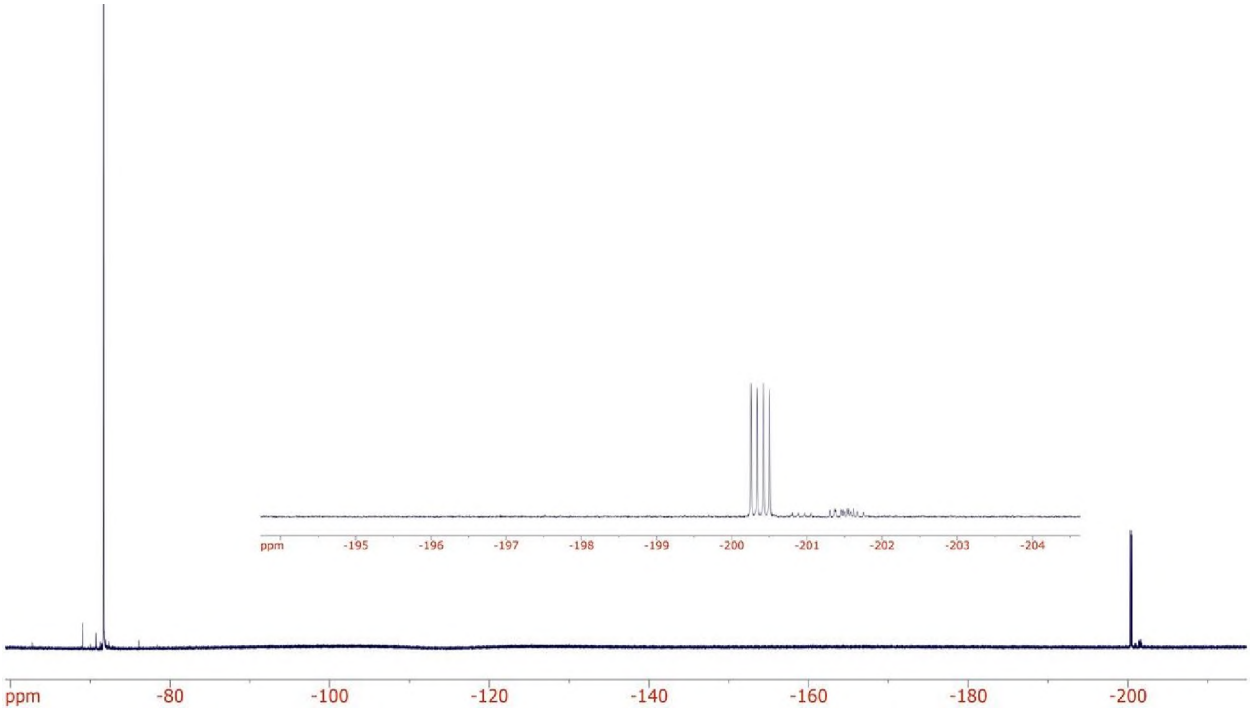

Figure A.33. ^{19}F NMR spectrum of Mosher ester product of 4b (KRED 130) and (*S*)-Mosher's acid.

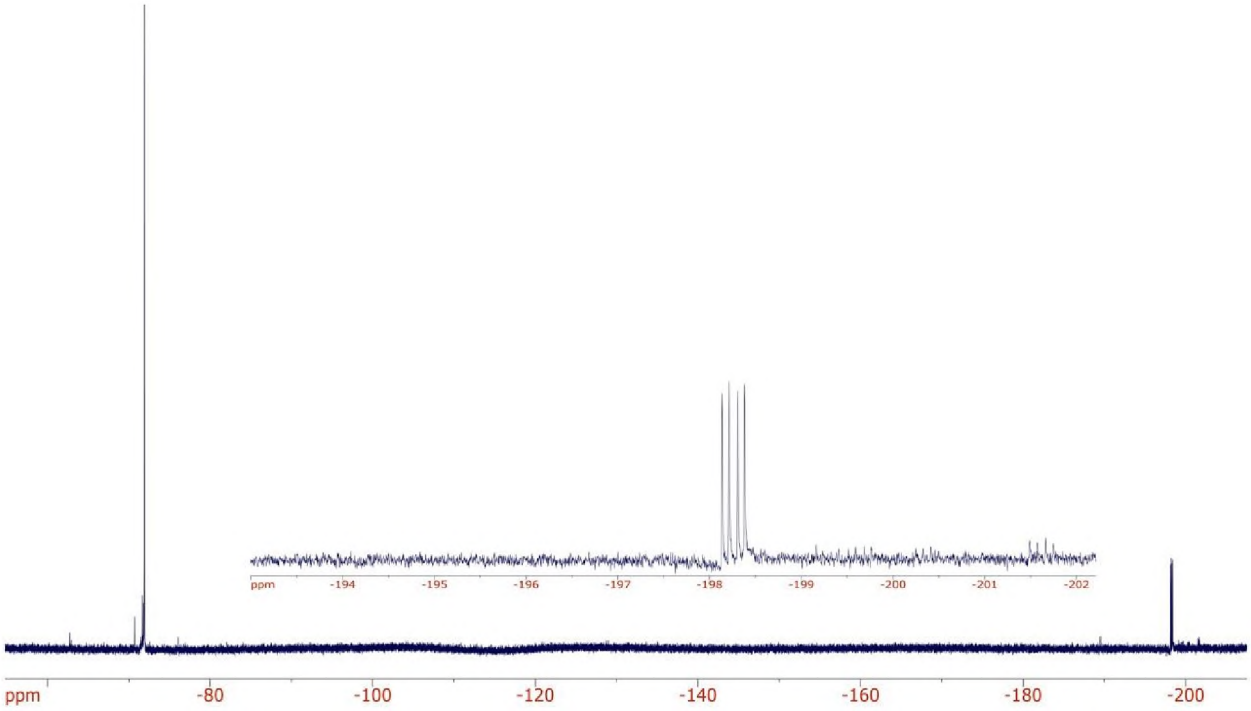

Figure A.34. ^{19}F NMR spectrum of Mosher ester product of 4b (KRED 130) 4-methoxy derivative KRED 130 product and (*R*)-Mosher's acid.

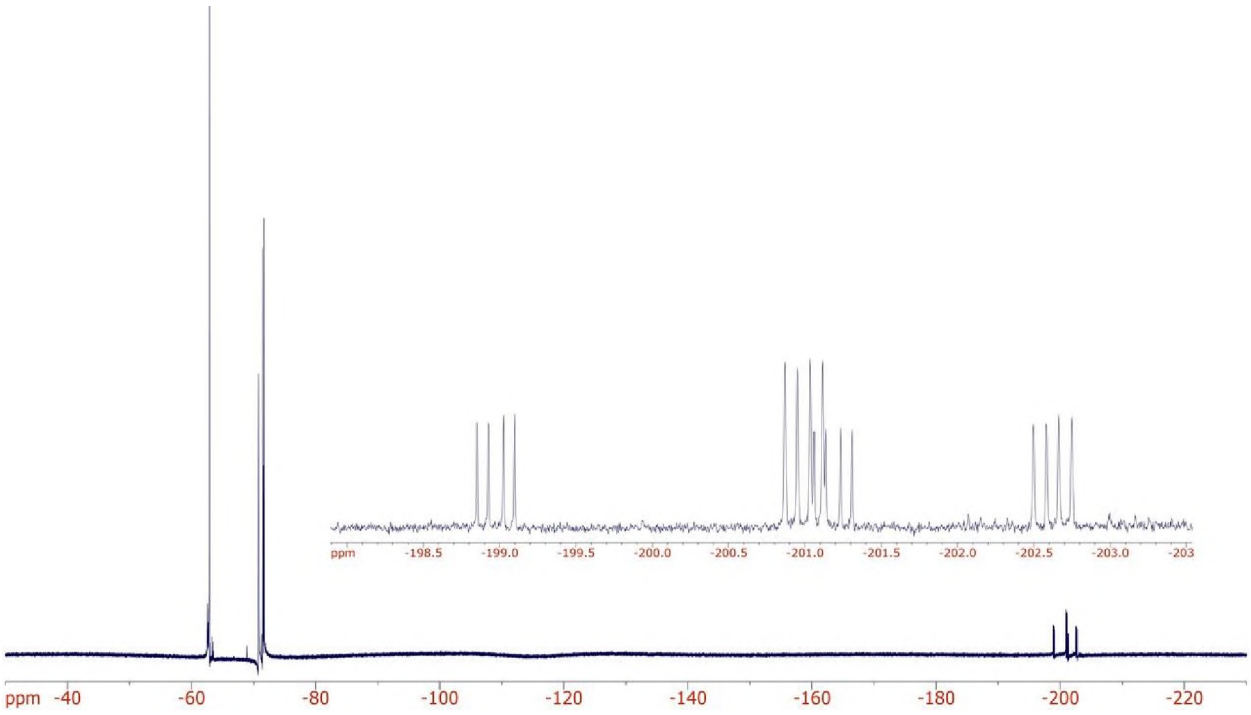

Figure A.35. ^{19}F NMR spectrum of Mosher ester product of racemic 4-trifluoromethyl derivative, 2c, and (*S*)-MTPA.

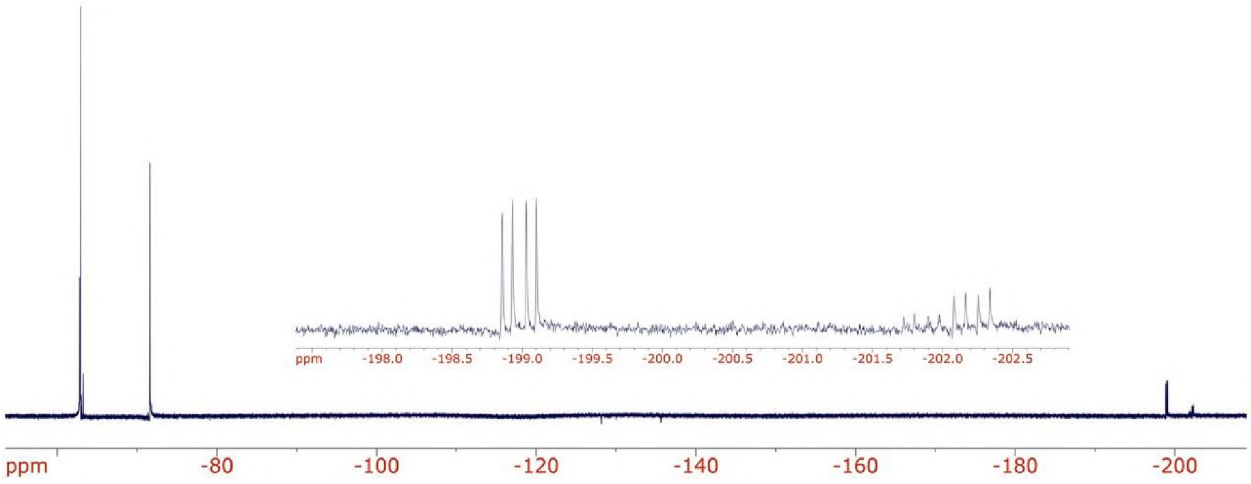

Figure A.36. ^{19}F NMR spectrum of Mosher ester product of 4c (KRED 110) and (*S*)-Mosher's acid.

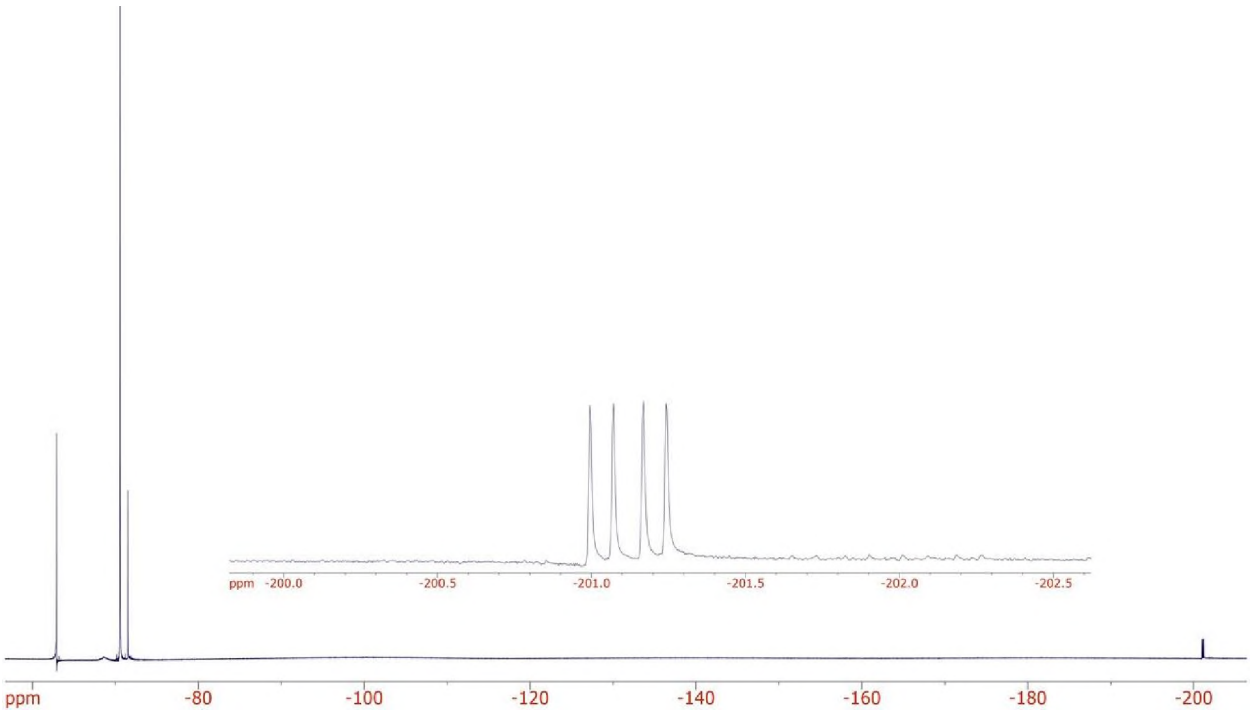

Figure A.37. ^{19}F NMR spectrum of Mosher ester product of 4c (KRED 110) and (*R*)-Mosher's acid.

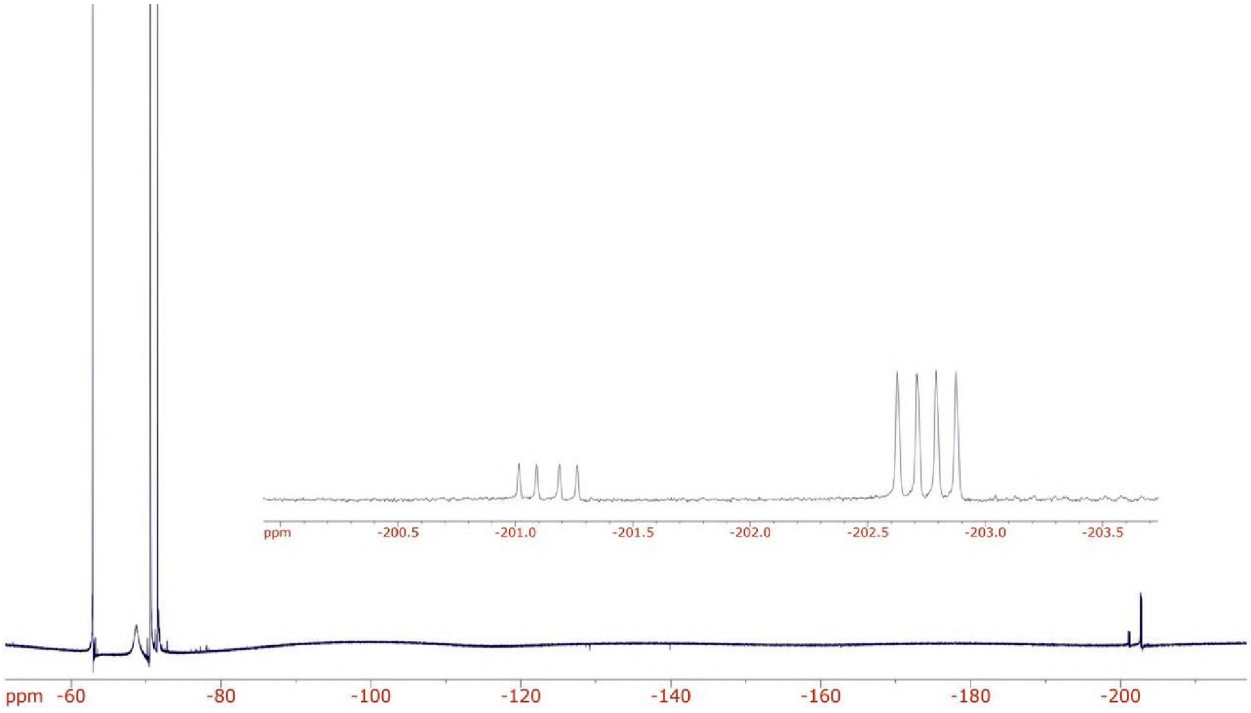

Figure A.38. ^{19}F NMR spectrum of Mosher ester product of 4c (KRED 130) and (*S*)-Mosher's acid.

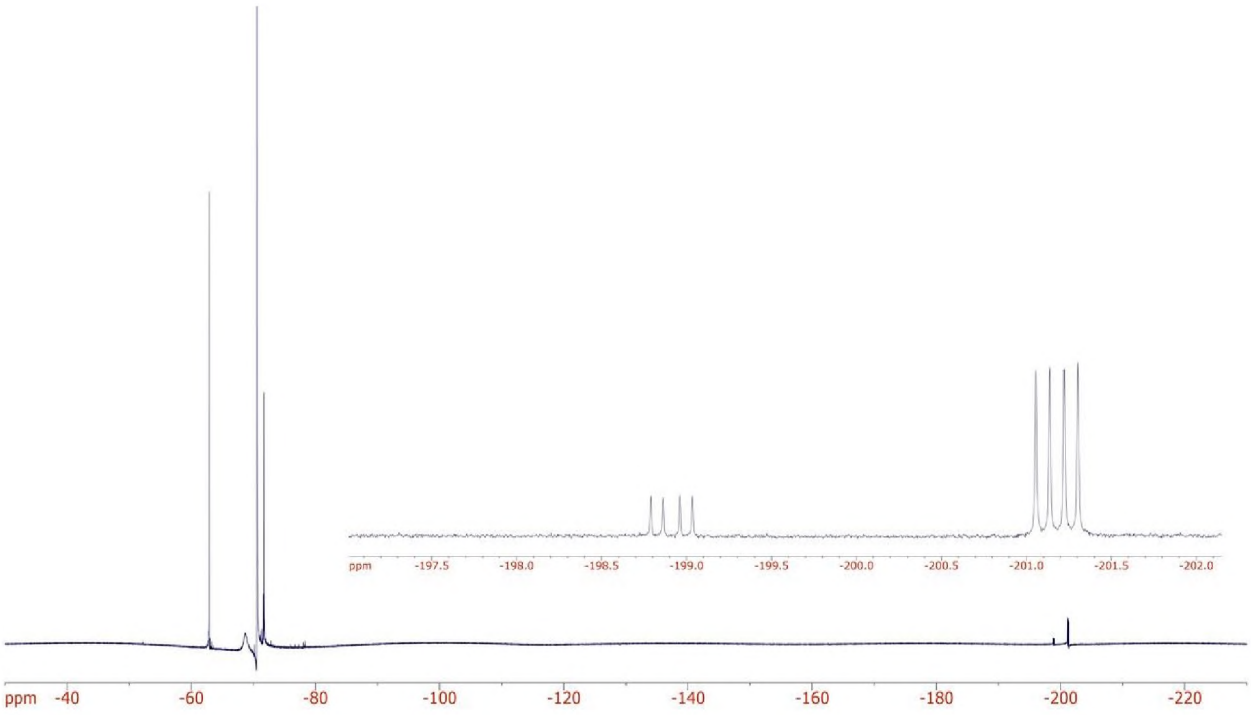

Figure A.39. ^{19}F NMR spectrum of Mosher ester product of 4c (KRED 130) and (*R*)-Mosher's acid.